Excitation energy propagation and angular momentum generation in the nuclear fission process

A thesis presented for the degree of Philosophiae Doctor

Dorthea Gjestvang
Department of Physics
University of Oslo

Spring 2023

Series of dissertations submitted to the
Faculty of Mathematics and Natural Sciences, University of Oslo
No. 2627

ISSN 1501-7710

Cover: UiO.
Print production: Graphic Center, University of Oslo.

Til Mamma og til Farmor
Glad i Dere

Abstract

In the nuclear fission process, the stretching and subsequent rupturing of a heavy nucleus results in the creation of two or more smaller fission fragments. The significant difference in binding energy between the heavy nucleus and the fragments gives rise to the release of large amounts of energy, which manifest as kinetic energy of the fission fragments as well as emission of neutrons and γ rays from the fragments.

Though perhaps most commonly known for the applications of the energy release, the fission process is also an interesting arena for studying the behaviour of the nuclear and Coulomb forces in a many-body system. Due to the complexity of the fission reaction, with a range of experimental observables and inter-dependencies that must be understood, the nuclear fission process is still not completely described by fission theory.

With the aim of learning more about how the fragment excitation energy E_{x} and angular momentum J are determined, this thesis investigates specifically the generation of angular momentum in the fission fragments and propagation of excitation energy throughout the fission process. This study is carried out experimentally by introducing changes to the fissioning system and observing the impact on the γ rays emitted from the fission fragments.

In this thesis, we present three papers that all investigate different excitation energy and angular momentum effects in fission. First, prompt fission γ rays (PFGs) are measured following the reaction ^{240}Pu$(d,p\mathrm{f})$, and the spectral characteristics are studied as a function of the excitation energy of the compound nucleus. The extracted energy dependence is interpreted and discussed and also compared to model predictions from the fission simulation code FREYA. We find that only a small fraction of the added excitation energy emerges as increased γ-ray emission, which implies that most of the energy must go elsewhere. Other recent results support our findings. We also present the open question of how the angular momentum of the compound nucleus impacts the subsequent PFG emission, and propose a new project that will shed light on this.

Furthermore, the average angular momentum $\bar{J}$ of a range of different fission fragment masses A are deduced following the ^{238}U(n,f), ^{232}Th(n,f), and ^{252}Cf(sf) reactions. The resulting shape of $\bar{J}(A)$ confirms the existence of a universal angular momentum sawtooth. We show for the first time that the $\bar{J}$ magnitudes of two partner fragments are observed to be uncorrelated. This experimental result gives new insight into the mechanism behind angular momentum generation in fission, and it is proposed that the generation is driven by the available excitation energy of the fission fragments at scission.

The last paper investigates what impacts the isomeric yield ratios (IYRs) of fission fragments. IYRs, i.e. the relative frequency of which isomeric states are populated, are angular-momentum sensitive observables. Though measurements are restricted to fission fragments with isomeric states, they may give a detailed understanding of structural

effects that impact the angular momentum generation. We study how the IYRs of the fission fragment ^{134}Te vary with changes in mass and energy of the fissioning system, as well as the minimum J of the binary fission partner and the observed neutron multiplicity. For this, a new method for extracting IYRs is developed. The new method opens for the extraction of isomers with half-lives on the order of 10^{-8} – 10^{-6}s, in addition to enabling the unique ability of studying the IYR dependence on partner properties. IYRs of ^{134}Te are found to be largely independent of the mass and energy of the fissioning system, as well as the emitted neutron multiplicity and angular momentum of the partner fragment. We discuss what the results imply for the behaviour of angular momentum generation, and remark on how isomer feeding saturation might impact the sensitivity of the IYRs to changes in the angular momentum.

The broader understanding of the results is presented and discussed in the light of other results in the literature. New projects that explore still unknown aspects of the generation and propagation of excitation energy and angular momentum in fission are proposed.

Sammendrag

Kjernefysisk fisjon finner sted når en tung kjerne strekkes til den ryker, og to eller flere lettere fisjonsfragmenter blir dannet. Den store forskjellen i bindingsenergi mellom den opprinnelige kjernen og fisjonsfragmentene fører til frigjøring av mye energi som går til kinetisk energi til fisjonsfragmentene, samt utsendelse av nøytroner og γ-stråler fra fragmentene.

Fisjonsprosessen er kanskje mest kjent for hva den frigjorte energien kan brukes til, men den er også en interessant arena for å studere hvordan den sterke kjernekraften og Coulombkraften oppfører seg i et mangepartikkel-system. Fisjon er en svært kompleks reaksjon, med en rekke egenskaper og gjensidige avhengigheter som må undersøkes og forstås. Fisjonsteori kan enda ikke beskrive alle aspekter av denne prosessen.

Målet med denne avhandlingen er å lære mer om hvordan fragmentenes E_{x} og angulærmoment J blir bestemt, og vi studerer spesifikt hvordan angulærmomentet til fragmentene blir generert samt hvordan eksitasjonsenergi blir propagert gjennom fisjonsprosessen. Dette undersøkes eksperimentelt ved å innføre endringer i systemet som fisjonerer, og observere hvordan disse endringene påvirker γ-strålende som blir sendt ut fra fisjonsfragmentene.

Denne avhandlingen beskriver tre artikler som alle undersøker forskjellige eksitasjonsenergi- og angulærmoment-effekter i fisjon. Først måler vi utsendelsen av γ-stråler fra reaksjonen ^{240}Pu(d,pf). Disse kalles PFGs (prompt fission γ rays), og vi studerer egenskapene til disse γene som funksjon av eksitasjonsenergien til kjernen som fisjonerer. Energiavhengigheten blir ekstrahert og diskutert, samt sammenliknet med utregninger fra fisjonsimuleringsmodellen FREYA. Resultatene tyder på at en minimal andel av den ekstra energien går til γ-utsendelse, hvilket impliserer at mesteparten av energien ender andre steder. Dette støttes av funn gjort i andre nylige publikasjoner. Vi diskuterer også det åpne spørsmålet om hvordan angulærmoment blir propagert gjennom fisjonsprosessen, og foreslår et nytt forskningsprosjekt som kan kaste lys på dette.

I den neste artikkelen presenterer vi målinger av det gjennomsnittlige angulærmomentet $\bar{J}$ som funksjon av fisjonsfragment-massen A fra reaksjonene ^{238}U(n,f), ^{232}Th(n,f) og ^{252}Cf(sf). Kurven $\bar{J}(A)$ har form som en sagtann, hvilket bekrefter tidligere funn. Sagtannformen er også uavhengig av hvilken reaksjon som skapte fragmentet. Vi oppdager at størrelsen på angulærmomentene til to partner-fragmenter er uavhengige av hverandre. Dette eksperimentelle resultatet gir ny innsikt i mekanismen bak generering av angulærmoment i fisjon, og vi foreslår at det er den tilgjengelige eksitasjonsenergien i fragmentene etter fisjonsøyeblikket som driver generasjonen av angulærmomentet til fisjonsfragmentene.

Den siste artikkelen bruker det samme datasettet på ^{238}U(n,f), ^{232}Th(n,f) og ^{252}Cf(sf) til å utvikle en ny metode for å måle hvor ofte isomere tilstander blir populert i fisjons-

fragmenter (såkalte IYR, Isomeric Yield Ratios). Disse relative frekvensene er sensitive til angulærmomentet til fisjonsfragmentene. Målinger av IYRer er begrenset til fisjonsfragmenter som har slike langlivede isomerer, men de kan også gi en detaljert forståelse av hva som påvirker angulærmomentet til et fisjonsfragment. Med den nye metoden kan IYRs fra isomerer med halveringstider rundt 10^{-8} – 10^{-6}s ekstraheres, samt at metoden åpner opp den unike muligheten til å studere hvordan IYRer avhenger av egenskaper til partnerfragmentet. Vi måler IYRer til fisjonsfragmentet ^{134}Te, og finner at disse stort sett er uavhengige av massen og eksitasjonsenergien til systemet som fisjonerte, samt massen og angulærmomentet til partnerfragmentet. Vi diskuterer hva disse resultatene betyr for hvordan vi forstår generering av angulærmoment i fisjon, og peker på hvordan en metning av isomer-populeringen kan påvirke hvor sensitiv en IYR er til endringer i fragmentets angulærmoment.

Til slutt presenterer vi helhetsforståelsen av de nye eksperimentene, og diskuterer disse i lys av tidligere resultater. Vi foreslår også nye prosjekter som undersøker fortsatt ukjente aspekter av generering og propagering av eksitasjonsenergi og angulærmoment i fisjon.

Acknowledgment

They say it takes a village to raise a child. Similarly, a full support group is needed to write a thesis.

To my amazing supervisors, Sunniva and Jon: thank you for everything you have taught me, for giving me a boost when I need it, and most of all, for believing in me. You treat me as an equal in scientific debates, and give me the freedom to pursue my own projects and pathways. I'm so grateful that I can come to you for academic questions as well as personal problems. Without you, this thesis would not have been written.

To all my friends - thank you for the teatimes and coffee breaks, afternoon walks, library chats, and wine nights. I'm so grateful that I am surrounded by all you awesome people - that I can both rant about my problems, and also completely forget about the PhD stress while we have a good time. You have all saved me a huge therapy bill (hehe).

Til Mamma, Andrea og Karina: tusen takk for at dere spør hvordan det går med meg, og synes det jeg driver med er kult og spennende. Farmor, det er så utrolig gøy at du vil vite akkurat hva jeg holder på med. Jeg er så stolt av å vite at jeg stammer fra, og er omkranset av, en rekke med viljesterke damer.

Tilslutt, kjære Stianmin - du gifta deg med meg ikke bare én, men to ganger i løpet av denne tida. Tusen takk for all støtten jeg får fra deg, for at du holder rundt meg når jeg trenger det, og gjør dagene mine bedre når jeg er i grøfta (så er det ekstra bonus at du heller ikke har innsigelser mot pretty-book-terapien min) < 3

Contents

Abstract **1**

Sammendrag **3**

Acknowledgment **5**

1 Introduction **9**

2 An overview of the fission process **11**
2.1 Some fission basics 11
2.2 Energy sharing in fission 13
2.3 Fission fragment de-excitation 15
2.3.1 Studying the excitation energy and angular momentum 16

3 Excitation energy-dependent emission of prompt fission γ rays **19**
3.1 Overview of main points in literature 20
3.2 Paper I: Excitation energy dependence of prompt fission γ-ray emission from $^{241}Pu^{*}$ 20
3.2.1 Summary of key results 22
3.2.2 Further developments 22
3.3 Discussion 23
3.4 Impact of compound nucleus angular momentum on prompt fission γ-ray emission 24
3.5 Future work 26

4 Angular momentum generation in fission **27**
4.1 Overview of main points in literature 28
4.2 Paper II: Angular momentum generation in nuclear fission 29
4.2.1 Summary of key results 30
4.3 Discussion 31
4.4 Further work 33

5 Isomeric yield ratios of fission fragments **35**
5.1 The basis of isomeric yield ratio measurements 35
5.1.1 Techniques 36
5.1.2 Transforming from isomeric yield ratio to angular momentum . . . 37
5.2 Overview of main points in literature 39
5.3 Paper III: What impacts the isomeric yield ratios of fission fragments? . . 40
5.3.1 Summary of key results 40
5.4 Discussion 41
5.5 Future work 43

6 What have we learned? **45**
6.1 Summary of results 45
6.2 Sawtooth patterns in fission 46
6.3 Excitation energy dependence 47
6.4 Dependence on fissioning system 48
6.5 Final thoughts 49

I Excitation energy dependence of prompt fission γ-ray emission from $^{241}Pu^{*}$ **51**

II Angular momentum generation in nuclear fission **63**

III What impacts the isomeric yield ratios of fission fragments? **85**

Bibliography **99**

Chapter 1

Introduction

Out of the various reactions a nucleus may suffer, the nuclear fission process is perhaps the most infamous. The fission process occurs when a heavy nucleus is stretched until it ruptures, creating two (or occasionally more) fission fragments. As the fission fragments are in sum less massive than the original nucleus, the difference in mass is released as enormous amounts of energy [1], and this energy release explains why the fission process is so prominently known - it is an important energy source for both peaceful and military applications.

However, there are more aspects to the nuclear fission process than simply the large energy release. As the fissioning nucleus consists of hundreds of nucleons (neutrons and protons), fission is a pertinent arena for observing how the nuclear and Coulomb forces behave in a many-body system. This behaviour is in fact so complicated that even though fission was first discovered in 1939 [1, 2], there is yet no complete theoretical description of fission.

One way to learn more about nuclear fission is to study the process experimentally. There are plenty of observables to be measured: the fission fragments emerge with a distribution of different masses, with varying kinetic energies, and emit a handful of neutrons and γ rays as they de-excite. We can, for example, measure the fission fragment mass yield and kinetic energies, or the multiplicity, energy, and emission angle of the neutrons and γ rays. However, to measure these independently is not enough. By determining event-by-event correlations between the different observables, we may get a deeper understanding of the mechanisms that are at play in fission. In addition to revealing new aspects of fission, the experimental measurements are used to benchmark fission models, and the comparison between experiments and models indicates whether the physics behind these models is correct.

In fission research, two quantities of interest are the excitation energy E_{x} and the

angular momentum J that the fission fragments emerge with. These are not directly observable in experiments, but correlate strongly with the neutron and γ emission as the de-excitation process rids the nucleus of excess E_{x} and J. Two central questions in fission research are thus how the excitation energies of the fission fragments are determined in fission, and how the angular momenta of the fragments are generated. Studying neutron and γ emission gives us insights into these questions. Neutron and γ-emission characteristics, as well as the correlation between them, have therefore been measured for different fissioning systems, see for example Refs. [3, 4]. In addition to basic science interest, understanding the E_{x} and J is also important for energy applications, as neutrons maintain the chain reaction in nuclear reactors and γ rays contribute to reactor heating [5].

In this thesis, the central questions are: how are the excitation energy and angular momentum of the fission fragments determined, and how do they evolve with changing properties of the fissioning nucleus? In other words, how are changes to the E_{x} and J of the fissioning system propagated through the fission process? These questions will be investigated by introducing perturbations to the fissioning nucleus and observing the impact on the measured γ-ray emission from the resulting fission fragments.

This thesis is based on three papers, all taking different approaches to investigating the central questions presented above. After the overview of the nuclear fission process in Ch. 2, experimental results are presented in Ch. 3 where the average γ-ray multiplicity and energy are measured for the compound nucleus (CN) $^{241}\mathrm{Pu}^{*}$. Here, the propagation of excitation energy through the fission process is studied by varying the available excitation energy in the fissioning nucleus. Furthermore, the work discussed in Ch. 4 represents an important step forward in understanding how angular momentum is generated in fission, revealed by studying the average deduced angular momentum of fission fragments from different fissioning systems. In Ch. 5, we scrutinize the angular momentum of the fission fragment $^{134}\mathrm{Te}$ produced by different fissioning nuclei and fission configurations. Finally, in Ch. 6 we take a step back to discuss the broader picture of what we have learned about angular momentum generation and excitation energy propagation in this thesis.

Chapter 2

An overview of the fission process

Before delving into the experimental works in this thesis, we will here give an overview of the nuclear fission process - both some key elements to it, as well as a broad understanding of what is known, and what is still unknown, about this process.

2.1 Some fission basics

Figure 2.1 shows fission as it is commonly depicted, with a heavy nucleus that stretches until it breaks apart, and the two fission fragments that emerge along with some neutrons and γ rays. In the introduction in Ch. 1 we touched upon why nuclear fission can occur: the mass of the heavy nucleus is larger than the sum of the fragment masses. A more precise explanation is given in terms of the average binding energy per nucleon. Heavy nuclei in the actinide region are less tightly bound than the nuclei in the $A \sim 100$ region, and thus the system of two lighter fragments is more tightly bound than the initial nucleus. The difference in binding energy results in an energy release of about 200 MeV per fission reaction [6]. When comparing this to the typical energy release in a chemical reaction, e.g. what we get when we burn coal, the benefit of using fission for energy applications is clear: fission releases about seven to eight orders of magnitude more energy per reaction [1].

Nuclei want to exist in the lowest possible energy state, which is why radioactive nuclei decay; they have the possibility of reaching a less energetic configuration. It may therefore be surprising that despite the large energy release in fission, only a handful of nuclei have

[1] The large difference in energy release between chemical and nuclear reactions is also clear when we consider the respective energy scales used: energy release in chemical reactions is typically given in eV while nuclear reactions use MeV.

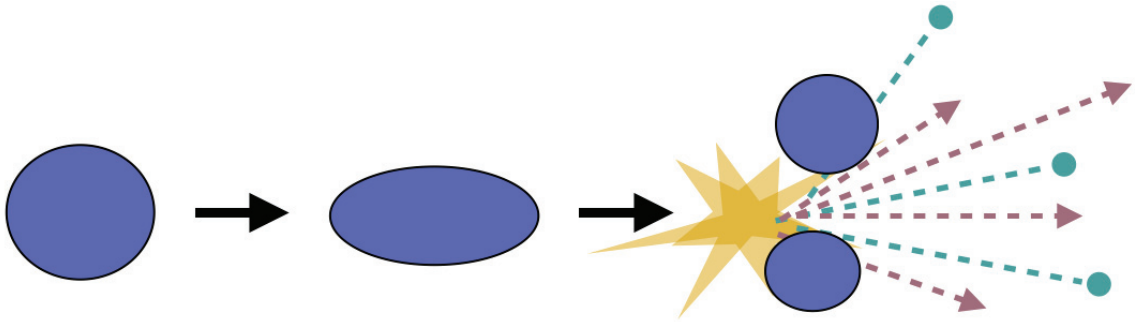

Figure 2.1: Illustration of the nuclear fission process, where a heavy nucleus stretches until it ruptures. Two fission fragments are formed, which emit neutrons (green circles) and γ rays (purple arrows) as they de-excite.

fission as their main decay mode. Even the well-known spontaneously fissioning nucleus ^{252}Cf only has an $\approx 3.1\%$ branching ratio to fission [7], overwhelmingly preferring to α decay despite the energy release being around 50 times smaller. The reason behind this can be understood by studying what happens as the nucleus stretches. Like L. Meitner and O. Frisch did in 1939 when first explaining the nuclear fission process [1] [2], we will begin by looking at the nucleus in terms of the (charged) Liquid Drop Model (LDM).

In order for the heavy nucleus to undergo fission, it needs to change its shape: it must stretch, as shown in Fig. 2.1. When changing the shape, there are predominantly two forces that come into play [9, pg. 8]. First is the Coulomb force, which pushes the charged protons in the nucleus apart and therefore aids the stretching process. On the other hand, the surface tension seeks to minimize the amount of surface the nucleus has. As the surface would increase with deformation, the surface tension thus works in the opposite manner from the Coulomb repulsion, and this surface tension needs to be overcome for a nucleus to fission. The challenge is thus to stretch the nucleus until the two halves break apart, referred to as scission. Scission occurs when the short-range nuclear force no longer keeps the two fragments together, and the Coulomb force then drives the fragments apart. In all existing nuclei, the surface term is larger than the Coulomb term, creating an energy barrier that hinders the nucleus from fissioning.

The energy barrier hindering fission is referred to as the fission barrier. For most nuclei, it is so large that fission is not a plausible reaction mechanism, thus explaining the very limited number of spontaneously fissioning nuclei. However, there is a subset of nuclei that can undergo spontaneous fission. For these nuclei, the barrier is sufficiently small such that there is a small probability that the nucleus can tunnel through it. These are referred to as spontaneously fissioning nuclei (sf), and the above-mentioned ^{252}Cf is among these.

[2] Here we also mention I. Noddack, who was the first to suggest that fission might be possible [8].

For other nuclei, especially in the actinide region, the fission barrier is too high for the nucleus to have a viable probability of spontaneous penetration. However, if the nucleus gets a "push" in the form of added excitation energy, it may be enough for them to overcome the barrier. This excitation energy might come from the absorption of a neutron, in which case the resulting reaction is referred to as neutron-induced fission. The excitation energy of the CN is then $E_{\mathrm{x}} = S_n + E_n$, where S_n is the neutron separation energy and E_n is the neutron kinetic energy. Fission can also be induced in other manners with light particles or even γ rays [10, pg. 481].

Fission cannot be fully described within the Liquid Drop Model. This is for example evident when measuring the shape of the fission barrier: where the liquid-drop model would predict a smooth, single-humped fission barrier, nuclear shell effects yield a fission barrier with two humps, named the double-humped fission barrier [9, pg. 14]. The reason for this double-humped shape is that halfway to fissioning, the nucleus reaches a super-deformed state that is more energetically favourable than neighbouring deformations [11]. The nucleus may exist for some time in this super-deformed well, known as a fission isomer, and it is possible to conduct spectroscopy of the states in this well, see e.g. Ref. [12] and references therein.

Another way that nuclear shell effects manifest in the fission process is the shape of the fragment mass yields. Where the LDM predicts that the two fragments should be of equal size on average, the measured yields from actinide fission often show distinctly asymmetric fission where one fragment is heavier than the other. This is mainly because of the influence of the double-magic shell closure around ^{132}Sn, resulting in the heavy fragment having a mass in this vicinity. Other shell closures can also impact the mass distribution [13]. However, predicting the exact mass distributions is difficult and remains an important research topic within the field of fission theory. The mass distributions are typically determined by calculating a potential surface that the nucleus must navigate on its way to fission. The shell effects influence this landscape, and thus impact the optimal way to tread the surface - resulting in different fragment mass distributions. For further description, see for example Refs. [13–15]. The challenge is thus to correctly predict the potential surface, which can be quite difficult and still yields surprising results. As late as in 2010, it was discovered that the nucleus ^{180}Hg, thought to fission symmetrically because of the influence of the ^{90}Zr shell closure, in fact fissioned asymmetrically [16].

2.2 Energy sharing in fission

The sharing of energy in fission will be an important topic for this thesis, as it determines the amount of energy available for de-excitation. The experimental works presented in Ch. 3 revolve around the measurement of γ rays stemming from this de-excitation process, and we therefore give a description of how this energy sharing proceeds.

First, the amount of energy released is defined as the Q-value of the reaction, which is given by the difference in mass between the fissioning nucleus and the fission fragments:

$$Q = m(\text{fissioning nucleus}) - m(\text{fragments}) \tag{2.1}$$

The Q-value is then distributed between the kinetic energy and excitation energy of the fragments.

As mentioned earlier, the fission fragments are driven apart at large velocities due to the Coulomb repulsion. This energy portion is commonly referred to as the TKE (Total Kinetic Energy) of the fragments, and makes up about 80% of the initial energy release [10, pg. 492]. Like the fission fragment mass distribution, the kinetic energy emerges as a mass-dependent distribution [17], and the light fragment typically has more kinetic energy than the heavy [10, pg. 491].

The rest of the available energy is given to the fragments as excitation energy, named TXE (Total eXcitation Energy), such that

$$Q = TKE + TXE. \tag{2.2}$$

The TXE is then distributed between the fragments,

$$TXE = E_{\mathrm{x},1} + E_{\mathrm{x},2}, \tag{2.3}$$

where $E_{\mathrm{x},1}$ and $E_{\mathrm{x},2}$ are the excitation energies of respectively fragment 1 and 2. The sharing of TXE between the two fragments is thought to be related to the ratio of the level densities in the two fragments [18], though the reproduction of experimental data is not perfect.

There is one final step to the excitation energy sharing process within each fragment. As the fragments typically emerge with some units of angular momentum [19, 20], a minimum amount of E_{x} must be bound into rotational energy. This is referred to as the yrast line: the minimum excitation energy that must be present to sustain a given angular momentum. Regarding the amount of angular momentum that the fragments emerge with, this will be discussed in more detail in Ch. 4. For now, we understand that the E_{x} of a fragment is decomposed in the rotational energy E_{rot} and statistical excitation energy E_{stat}:

$$E_{\mathrm{x}} = E_{\mathrm{rot}} + E_{\mathrm{stat}}. \tag{2.4}$$

A simple way of describing the initial condition of a fission fragment after fission is its position in a J vs E_{x} matrix. Such a matrix is illustrated in Fig. 2.2. Possible values of E_{x} vary and are also correlated with the value of J. This is due to the yrast line, and no positions below the yrast line are possible. We will use this figure when we in the upcoming section describe the final part of the fission process: fragment de-excitation.

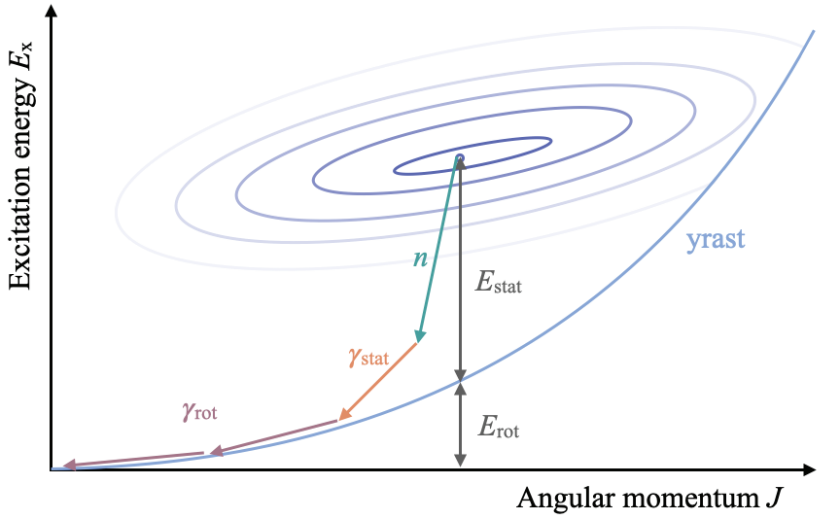

Figure 2.2: Illustration of the initial E_x vs J distribution of the fission fragments. The arrows indicate how they de-excite.

2.3 Fission fragment de-excitation

As we can see from Fig. 2.2 the newly formed fragments have significant amounts of excitation energy, and they rid themselves of this E_x through the emission of neutrons and γ rays. The initial fragments are quite neutron rich, as heavy nuclei need a higher neutron-to-proton ratio than lighter nuclei in order to combat Coulomb repulsion. Therefore, the de-excitation of a fragment typically starts with the emission of 1-2 neutrons, referred to as prompt fission neutrons (PFNs). They are called *prompt* as they arrive immediately after the moment of fission. To first order, neutrons are emitted as long as energetically possible, meaning that the available excitation energy is larger than the neutron separation energy S_n. For each neutron emitted, the excitation energy of the fragment decreases and we move down along the E_x-axis in Fig. 2.2 as illustrated by the arrows. The angular momentum J removed by each neutron is generally assumed to be small, such that neutron emission mainly exhausts the E_{stat} portion of the excitation energy. The assumption of negligible angular momentum removal by neutrons has recently been questioned [21], and we will return to this in Ch. 5.

When neutron emission ceases, the nucleus usually both has some E_{stat} and E_{rot} left, which is dissipated via γ-ray emission. Conforming with the name of the PFNs, the γ rays that are emitted immediately after the moment of fission are named prompt fission γ rays (PFGs). The first γ rays emitted are commonly referred to as statistical γ rays, marked in Fig. 2.2 as γ_{stat}. These occur within the statistical region of the nucleus with high density of nuclear levels and are thus typically $E1$ γ rays due to the high transition

probability of these transitions. Eventually, the de-excitation process reaches the yrast line and $E1$ γ rays are no longer possible. Thereafter, so-called rotational $E2$ γ rays γ_{rot} remove the last portion of the remaining E_{x} and J.

The assumption that neutrons are emitted as long as energetically possible is known to be a first-order approximation. The observation of PFGs with energies larger than S_n indicates that there must be some competition between γ ray and neutron emission even when $E_{\mathrm{x}} > S_n$ [22].

The de-excitation procedure described above paints a broad picture of the main features of the process, yet it is still quite simplified. We have omitted the descriptions of fragment-to-fragment variations because of differences in level scheme, that e.g. could cause the decay to flow in a band parallel to the yrast line instead of along it. We have also pointed out several unknown factors in the process that are currently being investigated, such as the γ-neutron competition and the angular momentum removal by neutrons. In this thesis, we will focus on the questions of how excitation energy of the fissioning nucleus is propagated throughout the fission process, as well as how the angular momenta of the fission fragments are generated.

2.3.1 Studying the excitation energy and angular momentum

The emitted neutrons and γ rays from fragment de-excitation carry information about the initial configuration of the fragment. As we see from Fig. 2.2, since the position of the initial nucleus in the J vs E_{x} matrix affects the de-excitation process, measuring the neutrons and γ rays gives us the ability to "add back" the quantities and reveal which configuration the fission fragment emerged in. Similarly, if a fragment emerges in a different position in the J vs E_{x} matrix, differences will be observed in the de-excitation process. This is the reason why all three of the scientific works presented in this thesis revolve around the measurement of fission γ rays from the primary fragments - we learn about the excitation energy and the angular momenta that the fragments emerged with.

However, it is only the γ rays emerging from the *primary* fission fragments that are of interest when unraveling the E_{x} and J. After reaching the ground state, the neutron rich fragments will β decay, and the β-delayed neutrons and γ rays do not carry information on the E_{x} and J of the initial fragment. It is thus necessary to ensure that the γ rays measured are indeed from the primary fragments. As the β particles are usually not measured when doing PFG measurements, it is common to put a time scale on what is defined as "prompt". This cut-off is usually set to about ±3 to ±10 ns after the moment of fission [23–25], dependent on the time resolution of the experiment.

There is an exception to this time cut. Some fission fragments will get stuck in long-lived isomeric states as they de-excite. In these states, the decay is delayed due to quantum number selection rules that make the transition improbable. This might, for example, be

a high difference in angular momentum between the initial and final state. The further decay of these fission fragments is thus delayed, and they can survive millisecond, seconds, or even hours after fission. When the isomer eventually decays, the γ rays in the cascade are still from the primary fragments. They therefore retain the information about the state the fragment emerged in, even a long time after the fission occurred. This we will exploit in Ch. 5 to investigate the initial E_{x} and J of fission fragments.

Chapter 3

Excitation energy-dependent emission of prompt fission γ rays

In the introduction, we raised the question of excitation energy propagation in the fission process: if we increase the E_{x} of the fissioning system, where does this energy end up? From energy conservation we know it must go somewhere, however the Eqs. 2.1 - 2.3 also illustrate that there is a multitude of ways to distribute the added energy. For example, it is known that the fission fragment mass distribution changes with increased compound nucleus (CN) energy [9, pg. 306], and that some of the energy goes to increased neutron emission [26]. In this chapter, we investigate the question: how does more available energy in the CN impact the emission of γ rays from the primary fragments?

In Ch. 2 prompt fission γ rays (PFGs) were defined as γ rays that arrive immediately after the moment of fission, and they are characterised by their multiplicity, average energy, and their energy spectrum. In addition to the basic science interest, knowledge of these PFG characteristics is also important for energy applications, as it is known that the PFGs contribute to the heating in reactors. Though only carrying a fraction of the energy released in fission, the γ rays travel large distances in matter, and thus may deposit significant amounts of heat in structures and components surrounding the reactor core. PFG characteristics from thermal neutron-induced fission were first measured for the major actinides in the 1970s [27, 28], and subsequently the field was dormant for some time. When the interest for fast reactors was picking up momentum in the early 2010s due to the development of generation-IV reactors, the question of PFG heating was brought up again: would the higher CN energy in fast fission give increased γ-ray heating? Therefore, there was a call for more studies of PFG characteristics for both thermal and fast fission [5], and the study of PFGs saw a renewed interest (see for example [23, 29–33]

and references therein).

3.1 Overview of main points in literature

At the point when this work was conducted, only a handful of E_x-dependent PFG measurements existed in the literature. An older measurement employing neutron-induced fission in the energy range $E_n = 1 - 15$ MeV showed a significant increase of total PFG energy with increased E_n [26]. Two newer (n,f) experiments compared the measured PFG characteristics at respectively two and three different neutron energies [25, 30], and the values below the thresholds for second-chance fission were consistent within a 2σ interval. E_x-dependent PFG characteristics had also been investigated at the Oslo Cyclotron Laboratory (OCL) [32], however they employed the old γ-ray detectors made of NaI and had challenges separating detector signals from PFGs and contaminating signals from fission neutrons. The measured values for the total PFG energy per fission in these experiments are shown in Fig. 3.1. Though they measure different fissioning systems, it is curious to compare the E_x dependence that they observe: there is little agreement on precisely how the total PFG energy should vary with E_x.

Despite the seeming disagreements between the experimental results, suggestions were made on how the PFG emission will vary with the CN E_x. In Ref. [34], a prediction on PFG change with CN energy was presented, where the variation was parametrised using the variation of PFN multiplicity with energy. The ENDF-B/VIII.0 evaluation in Ref. [35] presented recommended values for PFG characteristics and their dependence on E_x.

3.2 Paper I: Excitation energy dependence of prompt fission γ-ray emission from ^{241}Pu*

To contribute to answering the questions about the E_x-dependence of the PFGs, an experiment was conducted at the Oslo Cyclotron Laboratory (OCL) (Oslo, Norway) in April 2018. Here, the (d, p) reaction was used to induce fission of ^{241}Pu in an excited state [1] and the subsequent emitted γ rays were measured. The prompt fission γ-ray characteristics were extracted as a function of the CN E_x, for the first time using the $LaBr_3$ detector array OSCAR. The CN E_x range spanned 3 MeV below the threshold of second-chance fission, which simplifies interpretation as the mass of the fissioning system was the same over the whole energy range. Simulations were conducted with the fission simulation code FREYA (Fission Reaction Event Yield Algorithm) [36], and these simulations were then compared to the experimental data.

[1] Denoted ^{241}Pu*.

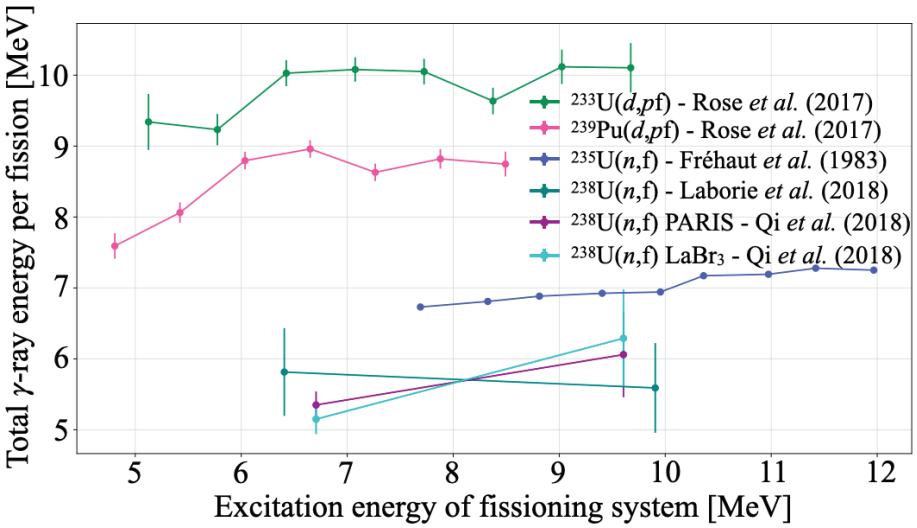

Figure 3.1: Experimental measurements of the variation in total PFG energy per fission with changing CN E_{x}. Only the data taken below the threshold of second-change fission are included. The references are Rose *et al.* (2017) [32], Fréhaut *et al.* (1983) [26], Laborie *et al.* (2018) [30], and Qi *et al.* (2018) [25]. Most show increasing trends, but there seems to be little agreement on the slope.

The experiment represented several advancements in the study of PFGs. This was the first time PFG characteristics from the fission of ^{241}Pu were studied. By studying different fission reactions, it is possible to look for system dependencies and deviations. The experimental setup illustrated in Fig. 1 of Paper I, is well-suited for the study of PFGs. By using the ^{240}Pu(d,p) reaction and detecting the ejected proton in the particle detector SiRi, the precise E_{x} of the CN ^{241}Pu* could be determined. The gas-filled fission fragment detector NIFF provided a tag on fission events by detecting one fission fragment. The OSCAR array used to detect the γ rays had a high angular coverage and a time resolution of 3 ns FWHM. This allowed for the time-of-flight discrimination between neutrons and γ rays where most neutrons below 10 MeV could be rejected. In combination, the experimental setup enabled the extraction of PFG characteristics over a range of CN excitation energies.

There are also several advantages with using (d,pf) compared to neutron-induced fission. Firstly, a beam of charged deuterons is easy to create and control, contrary to a neutron beam that will not be guided by magnetic fields. Secondly, as the ejected proton will carry energy out from the compound system, the reaction may populate the excitation-energy region below the neutron separation energy, which is unreachable by $(n$,f).

3.2.1 Summary of key results

The key points of Paper I are summarized here.

When comparing the benchmark measurement of the PFG spectrum from ^{252}Cf(sf) to previous measurements [37, 38], a deficit of γ rays below 0.5 MeV was observed. A correction factor was therefore applied to the measured PFG characteristics to account for this deficit. The main objective of the paper was to study the excitation energy dependence, and this was not diminished by the introduction of the correction factors.

The measured PFG characteristics from the ^{241}Pu$(d,p$f$)$ reaction changed minimally in the CN excitation energy region 5.5−8.5 MeV. This is demonstrated in Fig. 6 of Paper I.

The FREYA simulations reproduced the corrected experimental PFG characteristics within a 8% deviation, and also well reproduced the shape of the γ-ray energy spectrum.

Furthermore, we introduced new parameters for describing the slope of PFG characteristics with E_{x}, and uncertainty-weighted slopes were extracted both for our and previous results. Due to the significant uncertainties on some of the previous experimental results, we found the slopes to be largely consistent. The agreement between the (at the time) available experimental data indicated thus solely a weak or nonexistent dependence on E_{x} between the fission barrier and the threshold for second-chance fission. However, the slopes of the PFG characteristics with E_{x} were not in agreement with a published prediction and the most recent evaluation, which both expected more positive slopes of the PFG characteristics with E_{x}.

A question left open by the article was the impact of using the surrogate reaction $(d,p$f$)$ to induce fission compared to the $(n$,f$)$ reaction. Heavier beams are expected to induce more angular momentum in the CN, and thus this is a question of how angular momentum J of the fissioning system is propagated in fission. This lead to the planning of a new experiment, which is described in Ch. 3.4.

3.2.2 Further developments

As explained above, the article showed a γ-ray deficit below 0.5 MeV in the ^{252}Cf(sf) benchmark PFG spectrum, which was corrected for in the analysis. After the article was published, it was discovered that this was caused by timing challenges in the data acquisition resulting in some low-energy γ rays being time-stamped with artificially high times, consequently falling outside the prompt time window used in the analysis. This had not been discovered previously due to experiments at OCL mostly focusing on γ rays above 1 MeV. After this was rectified, a new ^{252}Cf(sf) benchmark measurement of the PFG spectrum was conducted. This time, our measured spectrum reproduced the previous measurements, see Fig. 3.2.

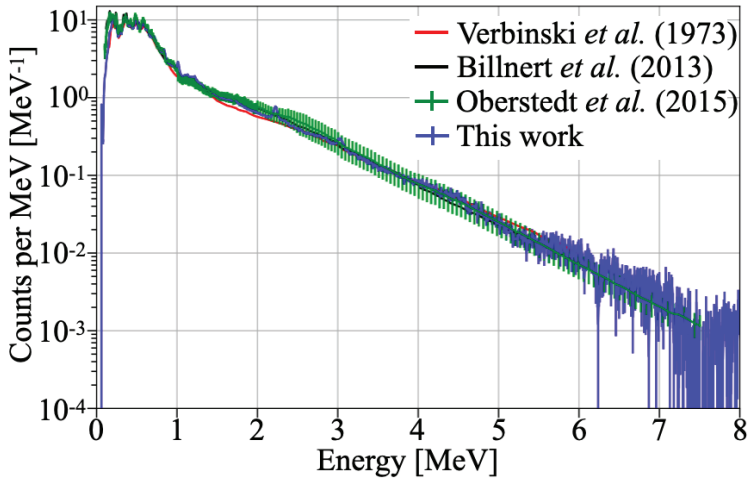

Figure 3.2: New measured PFG spectrum from ^{252}Cf(sf) compared to previous measurements from Verbinski *et al.* (1973) [28], Billnert *et al.* (2013) [37], and Oberstedt *et al.* (2015) [38].

3.3 Discussion

More experimental results have emerged on the behaviour of the PFGs with E_x. In Ref. [39], the PFG spectrum was measured for the ^{232}Th(n,f) reactions for the neutron energies E_n = 1.5, 2.1, and 2.8 MeV. They observed no change in the PFG spectrum over this energy range, and their values for the average γ-ray energy are comparable to the ones in Paper I. We use weighed linear regression to extract their slope of average γ-ray energy, and find that it is 0.11 ± 0.05, which is slightly higher than the slope in Paper I of -0.01 ± 0.01.

Furthermore, Ref. [40] measured PFGs following the ^{239}Pu(n,f) reaction in the range $E_n = 2$ to 40 MeV, and the determined slope in γ-ray multiplicity is 0.085 ± 0.010 MeV^{-1}, which is the same as Paper I's slope of 0.08 ± 0.03 within the uncertainties. This trend is observed over a significantly larger energy range than our range, and even across the barrier for second- and third-chance fission. The findings in Refs. [39, 40] thus support the conclusion in Paper I of a small variation in the prompt γ-ray emission with increased E_x.

The increase in γ-ray multiplicity with E_x is small yet statistically significant in both Ref. [40] and Paper I. In Ref. [40] they find it is the number of γ rays in the E_γ range 0.5 to 1.0 MeV that increases with increased CN E_x. This energy range is characteristic for E2 yrast transitions, referred to in Ch. 2.3 as rotational γ rays γ_{rot}. A higher number of γ_{rot} indicates that the initial fission fragment has more angular momentum J, as shown

in Fig. 2.2. Therefore, Ref. [40] uses this increased γ-ray multiplicity in the 0.5 - 1.0 MeV region to argue for the direct observation of a correlation between E_{x} and J: an increase in CN E_{x} gives an increase in J. This supports the statistical model for angular momentum generation presented in Paper. II. However, in Fig. 5 of Paper I we do not see a similar significant change in the γ-ray multiplicity in the noted energy region, and neither did Ref. [32] nor Ref. [39]. In Paper I and Ref. [32], the small increase in γ ray multiplicity seems more evenly distributed over the whole γ-ray energy range. Though studying a broader E_{x} range than Paper I and Ref. [32], Ref. [40] shows in their Fig. 4 that the change should be notable even with a E_{x}-range of 3 MeV. More investigations with higher statistics are therefore needed to understand if the trend in Ref. [40] is real.

3.4 Impact of compound nucleus angular momentum on prompt fission γ-ray emission

In Paper I, we compare the PFG results where fission is induced by the (n,f) process to our measurements using the (d,pf) reaction. We have presented some benefits of using the (d,pf) reaction as a surrogate for neutron-induced fission. Nevertheless, the two reactions are not equivalent, due to the more massive deuteron beam inducing more angular momentum in the CN. The impact of using a surrogate reaction with heavier beam has, for example, been observed in the radiative-capture cross section measurements of Ref. [41], where the cross section was significantly higher compared to neutron emission. A theoretical work presented in Ref. [42] suggests that the angular momentum J_{CN} of the CN has little influence on the J of the fragments. However, there is no experimental measurements of PFGs where the CN was populated using two different reactions [2], so it is not known whether the PFG characteristics are perturbed by the use of a surrogate reaction.

The open question posted in Paper I is thus: will the difference in the initial angular momentum impact the emission on PFG emission? As we saw in Ch. 2, PFGs are emitted when a nucleus decays to get rid of excitation energy and angular momentum. Hence, if the angular momentum of the fission fragments are impacted by the change in CN angular momentum, this will be evident by looking at differences in the PFG characteristics. Therefore, the question regarding the similarities of the (d,pf) and (n,f) reactions are rooted in the main question of this thesis: how will the initial angular momentum of the CN affect those of the fission fragments? Or, rephrased: how is angular momentum propagated throughout the fission process?

[2] Ref. [40] was recently published, and provided data on the ^{239}Pu(n,f) reaction that can be compared to the ^{239}Pu(d,pf) results of Ref. [32]. However, Ref. [40] studied a very limited range in γ-ray energy, only detecting about 60% of the multiplicity. At the same time, Ref. [32] had challenges with prompt neutron contamination. Comparisons between the two are therefore difficult.

To investigate this question, and as a part of the work in this thesis, we proposed a new experiment at the Oslo Cyclotron Laboratory. Here, the same compound nucleus would be populated using two very different reactions to directly look for differences in the PFG emission. The $(p, p'\mathrm{f})$ and $(\alpha, \alpha'\mathrm{f})$ reactions were chosen, corresponding to the lightest and heaviest beam the Oslo cyclotron can accelerate. The large mass difference would achieve the highest possible contrast in CN angular momentum. It would also be the first time PFG characteristics were measured following these reactions. We planned to use a target of ^{239}Pu, which had been used previously in Ref. [32] with the (d, p) reaction. The optimal beam energies were determined by considering that the particles should be stopped in the particle detector and while at the same time achieving sufficient reaction rates, and were found to be 17 MeV protons and 32 MeV αs. The excitation energy of the fissioning nucleus would also be calculated event-by-event, and so both excitation energy and angular momentum propagation could be studied simultaneously. The measurements would be conducted back-to-back using the same experimental setup to avoid potential systematic errors originating in different experimental conditions.

Following the experience gained from the ^{240}Pu(d,pf) experiment in Paper I, several adjustments were also made to the experimental setup and data acquisition.

Firstly, improvements were made to the time-of-flight separation between neutrons and protons. In Paper I, the prompt time cut of ±3 ns was used to select PFGs, corresponding to $\pm 1 * \mathrm{FWHM}$ of the time resolution. This range is smaller than the recommended value in Ref. [23] of using $\pm 2.5 * \mathrm{FWHM}$ as the time gate to better enable comparisons between experiments with different time resolutions. To enable the use of the recommended time cut, the target-detector distance had to be larger to increase the arrival-time difference between the neutrons and γ rays in the $LaBr_3$ detectors. As a tradeoff between angular coverage and PFN discrimination, the target-detector distance was chosen to be 35 cm.

Since the experimental setup changed, the detector response function, used to correct the measured γ-ray spectrum for the detector response, was also expected to change. The changes to the experimental setup were therefore implemented in Geant4 such that the effect could be investigated. As it turns out, the impact on the response was minimal and the old response function could be used with an adjusted value for the geometric efficiency. The quality of the detector response function is demonstrated through the reproduction of the ^{252}Cf PFG spectrum in Fig. 3.2.

Lastly, the gas-filled fission fragment detector NIFF was rebuilt, as it was destroyed at the end of the ^{240}Pu(d,pf) experiment. Unfortunately, an error at the very beginning of the beam time led (again) to the destruction of this fragile fission detector, abruptly ending the experiment after 30 min of beam time. As the collection of sufficient statistics was calculated to take about 24h of beam time, this was too little data to analyze.

3.5 Future work

The question of angular momentum propagation in fission remains largely unexplored, and thus there is still a lot of interest for conducting an experiment comparing PFG characteristics from the $(p, p'\mathrm{f})$ and $(\alpha, \alpha'\mathrm{f})$ reactions. In collaboration with researchers at the Institute for Nuclear Research in Debrecen, Hungary, we are therefore working to integrate their newly patented fission fragment detectors [43] as a part of the OCL experimental setup. The experiment is scheduled for the fall of 2023, and the data set will be analyzed by M. Sc student H. Haug, whom I co-supervise.

Chapter 4

Angular momentum generation in fission

In Ch. 2 we said that the fission fragments are created with some excitation energy E_{x} and angular momentum J, and these initial conditions govern the subsequent neutron and γ-ray emission. We can understand that the fragments start with E_{x}, even in the case of spontaneous fission: the large, positive Q-value in fission results in an abundant supply of energy and some of this ends up as excitation energy. However, it was also discovered early that the fragments also have angular momentum [44], even when the CN has an initial angular momentum of $J_{\mathrm{CN}} = 0$. Even more puzzling, the average angular momentum was quite high as well, about $5 - 9\hbar$ on average [20, 44]. This raises the very intriguing question, which is central in this thesis: how can a system at rest produce two spinning fragments after splitting? Rather than angular momentum *propagation*, how is this angular momentum of the fission fragments *generated*?

There are a multitude of reasons why the question of angular momentum generation is relevant. We stated in Ch. 2 that γ-ray emission is expected to remove the majority of the angular momentum of the fission fragments. This forms a strong link between a fragment's J and emitted fission γ rays, and the study of these γ rays was already motivated in Ch. 3. Since the initial J heavily influences the γ emission, understanding the generation of J gives us a direct comprehension of what impacts the γ-ray emission. For example, rather than conducting separate measurements as in Ch. 3 to investigate the impact of fast-fission on PFG emission, this could be predicted if we had a representative model for J generation. Furthermore, J generation is a very curious quantum mechanical challenge, and by understanding the process microscopically, we evolve our understanding of the nuclear forces.

4.1 Overview of main points in literature

When the angular momenta of fission fragments were first investigated, different experimental techniques were used to study them. Two of these were γ-ray multiplicity studies (see e.g. Ref. [19]) and isomeric yield ratio (IYR) measurements (like in Ref. [45]). A higher initial angular momentum J will result in more γ rays being emitted from the fission fragments before reaching the ground state, and γ-ray multiplicity measurements are therefore indicative of J. However, it is not known precisely how much J each γ ray carries and therefore the method can only estimate J, and the result will be highly model dependent. Extracting the mass-dependent multiplicity also requires precise physical collimation to measure only the γ ray from one fragment rather than both.

IYR measurements determine the relative population frequency of long-lived excited states and carry information on the initial distribution of angular momentum states in the fragment. How IYRs are measured will be thoroughly presented in Ch. 5, but we can already comment that IYR measurements do not give a direct value for J. Instead, models must be employed to convert the IYR to a value for the average angular momentum $\bar{J}$. Moreover, not all fission fragments have isomeric states, and IYR measurements are therefore not a tool that can be universally applied.

When measuring the γ-ray multiplicity as a function of fragment mass, a sawtooth was observed [46] similar to the sawtooth known to exist in neutron multiplicity measurements. This indicated that the angular momentum of the fragments followed the same trend, and Ref. [19] suggested that the J of a fragment corresponded to the deformation of the initial fragment. However, over a decade later Ref. [47] presented experimental event-by-event data that did not show the sawtooth, and argued that the sawtooth was a consequence of the collimation method applied in the previous measurements. A comparison of the results in Refs. [46] and [47] is shown in Fig. 4.1.

The confusion on the existence of the J-sawtooth was further strengthened when no pattern was observed in J-values deduced from a range of IYR measurements [48], though a previous IYR measurement did observe it [49]. There was also no consensus in IYR studies regarding the impact of different fissioning systems: some observed differences with changing CN [50, 51], while one did not [45].

In the theoretical field, several mechanisms for angular momentum generations had been proposed, for example bending/wriggling of the nucleus [52] and Coulomb-driven angular momentum generation [44].

As seen from the works presented above, the available experimental data was inconsistent regarding the existence of the sawtooth. Therefore, it was also unclear what models for angular momentum generations should predict.

Despite the conflicting results regarding the J-sawtooth, important observations were

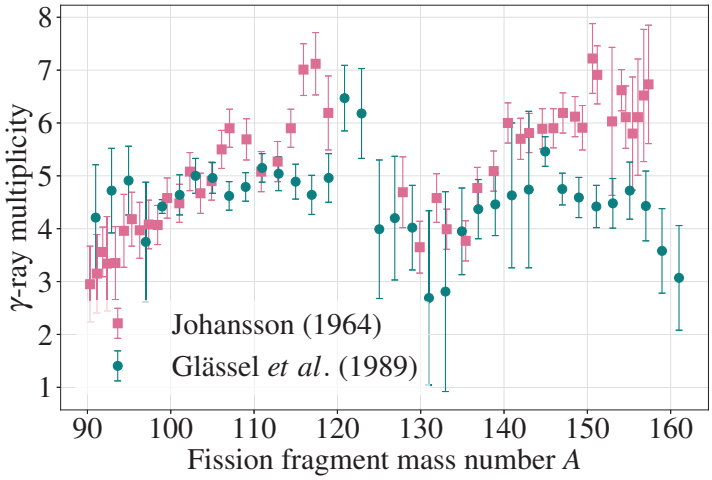

Figure 4.1: A sawtooth or not a sawtooth... The figure shows a comparison of the γ-ray multiplicity measurements presented in Johansson (1964) [46] and Glässel *et al.* (1989) [47], both measuring the γ-ray multiplicity as a function of fragment mass A following the spontaneous fission of ^{252}Cf.

made on the nature of angular momentum generation. In Ref. [53], J were deduced from IYR measurements along a chain of nuclei with odd and even atomic number Z and it was found that the unpaired proton gave a visible contribution to the J of the fragment. Furthermore, Ref. [54] simultaneously measured the IYR and kinetic energy KE of ^{132}Sn, and found them to be anti-correlated. Low KE-values are expected to emerge from deformed scission configurations. This is because when a nascent fragment is deformed, the distance to the center of charge in the partner fragment is large. The Coulomb repulsion between them is therefore weaker - resulting in a lower kinetic energy after scission. Since the KE was found to be anti-correlated with the IYR, this points to deformed fragments gaining more angular momentum, and this result is illustrated in Fig. 4.2. The suggestion of a deformation-driven angular momentum generation mechanism was also in agreement with the suggestions of Ref. [19].

4.2 Paper II: Angular momentum generation in nuclear fission

The three experiments forming the basis of the article were conducted during the ν-Ball campaign in Orsay, France in 2017/2018. Measurements were made of γ rays following the reactions ^{238}U(n,f) and ^{232}Th(n,f) at the average neutron energies $\bar{E}_n$ = 1.9 MeV

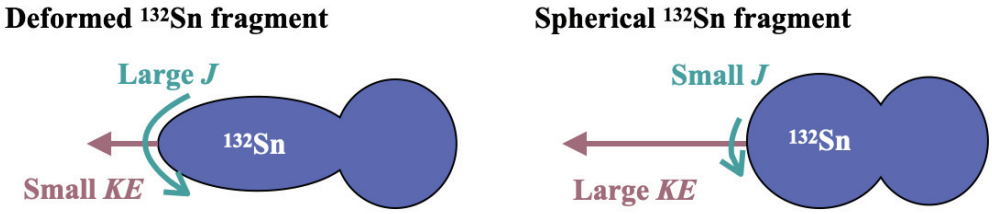

Figure 4.2: Illustration of the results presented in Ref. [54]. When ^{132}Sn is deformed, the distance to the partner fragment charges increases. The deformation therefore results in a smaller kinetic energy KE of the ^{132}Sn fragment following scission. Ref. [54] observes the KE to be anti-correlated with the isomeric yield ratio, which therefore suggests that deformed fragments emerge with higher angular momenta J.

and $\bar{E}_n = 2.0$ MeV, respectively, as well as the spontaneous fission of ^{252}Cf. A large array of 10 co-axial Ge detectors and 24 clover Ge-detectors were used to identify discrete transitions from fission fragments.

None of the questions on angular momentum generation presented above were the original objective for these experiments. Instead, fission was used as a reaction mechanism to populate nuclei of interest in nuclear structure studies. One goal was to measure the level scheme of ^{82}Ge, but there was a challenge: though the average angular momentum of fission fragments were quoted in literature to be about $7\hbar$ on average, levels in ^{82}Ge with an angular momentum above $6\hbar$ were weakly populated.

This triggered an investigation of the average angular momentum in different fission fragments, where the method presented in Ref. [55] was used to deduce the average J of the full mass range of fission fragments. The method uses the feeding intensities of known levels to determine the value of J when the de-excitation enters the known level scheme. As the method is based on the knowledge of the level scheme, the initial angular momentum J preceding neutron and statistical γ-ray emission is still shrouded. We will return to the question of angular momentum removal by neutrons in Ch. 4.3.

4.2.1 Summary of key results

Paper II deduced the average angular momentum of a range of fission fragments following the three reactions ^{238}U(n,f), ^{232}Th(n,f), and ^{252}Cf(sf). In all three reactions, the compound nucleus starts with zero or close to zero CN angular momentum J_{CN}, and thus the J of the fission fragments are almost purely generated through the fission process. The key results of Paper II are highlighted here.

The average angular momenta of fission fragments from all three systems form a sawtooth shape as a function of fragment mass number, see Fig. 1 of Paper II. This

sawtooth is observed to be universal, i.e. the average angular momentum $\bar{J}$ of a given fragment seems to be independent of the fissioning system that formed it. Furthermore, the heavy fragment has more angular momentum on average than the light fragment. The deduced average angular momentum values $\bar{J}$ were consistent with previous estimates in Ref. [20].

When studying the average angular momenta $\bar{J}_1$ and $\bar{J}_2$ of two partner fragments that emerge in the same reaction, no correlation was observed between their magnitudes. If the minimum observed J_1 of fragment 1 was increased, this had no impact on $\bar{J}_2$. This is visualised in the flat correlation trends in Fig. 2 of Paper II.

None of the available theoretical models were thought to be able to explain both the observation of an angular momentum sawtooth and the uncorrelated J magnitudes. The angular momentum generation was therefore explained microscopically by the statistical population of angular momentum states outside closed nuclear cores. Thus, the angular momentum-sawtooth (and consequently also the γ-ray multiplicity sawtooth) were thought to be connected, as they both originate from the sawtooth in excitation energy as a function of fragment mass. This will be further discussed in Ch. 6. The sawtooth also solved the mystery of the population of states in ^{82}Ge. Being close in mass to the double-magic nucleus ^{78}Ni, there are few nucleons outside the closed core that contribute to generating angular momentum.

4.3 Discussion

The work presented in Paper II generated scientific interest, both experimentally and theoretically. Experimentally, the existence of the γ-ray multiplicity sawtooth was confirmed in a separate measurement [56] shortly after Paper II was published. The reason for the lack of a sawtooth pattern in Ref. [47] was also explained.

For the theoretical models, the experimental results or Paper II provide benchmarks that must be reproduced in the predictions of the theories. The models must explain the origin of the sawtooth and why it is universal for a fission fragment no matter the original system, as well as why the average magnitudes $\bar{J}_1$ and $\bar{J}_2$ from a pair of fission fragments are observed to be uncorrelated and why the heavy fragment has a higher angular momentum than the light. I have included some of the theoretical works discussing the results of Paper II below.

Initially, we believed that some of the previous models for angular momentum generation were ruled out as they were not in agreement with the experimental observations. Following the publication of Paper II however, several theoretical works were published that explained how some of these mechanisms were still viable explanations. In Ref. [57] it was demonstrated that statistical population of bending/wriggling modes give values

for J_1 and J_2 that are observed uncorrelated in magnitude, even though they are highly correlated in direction. The sawtooth is explained to originate from the moment of inertia of the fragments, i.e. it is the deformation at scission that drives the J generation. If the shape of the fragment at scission is the same for all three fissioning systems, this also explains why the J seems to be system independent. Thus, statistical population of bending/wriggling modes could still be the mechanism that generates angular momentum in fragments.

The generation of angular momentum through Coulomb forces was in Paper II commented to be, if existent, a second-order effect as no dependence on J was observed on the charges $Z_1{}^*Z_2$ of fragments pairs. Later, Ref. [58] showed that the Coulomb mechanism for J generation is also highly dependent on the distance between the fragments and the angle between them. Therefore, the independence of the J's of partner fragments does not necessarily falsify the model of J generation through Coulomb repulsion. Furthermore, Ref. [58] comments that the $J(A)$-sawtooth may be explained by the deformation of the fragments. Again, this explains both the universal sawtooth and the uncorrelated J magnitudes.

In Ref. [59], the microscopic calculations of angular momentum generation were presented. They found that the shell structures of the fragments strongly influence the J generation. However, this leads to the prediction that the heavy fragment on average carries less angular momentum than the light fragment, which is opposite of what Paper II observed experimentally. Also, the $\bar{J}(A)$-pattern presented in their Fig. 1 is not quite the sharp sawtooth observed experimentally. It will be interesting to see if further microscopic studies manage better reproduction of the experimental data.

The angular momentum generation theories that incorporate fragment deformation at scission also explain the event-by-event decrease in J with higher fragment kinetic energy as observed in Ref. [54], as well as why even-even nuclei have less angular momentum than their odd neighbors [53].

There is also a study that doubts the connection between the sawtooth and initial fragment J [21]. As commented above, the method employed in Paper II to extract the angular momentum only determines J after statistical emission. The change in J during statistical emission was estimated from RAINIER in Paper II, but as Ref. [21] comments, it builds on the assumption that neutron emission does not significantly change the angular momentum of the fragment. Ref. [21] showed neutron emission may dissipate more J than assumed by the literature consensus, $> 1\ \hbar$ per neutron on average, and still reproduce the experimental results of Paper II. The result is that the J distribution after statistical emission will be distorted compared to the initial fragment angular momentum J. If this is accurate, then measurements of γ rays alone might not be enough to learn about the J of fission fragments. To our knowledge, there are currently no published works investigating the angular momentum removal by neutron emission, and this will

be further explored in Ch. 5.

4.4 Further work

With the new experimental results on the behaviour of fission fragment angular momentum, new benchmarks have emerged that models must reproduce. In Paper II, theories that did not seem to reproduce the experimental results were dismissed. The reality, however, is that the theories instead have adapted and evolved such that the experimental observations are reproduced. Therefore, more experimental investigations must be conducted to learn more about the behaviour of the angular momentum of the fission fragments.

As several of the methods for determining J rely on measuring γ rays, it is clear that the question of J removal by neutron emission needs to be answered. If the suggestions of Ref. [21] are true, then the J determined from IYR and γ-ray multiplicity measurements give little to no indication of the fragment's initial angular momentum.

We have discussed the correlation of the angular momentum magnitudes J_1 and J_2. A question that is currently being discussed is the direction of the $\vec{J}_1$ and $\vec{J}_2$ (the angular momentum *vectors*) with respect to the fission axis and each other. Here, different models predict different angular correlations, and more experimental data on this will therefore be useful when differentiation between different scission models [60]. One question is whether the $\vec{J}$s are exclusively perpendicular to the fission axis, i.e. the m quantum numbers are zero. Early studies indicate that the experimental data were consistent with perpendicular $\vec{J}$s [20, 61], however there are also experiments that show a significant deviation from $m = 0$ [62]. A new question is thus whether this deviation $m \neq 0$ exists, and if so, how this component is generated. The question of the directions and correlation of $\vec{J}_1$ and $\vec{J}_2$ are illustrated in Fig. 4.3.

Finally, there is the question about fragment-to-fragment variations in their angular momentum. Such individual variations may explain some of the deviation from the universal sawtooth of Paper II. We have already commented on the observed effect of single, unpaired particles on the J [53]. In Paper II, the angular momentum of a given fragment is observed to be independent of the fissioning system, however, system dependencies have previously been observed. For example, in Ref. [50] Sn isotopes were determined to have a higher angular momentum following the $^{\mathrm{nat}}$U(p,f) reaction compared to the ^{232}Th(p,f), while the opposite was true for Y isotopes. This indicates that there might be more to angular momentum generation rather than just a universal sawtooth. The angular momentum of specific fission fragments will be investigated in Ch. 5.

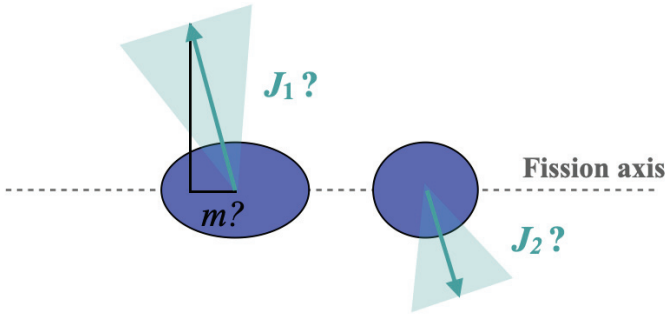

Figure 4.3: The figure illustrates the direction of the angular momentum vectors $\vec{J}_1$ and $\vec{J}_2$ of the two fragments. From the experimental work of Paper II, we have learned that the angular momentum magnitudes $\bar{J}_1$ and $\bar{J}_2$ of the two fragments are observed to be uncorrelated. However, questions remain of the directions of $\vec{J}_1$ and $\vec{J}_2$ - are they correlated in direction, and are they perpendicular to the fission axis (i.e. m quantum number equal to zero)?

Chapter 5

Isomeric yield ratios of fission fragments

One of the main experimental results presented in Ch. 4 was the universal angular momentum sawtooth: no matter the fissioning system, the angular momentum J of the fission fragments fell on the same pattern. At least this was the observation within the sensitivity of the method used to determine the angular momenta. However, we also commented that previous isomeric yield ratio (IYR) measurements had seen system-to-system variations in the generated angular momentum. In this chapter, we will therefore study the same data set as in Paper II , but with the complementary method of IYR measurements. We will both look at excitation energy propagation and angular momentum generation within the specific fragment of ^{134}Te, and scrutinize what impacts the J that this fragment is produced with. At the same time, we get a deeper understanding of the strengths and weaknesses of IYR measurements, as well as what fission parameters that impact the IYR of fission fragments.

5.1 The basis of isomeric yield ratio measurements

As the name implies, the method of studying isomeric yield ratios relies on the population of a long-lived state, and thus the method is confined to fragments that have isomeric states. Luckily, there are plenty of such fragments where the decay gets stuck in an excited state; about 150 fission fragments are known to have isomeric states, and many more are expected to exist [63]. Fragment yields and isomer half-lives limits which fragments can be studied experimentally. The idea of IYR measurements is to determine how often the isomeric state is populated compared to how often the decay bypasses this state. The excitation energy and angular momentum of the isomeric state are known, and the population frequency of the state is therefore indicative of the initial values of E_{x} and

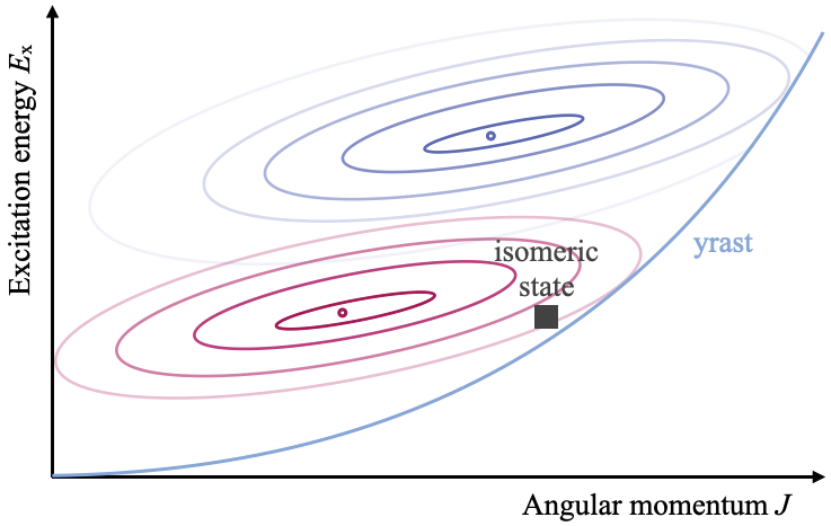

Figure 5.1: Illustration of the initial E_x vs J distribution that a fission fragment emerges with, and how these initial conditions affect the IYR of a fragment. The distribution of E_x and J to the right (blue) has a higher probability of populating the isomeric state than the one to the left (pink).

J that the fragment started with. This is illustrated in Fig. 5.1: depending on the initial distribution of E_x and J in the de-exciting fission fragment, the isomeric state has different probabilities of being populated. Thus, IYR measurements of fission fragments give information on the initial conditions of the fragment after it is created in fission. Note that the measured IYR depends on both the distribution of J in the primary nucleus as well as E_x distribution.

5.1.1 Techniques

Over the years, different methods have been developed to measure IYRs. Initially, the element of interest was first isolated through radiochemical methods before γ rays from the sample were measured (see Refs. [64, 65] and references therein). The radiochemical separation reduced the background of transitions from other fission fragments. Later, ion-guide isotope separators could be used to select the isotopes of interest before measuring γ rays from the decay (e.g. Ref. [49]). In recent years, a new principle of measurements was also demonstrated: instead of relying on γ-decay from the isomeric state, a Penning trap with good mass resolution could be used to separate the mass of the nuclei in the ground state from the slightly more massive nuclei in the isomeric state [50].

The different IYR measurement techniques have different challenges associated with

them. In all cases described above, the measurement is not done precisely at the moment of fission: there is some time in between the fragment production and when the decay is measured. For example, an isomer produced in fission might decay during the time it takes to conduct radiochemical separation, or during transport to the Penning trap. As long as the time between production and measurement is precisely known, this decay can be corrected for by applying the radioactive decay law, though it introduces an additional source of uncertainty to the measurement. The isomeric half-lives available to the different methods also depend on this transportation time between production and measurement. Only the longest-lived isomers can be investigated with radiochemical separation, and continually lower isomeric half-lives are reachable with the gradual decrease of transport time.

Another source of uncertainty in IYR measurement that was recently pointed out [63], is that some of the IYR measurement techniques need knowledge of γ-ray feeding probabilities in between discrete levels in the nucleus of interest. If the relative amount of discrete γ-ray transitions are used to determine the IYR, then it is necessary to know the branching ratios between the levels to calculate it.

Finally, contaminant production of the fragment through β decay might impact the IYR and thus also the J that we deduce from the IYR. When studying angular momentum of fission fragments, we are only interested in the J they gain throughout the fission process. However, if the technique has a significant transport time, there is a chance that the fragment of interest will be produced following β decay. As the isomer population ratio from β decay might be quite different compared to fission, this is a potential contaminator in the measurement. Depending on the fragment yield in fission and lifetime of the precursor nucleus, the amount of contamination might vary from negligible to notable, and it is thus important to be aware of this potential contamination. To correct for it, the yield of the precursor must be known along with its half-life and which levels in the daughter nucleus that will be populated following β decay.

5.1.2 Transforming from isomeric yield ratio to angular momentum

From the IYR measurement, we get a number that describes the probability of a given fragment being populated in this isomeric state following fission. The extracted IYR values for the same fragment can be directly compared in order to investigate for example how the IYR changes when using different fission reactions to create the fragment. We may learn even more about the angular momentum if we try to extract the initial angular momentum J from the IYR, and for this we need a model connecting the isomer population frequency to the initial values of E_{x} and J of the fission fragment.

A model that has frequently been used as the model to extract the J distribution

from the IYR, is the so-called Madland-England model presented in Ref. [66]. Other, similar models had also been suggested earlier, see for example Ref. [67]. In both cases, the angular momentum is thought to be a distribution on the form of Eq. 5.1 obtained from statistical theory [68, 69]:

$$P(J) \propto (2J+1)\exp\left\{-\frac{(J+0.5)^2}{B^2}\right\}, \tag{5.1}$$

where B governs the spread of the angular momentum distribution. In the Madland-England model, the value of the IYR is assumed to mainly depend on the angular momentum differences of the states in the γ-ray cascade, as well as the J quantum number of the ground state and isomeric state. In Ref. [66], they fit their model to experimental data to find a universal value for B, and use this to predict expected IYR values for a range of fragments. In this model, the de-excitation pattern has been heavily simplified and solely depends on whether the initial J of the nucleus is closest to the one of the ground state or isomeric state. The procedure can also be conducted in reverse, where the measured IYR value is used to deduce the B of the angular momentum distribution in Eq. 5.1. However, it has been commented that the Madland-England model is too simple. Ref. [63] showed that the Madland-England model works well for predicting IYRs of nuclei in the heavy-mass region to which it was fitted, however does not reproduce data for light fission fragments. The extraction of the $\bar{J}$ using this model assumes both that the spin distribution has the shape described in Eq. 5.1, which may not always be representative. Furthermore, as Ref. [66] themselves comments, the de-excitation pattern is heavily simplified. The use of such a basic model to extract the angular momentum of fission fragments in the experimental results presented in Refs. [48, 63] could explain why no sawtooth shape was observed in $\bar{J}(A)$.

A significantly more refined method of extracting the J distribution from IYR measurements is to use the Hauser-Feshbach decay code TALYS [1] in combination with a fission simulation code. In Ref. [70], a method for this was developed where TALYS de-excited the fission fragment according to initial conditions given GEF (GEneral model of Fission). By varying the initial conditions, it is possible to determine the relation between the IYR and the average J it corresponds to. As this method both uses a more sophisticated decay model as well as considers the level scheme of individual nuclei and its initial conditions, this method is expected to yield more accurate values for J.

[1] Ref. [66] actually comments that the best way to calculate IYRs would be to preform statistical cascade calculations - but the nuclear data needed for such a calculation was not available at the time. Now, over forty years later, we have this option.

5.2 Overview of main points in literature

We have already discussed some of the relevant published works on IYR, but we will here present them systematically and point out some key aspects of interest.

Some of the published works on IYRs investigate how changes in the fissioning system, like e.g the mass and energy of the fissioning nucleus, impacts the determined IYR of a fragment. One example is to study the change in the IYR of a given fragment when changing the fissioning system, similar to what was done in Paper II for the average angular momentum. A recent example of this that we have mentioned earlier, is presented in Ref. [50] where the yield of Sn and Y isotopes were extracted following the reactions $^{\mathrm{nat}}$U(n,f) and ^{232}Th(n,f). Here, it was found that the IYR was higher for Sn in $^{\mathrm{nat}}$U(n,f), while the opposite was true for Y. On the other hand, both Refs.[45, 71] found the IYR of different Sn, Sb, Te and I fragments to be independent of whether it was produced in ^{235}U(γ,f) or ^{238}U(γ,f), which also is in agreement with the conclusion drawn in the recent review of available IYR measurements [63].

Seemingly inconsistent results also emerge when studying the impact of the energy of the CN on the IYR. Ref. [63] concludes that no change is seen when comparing IYRs from thermal or fast fission, however other studies have found such CN E_{x} dependencies [71, 72]. Here, the span of different excitation energy studies might explain the contradiction, as Ref. [63] considered a much narrower energy difference compared to the other studies.

The impact of the fission configuration on the IYR has also been investigated. We have already mentioned Ref. [54], where the IYR of ^{132}Sn was anti-correlated with the kinetic energy of the fragment, which was interpreted as increased fragment deformation resulting in more angular momentum being generated in that fragment.

All the studies presented above have compared the IYR of a single fragment from different fission reactions and configurations. It is also possible to look for systematic effects in between different fission fragments by comparing the IYRs from different fragments. This is more challenging because the IYR values are not directly comparable, as it depends on the angular momentum quantum number of the isomeric state as well as where in the level scheme the isomeric state is found. It is therefore necessary to use a method like the ones presented in Ch. 5.1.2 to transform from IYR to J, which can make the comparison less clear. Nevertheless, structural dependencies have been observed through IYR measurements, like the contribution of single particles to the angular momentum which results in odd-even staggering [53, 73], as well as the correlation between fragment quadrupole moment and angular momentum [20, 53, 73].

We point out here that some of the angular-momentum sensitive studies extract the average angular momentum of the fission fragment $\bar{J}$, as done in Paper II, while other uses the root-mean-square J_{rms}. As has been shown before [20], these quantities are not equivalent, and there is no way of transforming in between them without having the full

data set. We therefore need to be careful when comparing to earlier results to ensure that we are, in fact, using the same variable for the measurement.

5.3 Paper III: What impacts the isomeric yield ratios of fission fragments?

The experimental data analysed in this work is the same as the one presented in Paper II, collected during the ν-Ball experimental campaign. Using this data, a new technique for measuring isomeric yield ratios was developed, and it is based on measuring the time-dependence of the emitted γ rays from the fission fragments. This measurement was possible due to the large number of Ge-detectors in the experimental setup. Rather than conducting the procedure of transportation and measurement of previous techniques, this new method measure the γ rays from the instance the fission fragments are produced. We study the time-dependent emission of γ rays that lie below the isomer in the level scheme. These γ ray may either be emitted either when the decay bypasses the isomeric state or following the decay of the isomer, which results in the time-of-arrival spectrum taking the shape illustrated in Fig. 5.2. The shape of this spectrum will include an (approximately) Gaussian component representing instances where the decay bypassed the isomeric state, as well as an exponential decay curve from when the γ rays are emitted following the decay of the isomer. By determining the respective integrals of the two components, the isomeric yield ratio can be determined. Furthermore, if both fission fragments are stopped immediately after fission, we can also determine the properties of the partner nucleus that the fragment emerged with, enabling the extraction of the IYR dependent on partner properties. This is a unique feature, which opens a lot of interesting opportunities for studying more aspects of what impacts the angular momentum of the fission fragment.

We study the same experimental data as in Paper II, but with another method. This is advantageous because there are no systematic differences in the experimental conditions, and new aspects may be revealed due to differences in sensitivity of the two methods.

5.3.1 Summary of key results

In Paper III, the new IYR measurement technique is presented and demonstrated on the fission fragment ^{134}Te, where the IYR is extracted for the first time. Furthermore, we combined the fission simulation code FREYA and TALYS in order to extract the average angular momentum of ^{134}Te. Some key results are summarised below.

The isomeric yield ratio of ^{134}Te is extracted from the three fissioning systems ^{238}U(n,f), ^{232}Th(n,f), and ^{252}Cf(sf). There might be a slope of the IYR with increasing mass number, but for the current measurement this slope is on the verge of statistical insignificance on a 2σ interval.

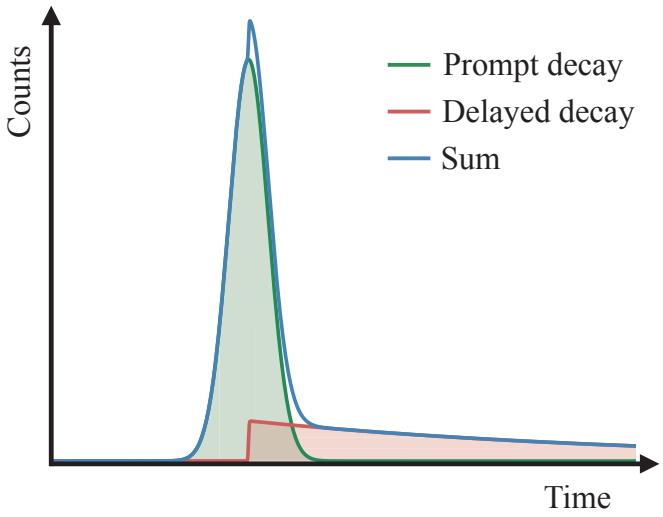

Figure 5.2: Illustration of the shape of the time-of-arrival spectrum of the new method. A prompt Gaussian component (green) represents the fragment decays that bypass the isomeric state, while the delayed exponential component (red) represents the portion of the decay that populates the isomer. The sum of the two is the shape of the double-gated time spectrum.

The IYR extracted for ^{238}U(n,f) at two different average neutron energies $\bar{E}_n$ = 1.9 and $\bar{E}_n$ = 3.4 are the same within the uncertainties.

When extracting the IYR of ^{134}Te as a function of the number of prompt neutrons emitted from the combined system, we find no significant change in the IYR value. On the other hand, when studying the IYR dependence on the minimum angular momentum of the partner nucleus, contradicting results are observed.

FREYA+TALYS simulation enables the extraction of the average angular momentum $\bar{J}$ from the IYR, and we find that the average angular momentum of ^{134}Te following ^{238}U(n,f) at $\bar{E}_n$ = 1.9 MeV is 6$\hbar$. The sensitivity of the IYR measurement on the J is discussed. We also point out the impact of isomer population saturation at high J, where the IYR is no longer sensitive to changes in the angular momentum distribution of the fragment.

5.4 Discussion

Paper III was not published at the point when this thesis was submitted, and no new developments can therefore be presented. This section presents some more ideas and

discussions of this topic.

A main point of interest for those who perform IYR measurements is to reconcile the contradicting observations with regards to the behaviour of the IYR dependence on the fissioning system. Though the review of historical data in Ref. [63] commented that they saw no system dependence (which was in agreement with Paper II), some of these measurements have rather high uncertainties and are therefore correspondingly insensitive to small changes in the system. In our new results of Paper III, there is an indication of either an independence or small positive slope with the mass number of the fissioning system. However, this positive slope is not universal. As we have commented before, some angular momentum studies find a dependency on the fissioning system [50], while others do not [45, 63, 71]. Opposing trends are also seen for the IYR dependence on excitation energy [63, 71, 72]. Of course, these potential conflicts might be caused by differences in experimental setup, IYR sensitivity, or how different the systems are that they compare. However, it is also a possibility that these contradicting results originate from actual structural dependencies and differences in the individual fragments. The experimental results of a "universal sawtooth" in Paper II allows for some such deviations: as seen by the curves in Fig. 1 of Paper II, there are some fragments that deviate from the trend. It is therefore interesting to speculate where these differences might come from.

A reason for fragment-to-fragment differences might come from the IYR saturation effect. As discussed in Paper III and shown in Fig. 7 of Paper II, there are some regions of J where a given isomer is highly sensitive to changes in the distribution, and other regions where the IYR is saturated and even large changes in J will not affect the IYR. This might explain why some fragments have different IYRs for different fissioning systems, while others do not. If the isomer is in the sensitive region, then small changes in the fragment's initial condition might impact the IYR. Other fragments that are saturated will not see any such change.

We described in Ch. 5.1.1 the possible contamination of β decay in experimental results where there is a significant time between the fission reaction and the measurement. If the contamination is large and the measured IYR is used to extract J, then this can lead to the J being significantly wrong. This contamination is also dependent on the properties of the precursor nucleus, and thus might impact various fragments differently. The result could be that the trends of the J are distorted, like for example when looking for a sawtooth pattern as was done in Refs. [48, 49].

When using TALYS or a similar decay code to extract J from the IYR, then knowledge of the level scheme in the nucleus is needed. Ref. [74] demonstrated the impact of the lack of level scheme knowledge when determining J. If lacking, this might cause significant perturbations in the determined J.

It would be curious to investigate further if any of the above-mentioned challenges might explain the contradictions in IYR measurements when it comes to J-trends as well

as the impact of perturbing the fissioning system.

When presenting the simple model for fission fragment de-excitation in Ch. 2, it was commented that neutron emission was expected to remove negligible amounts of angular momentum from fission fragments, despite there being no experimental confirmation of this assumption. In Ch. 4, we showed how this lack of experimental evidence opened up for Ref. [21] to argue that there is a possibility that the neutrons carry significantly more angular momentum than previously assumed, and that this leads to the initial fragment angular momentum being decoupled from the angular momenta we determine using techniques like the ones presented in Papers II and III. However, the neutron multiplicity gating technique presented in Paper III is a direct determination of the impact of neutron emission on the angular momentum of fission fragments, and is as far as we know the first of its kind. It may therefore be used to determine the amount of angular momentum removed by prompt neutron emission. Though the neutron-emission dependent IYR measurements in Paper III show no dependence on neutron multiplicity, the measurements has significant uncertainties. The measurements may therefore not be sensitive to the difference in angular momentum ΔJ carried away by neutron emission. By conducting measurements with increased statistics, upper bounds for J removal by neutron emission can be established, which will be the goal of future work.

5.5 Future work

The new technique for measuring IYRs open exciting possibilities for further studies, both when it comes to investigating isomeric states with shorter half-lives as well as further exploring the partner gating technique. A new and higher-statistics data set was recently collected during the νBall-2 experimental campaign. The increased statistics will be used to extract new IYRs of lower-populated fission fragments, especially in the light fragment region where fewer isomers have been measured. Furthermore, this allows for the neutron multiplicity-dependent IYR extraction for more fragments, and will be used to constrain the angular momentum removal though neutron emission.

Chapter 6

What have we learned?

In this thesis, several new works on excitation energy and angular momentum effects in fission have been discussed. Here we will summarize the findings and discuss the broader understanding they give us of the nuclear fission process.

6.1 Summary of results

In Paper I, we showed that when increasing the E_{x} of the fissioning nucleus, this only had a minor impact on the total number and energy of the γ rays that were emitted in fission. This points to the added energy being distributed somewhere else. The generation of angular momentum was the main topic of Paper II, and results were presented that showed how the average angular momenta of fission fragments all fall on a sawtooth curve which is independent of the fissioning system. Based on this, it was suggested that angular momentum is generated statistically, and thus closely linked to the excitation energy of the nascent fragment. It was also shown that the angular momenta of partner fragments were uncorrelated in magnitude, an observation that helps constrain physical models for angular momentum generation in fission. Finally, Paper III dived into the isomeric yield ratio of the fission fragment ^{134}Te and investigated how changes in the fissioning system impacted the measured IYR. The IYR was observed to potentially exhibit a positive slope with mass number of the fissioning system, contrary to the results of Paper II, however, the slope was statistically insignificant. No statistically significant change was found when increasing the neutron energy that induced the fission or when studying the impact of increased neutron multiplicity. Now let us look at how these experimental results fit together in a broader picture.

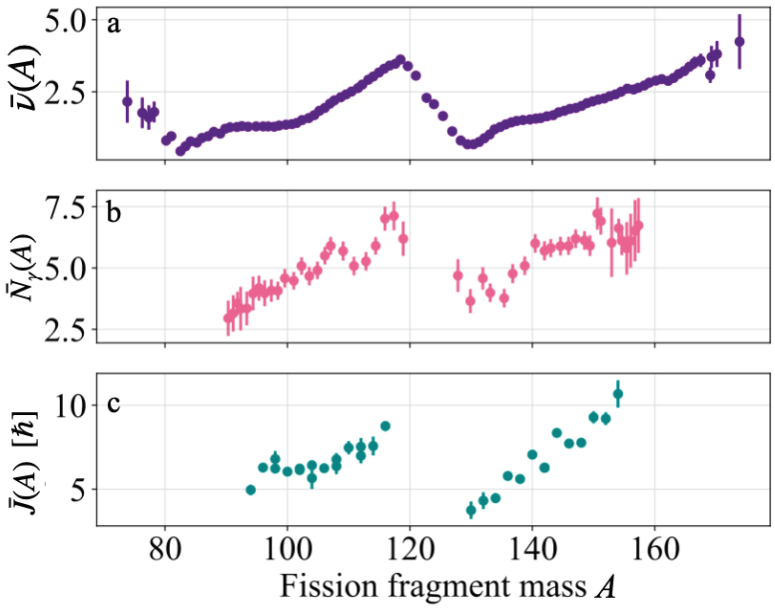

Figure 6.1: Sawtooth patterns observed in various observables as a function of fragment mass following ^{252}Cf(sf). In (a) the average neutron multiplicity $\bar{\nu}(A)$ from Göök *et al.* [17] is plotted, (b) shows the average γ-ray multiplicity $\bar{N}_\gamma(A)$ from Johansson [46], and (c) is the average angular momentum $\bar{J}(A)$ from Paper II.

6.2 Sawtooth patterns in fission

In this thesis, we have encountered quite a few different sawtooth patterns. In addition to the well-known sawtooth in the average neutron multiplicity $\bar{\nu}$ as a function of fragment mass A (see e.g Ref. [17] and references therein), Ch. 4 presented both historical results on the average γ-ray multiplicity $\bar{N}_\gamma(A)$ sawtooth as well as a sawtooth in average angular momentum $\bar{J}(A)$. Three experimental sawtooth patterns have therefore been observed as shown in Fig. 6.1, and this raises the intriguing question of how they might be connected.

To find the connection between $\bar{N}_\gamma(A)$, $\bar{J}(A)$, and $\bar{\nu}(A)$, we first comment that the number of neutrons emitted by a fragment is highly indicative of the fragment's excitation energy E_x. As illustrated in Fig. 2.2 neutrons remove a lot of E_x from the fragment as each neutron carries off the energy sum of the neutron separation energy and its kinetic energy. Therefore, it is expected that the curve $E_\mathrm{x}(A)$ follows the same sawtooth pattern as $\bar{\nu}(A)$. If the suggestions of excitation-energy driven angular momentum generation in Paper II are representative, then all the experimentally observed sawtooth patterns in Fig. 6.1 may be explained as follows.

The fragments emerge with some E_{x} that varies with A and fall on a sawtooth pattern. If the J-generation is statistically generated based on the E_{x}, then this also creates a sawtooth pattern for $\bar{J}(A)$. The primary fragment then de-excites, and the more E_{x} it started with, the more neutrons are emitted, giving a sawtooth in $\bar{\nu}(A)$. As explained in Ch. 2 and shown in Fig. 2.2, the J results in a fraction of the E_{x} being bound up in rotational energy E_{rot}. As emission of γ rays is the main way to dissipate E_{rot} from a fission fragment, a higher initial angular momentum will lead to an increased γ-ray multiplicity. A sawtooth in $\bar{J}(A)$ thus gives a sawtooth in $\bar{N}_{\gamma}(A)$. The $\bar{N}_{\gamma}(A)$, $\bar{J}(A)$, and $\bar{\nu}(A)$ sawtooth patterns can thus all be thought to originate from the $E_{\mathrm{x}}(A)$ sawtooth.

All the observed sawtooth patterns in Fig. 6.1 might thus be explained by a sawtooth in E_{x}. This potential link between the excitation energy and angular momentum sawtooth patterns thus forms a connection between the two topics of this thesis: the excitation-energy *propagation* might have a significant impact on the angular momentum *generation*.

It has also been suggested that the shape of $\bar{J}(A)$ can be explained by a combination of the shape of $E_{\mathrm{x}}(A)$ in addition to shell structures in the level densities of the fragments [75]. Another explanation for the J sawtooth is that the moments of inertia of the fragments at scission follow a sawtooth shape due to shell and deformation effects [57].

6.3 Excitation energy dependence

Moving on to the study of excitation energy propagation in fission, we have found that increasing the E_{x} of the compound nucleus only barely has an impact on γ-ray emission. This was found both in Paper I when studying PFG characteristics as well as in Paper III, when looking for changes in IYRs of ^{134}Te. The observation suggests that adding excitation energy to the CN only weakly impacts the γ-ray emission from the fission fragments and that the energy is mainly diverted elsewhere.

As discussed above, Paper II suggests that the generation of angular momentum is driven by the excitation energy available in the nascent fragments. As we found minimal to no changes in the PFG emission as well as the IYR of ^{134}Te as a function of compound nucleus E_{x}, this seems to indicate that the excitation energy of the fragments remain largely the same when the CN E_{x} increases. On the other hand, however, it is known that the neutron multiplicity increases with higher CN E_{x} [9, pg. 525]. As presented above, a higher neutron multiplicity indicates a higher excitation energy in the nascent fragment. This seems to suggest that if the J-generation is E_{x}-dependent, then we should see changes in the IYR and γ-ray emission - when we do not. At first glance, this seems to be at odds with the suggestion in Paper II that the angular momenta of the fragments are determined from the excitation energy.

This discrepancy may be resolved when taking into account that we only studied the

IYR of one specific fragment over a rather narrow energy range. Other studies of different fragments have found changes in the IYR with large increases CN E_{x}, see e.g. Ref. [72] and references therein. It could therefore be that we study a too small change in the E_{x} to observe the effect. Another explanation might be that the effect varies on a fragment-to-fragment basis. As the various fragments start with different amounts of excitation energy, it could e.g. be that the added CN E_{x} is distributed unevenly between the fragments. If so, it would explain why some fragments exhibit an increase in IYR with energy while others do not. This might also fit with the trend observed in Paper I: even though the PFG multiplicity slope is small with increased CN E_{x}, it is statistically significant. If the energy increase affected fragments differently, resulting in some fragments being created with larger J while others are unperturbed, this could in sum result in the weak but present increase in PFG multiplicity with CN E_{x} observed in Paper I.

A new aspect of E_{x}-dependent angular momentum generation has recently been observed. Ref. [76] measured the correlation between the E_{x} and γ-ray multiplicity $\bar{N}_{\gamma}$ of different fragments, and found that the $\bar{N}_{\gamma}$ first increased with E_{x} until a given point after which it did not increase any further. Due to the strong connection between $\bar{N}_{\gamma}$ and J, it was interpreted that the J first increases with E_{x} until it reaches a saturation point. After the saturation point, a further increase in E_{x} does not result in an increased J. They also found that some fission fragments emerge saturated, while others do not. This behaviour might therefore be one example of an effect that varies on a fragment-to-fragment-basis, and that could result in some IYRs being energy-dependent while others are not. It will be very interesting to follow the development of this topic.

6.4 Dependence on fissioning system

Paper II commented on the system-independent generation of angular momentum: no matter what the mass of the fissioning system was, the angular momentum of a given fragment seemed to be largely the same. Yet, the experimental results left some room for differences, and in Chs. 4 and 5 we discussed experimental results in the literature where the fissioning system was seen to both impact or not impact the J of fission fragments. The reason for this contradiction might be found in the sensitivity of the different studies: some studies, like Paper III, scrutinize small effects on specific fragments, while other studies, like Paper II, look at general trends across the whole fission fragment mass range. We have also in Ch. 5 presented thoughts on what may impact the sensitivity of IYR studies, and thus might lead to conflicting results.

At first glance, a system-independent J generation seems to be at odds with prompt neutron-measurements from the fission of ^{252}Cf(sf). It is known that this reaction emits in total more neutrons compared to the other reactions studied in Paper II. Where ^{252}Cf(sf) releases ≈ 3.76 per fission [77], less than 2.3 neutrons are released following ^{232}Th(n,f) at E_n = 2.0 [78] and the multiplicity is ≈ 2.6 for ^{238}U(n,f) at E_n = 1.9 [79]. If higher neu-

tron multiplicity reflects the E_x of fragments and the angular momentum is E_x-driven, how can this be reconciled with the system independence of Paper II? This can be explained by looking at the fission fragment mass distribution, which changes when the mass of the fissioning system changes. Though the J of a specific fragment A is about the same for all systems (see Fig. 1 in Paper II), the spontaneous fission of ^{252}Cf produces on average heavier fragments which in turn emit more neutrons. A specific fragment thus emerges with about the same angular momentum no matter the fissioning system, while the changing fission fragment mass distribution leads to a higher average angular momentum among the fragments. This can be seen in Fig. 4 of Paper II.

6.5 Final thoughts

So far we have discussed the experimental results in light of excitation-energy driven angular momentum generation presented in Paper II. However, we also pointed out in Ch. 4 that it has been suggested that it is the fragment deformation - and not excitation energy - that drives the angular momentum generation. Deformation-driven angular momentum can explain why the J is anti-correlated with the kinetic energy of a fragment and positively correlated with the fragment's quadrupole moment at scission. Yet, these two explanations might also be connected. We commented above that the sawtooth shape in angular momentum generation has both been interpreted as originating from the sawtooth in excitation energy as well as the moment of inertia of the fragments. In the statistical model described in Paper II, the sawtooth is related to the number of nucleons outside a closed, double-magic core. At the same time, fragments with more nucleons outside a closed core are also generally more deformed than fragments close to shell closures. The question of whether it is the deformation or excitation energy that drives the J generation might be closely related. By studying the fragment-to-fragment effects, we can learn more about the details of angular momentum generation in fission and understand the precise fragment properties that governs the J it ends up with.

A question that has been left open by this thesis [1] is how angular momentum of the CN is propagated through the fission process. We have in Paper II looked at cases where the compound nucleus starts with minimal angular momentum, but what happens if the CN is already rotating? Angular momentum conservation tells us this must go somewhere, but what will this look like experimentally? Will it impact both fragments equally, or will one fragment get a disproportional share of the J_{CN}? No matter what answers are found to these questions, it will bring a deeper understanding of the mechanisms at play in the fission process.

[1] This question is not left untouched by choice, but rather due to the unfortunate aspect of experimental physics that no matter how much work you put into an experiment, it will sometimes fail miserably.

Paper I

Excitation energy dependence of prompt fission γ-ray emission from ^{241}Pu*

Excitation energy dependence of prompt fission γ-ray emission from ^{241}Pu*

D. Gjestvang,[1,*] S. Siem,[1,†] F. Zeiser,[1] J. Randrup,[2] R. Vogt,[3,4] J. N. Wilson,[5] F. Bello-Garrote,[1] L. A. Bernstein,[2,6] D. L. Bleuel,[3] M. Guttormsen,[1] A. Görgen,[1] A. C. Larsen,[1] K. L. Malatji,[7,8] E. F. Matthews,[6] A. Oberstedt,[9] S. Oberstedt,[10] T. Tornyi,[11] G. M. Tveten,[1,‡] and A. S. Voyles[6]

[1]*Department of Physics, University of Oslo, N-0316 Oslo, Norway*
[2]*Nuclear Science Division, Lawrence Berkeley National Laboratory, Berkeley, California 94720, USA*
[3]*Nuclear and Chemical Sciences Division, Lawrence Livermore National Laboratory, Livermore, California 94551, USA*
[4]*Physics and Astronomy Department, University of California, Davis, California 95616, USA*
[5]*Université Paris-Saclay, CNRS/IN2P3, IJCLab, 91405 Orsay, France*
[6]*Nuclear Engineering Department, University of California, Berkeley, California 94720, USA*
[7]*Department of Subatomic Physics, iThemba LABS, P.O. Box 722, Somerset West 7129, South Africa*
[8]*Physics Department, Stellenbosch University, Matieland 7602, South Africa*
[9]*Extreme Light Infrastructure-Nuclear Physics (ELI-NP), Horia Hulubei National Institute for Physics and Nuclear Engineering (IFIN-HH), 077125 Bucharest-Magurele, Romania*
[10]*European Commission, Joint Research Centre, Directorate G for Nuclear Safety and Security, Unit G.2, 2440 Geel, Belgium*
[11]*Institute for Nuclear Research (Atomki), 4026 Debrecen, Hungary*

(Received 23 December 2020; accepted 16 February 2021; published 15 March 2021)

Prompt fission γ rays (PFGs) resulting from the ^{240}Pu(d,pf) reaction have been measured as a function of fissioning nucleus excitation energy E_x at the Oslo Cyclotron Laboratory. We study the average total PFG multiplicity per fission, the average total PFG energy released per fission, and the average PFG energy. No significant changes in these characteristics are observed over the range $5.75 < E_x < 8.25$ MeV. The physical implications of this result are discussed. The experimental results are compared to simulations conducted using the computational fission model FREYA. We find that FREYA reproduces the experimental PFG characteristics within 8% deviation across the E_x range studied. Previous excitation energy-dependent PFG measurements conducted below the second-chance fission threshold have large uncertainties, but are generally in agreement with our results within a 2σ confidence interval. However, both a published parametrization of the PFG energy dependence and the most recent PFG evaluation included in ENDF/B-VIII.0 were found to poorly describe the PFG excitation-energy dependence observed in this and previous experiments.

DOI: 10.1103/PhysRevC.103.034609

I. INTRODUCTION

Eighty years have passed since the discovery of nuclear fission [1,2] and yet important aspects of fission remain to be understood. Computational models aiming to describe fission rely on experimental data to benchmark their calculations. Therefore, precision measurements of fission fragments, neutrons, and γ rays, and the correlations between them, are vital to test the current understanding of how fission proceeds.

Following the revived interest in fission, originating from its role in the nucleosynthesis of heavy elements [3] and the development of Generation-IV reactor concepts [4], studies are broadened to include hitherto unexplored details of nuclear fission. Prompt fission γ rays (PFGs), emitted in the final stages of fragment deexcitation, were first measured in the 1970s for selected actinides [5,6] and were found to carry only a small fraction of the total energy release. They were thus long considered to be of little importance for understanding the fission process. However, PFGs carry the majority of the angular momentum generated in fission [7] and are therefore essential for understanding the state of the fragments just after scission. Furthermore, PFGs can deposit energy far away from where they are emitted, creating potential heating challenges in nuclear reactors [4]. Therefore, experiments measuring PFG characteristics for new fissioning systems and energy regions have been conducted [8–10], and progress has been made in accurate modeling PFG emission [11–14].

A key question, essential for reactor applications and basic fundamental physics, is how the prompt γ-ray emission in fission is affected when the excitation energy E_x of the fissioning system increases. Currently, only limited experimental data exist where the PFGs have been extracted for more than one E_x [8,15–19]. Here we present measurements of the PFG characteristics from the ^{240}Pu(d,pf) reaction, extracted over a range of ^{241}Pu* excitation energies. The characteristics investigated are the average total γ-ray energy emitted per fission, $\overline{E}_{\gamma,\mathrm{tot}}$, average total γ-ray multiplicity per fis-

*dorthea.gjestvang@fys.uio.no
†sunniva.siem@fys.uio.no
‡Present address: Expert Analytics AS, N-0160 Oslo, Norway.

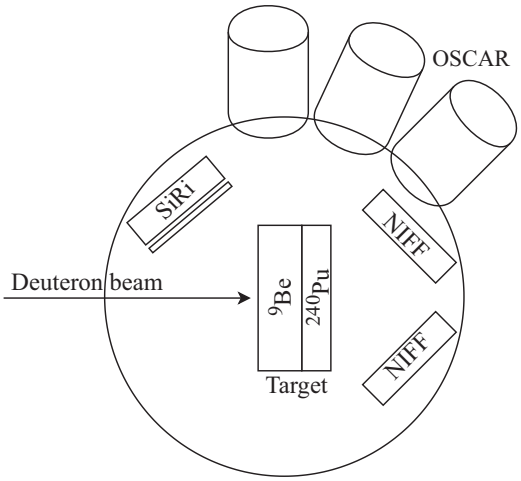

FIG. 1. Experimental setup for detecting PFGs from the ^{240}Pu(d,pf) reaction. Although only three $LaBr_3$ detectors are depicted, 28 were used in the experiment. Two of the four NIFF counters are illustrated. The figure is not to scale.

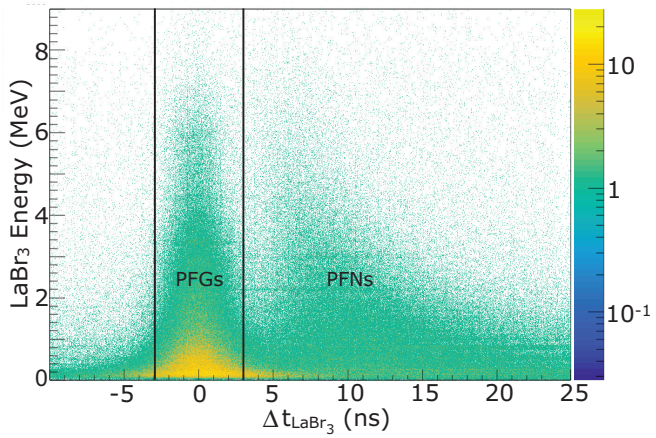

FIG. 2. Fission-gated spectrum showing the time difference Δt_{LaBr_3} between a proton in the ΔE detector and γ rays in OSCAR, plotted against the γ-ray energy detected by the $LaBr_3$. The time gates used to distinguish PFGs from PFNs via ToF are shown in black.

sion, $\overline{M}_\gamma$, and average γ-ray energy, $\overline{\varepsilon}_\gamma$. By studying how these quantities change with E_x, we investigate how increased excitation energy impacts γ-ray emission from the fission fragments. Furthermore, the measurements are compared to predictions made by the fission model FREYA (Fission Reaction Event Yield Algorithm), which simulates fission events where energy as well as linear and angular momentum are conserved [20]. This comparison between simulation and experiment is a benchmark of the current understanding of γ-ray emission in fission, and is expected to provide new insight into the fission process [21].

II. EXPERIMENT AND DATA ANALYSIS

The experiment presented in this paper was performed in April 2018 at the Oslo Cyclotron Laboratory (OCL). The experimental setup is illustrated in Fig. 1. A target of $\approx$0.4 mg/cm^2 thick ^{240}Pu on a fronting of 2.3 mg/cm^2 ^{9}Be, produced as described in Ref. [22], was bombarded with a beam of 13.5 MeV deuterons. The outgoing protons from the (d,pf) reaction were detected by SiRi, a silicon ΔE-E detector consisting of eight 1550 μm thick E pads each fronted with eight 130 μm thick ΔE strips [23]. SiRi was placed 5 cm away from the target, covering the angles 126°–140° with respect to the beam axis. By analyzing the energy and emission angle of the outgoing protons, the excitation energy of the compound nuclei (CN) ^{241}Pu* could be reconstructed [24].

To distinguish fission events from other reaction channels, fission fragments were detected using NIFF (Nuclear Instrument for Fission Fragments), consisting of four parallel plate avalanche counters (PPACs) [25]. NIFF is assembled in a lamp-shade geometry where each counter is placed at an angle of 45° with respect to the beam axis. The distance from the detector to the center of the target is about 5 cm, and an aperture in the center allows the beam to pass through. NIFF does not give a signal for light ejectiles such as ^{4}He and has no mass resolution, but provides high efficiency as only one of the fragments needs to be detected to tag a fission event.

The reaction chamber, containing the target, SiRi, and NIFF, was surrounded by the Oslo Scintillator Array (OSCAR). OSCAR consists of 30 new $LaBr_3$:Ce scintillator detectors used for photon detection. Each detector crystal is cylindrical and measures 3.5 in× 8 in (diameter × length) [26]. In this experiment, 28 of the 30 detectors were operational. $LaBr_3$ detectors are known for balancing good energy resolution with a fast decay time and are therefore well suited for coincidence experiments like PFG measurements. In the experiment, 27 of OSCAR's detectors were situated at a 20 cm distance from the target, while one was pulled back to 40 cm. The present work is the first use of OSCAR for PFG detection.

In this experiment, the data acquisition system was set to capture all events where the fission fragments and γ rays arrived within a $\pm$1.5 μs time interval relative to the detection of a proton. Details of the data acquisition will follow in Ref. [27]. In order to extract prompt fission γ rays, coincidence between a proton, a fission fragment, and a γ ray was required. These events are obtained by applying prompt time gates in the time-of-flight (ToF) spectrum. The fission-gated ToF spectrum for detected $LaBr_3$ energies is shown in Fig. 2, where Δt_{LaBr_3} is the time difference between the arrival of a proton in the ΔE detector and the arrival of a γ ray in OSCAR. Here the flight time of the proton has been corrected for, ensuring that the peak in Fig. 2 is centered around zero for both high- and low-energy proton events. The FWHM time resolution of the experiment was $\approx$3 ns. To separate the PFGs from the prompt fission neutrons (PFNs), which produce signals resembling γ rays in the $LaBr_3$ detectors, a time gate of $\pm$3 ns was chosen. This was a compromise between maximizing statistics and minimizing the PFN contribution. With this $\pm$3 ns time gate and 20 cm distance from the target to the detector, the majority of the neutrons below 10 MeV could be rejected.

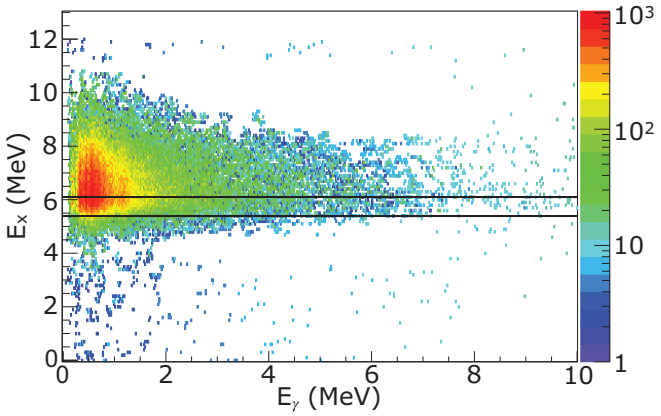

FIG. 3. Unfolded, background-subtracted coincidence matrix, showing the energies E_γ of γ rays from $(d,pf\gamma)$ events as a function of ^{241}Pu* excitation energy E_x. The values of the inner and outer fission barriers, 6.14 ± 0.5 MeV and 5.4 ± 0.5 MeV, respectively [32], are drawn in black.

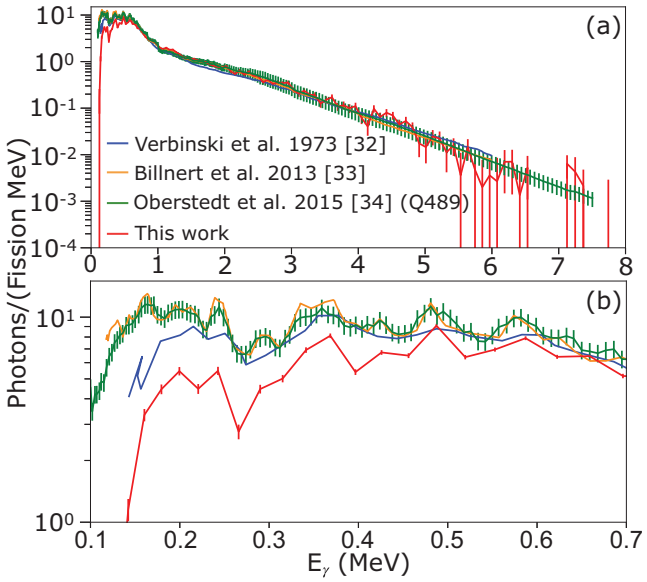

FIG. 4. Extracted prompt fission γ-ray spectrum for ^{252}Cf, compared to the previous measurements of Verbinski *et al.* [33], Billnert *et al.* [34], and Oberstedt *et al.* [35] (marked Q489). The latter two measurements were conducted using $LaBr_3$ detectors. (b) shows the same data as (a) magnified to highlight the low-energy region. The uncertainties on the spectrum in this work are statistical. The deviation at low energies can be explained by the difference in relative time gates, see text.

Similarly, a time gate on Δt_{NIFF} of ± 4.6 ns was used to select prompt fission fragments, where Δt_{NIFF} is the time difference between the arrival of a proton in the ΔE detector and the arrival of a fission fragment in NIFF. Here, the same relative width between the prompt time cut and the time resolution of the fission detectors were used as for the γ-ray detectors. As the NIFF time resolution was worse than the $LaBr_3$, the time scale of the events are best described by $\Delta t_{\mathrm{LaBr_3}}$.

The γ-ray response of OSCAR [28,29] was corrected for by applying the unfolding procedure described in Ref. [30]. This procedure has recently been further developed and now propagates the statistical uncertainties throughout the unfolding routine [31]. The unfolded, background-subtracted coincidence matrix showing the detected γ-ray energies E_γ for different ^{241}Pu* excitation energies E_x is shown in Fig. 3.

A. Verification using ^{252}Cf

The prompt fission γ-ray characteristics from the spontaneous fission of ^{252}Cf are well known and thus measurements of these serve as a benchmark for our PFG extraction routine. We measured PFGs emitted from a ^{252}Cf source, the activity of which was measured to 3.3 kBq in April 2012, using the same experimental setup as described in Sec. II. In Fig. 4, the PFG spectrum from ^{252}Cf(sf) measured in this work is compared to previous measurements [33–35]. There is good agreement for γ-ray energies above $\approx$0.5 MeV and the structures in the spectrum below $\approx$0.5 MeV also match those of earlier measurements. For $E_\gamma < 0.5$ MeV, we note that there is a depletion in the measured γ-ray multiplicity relative to the earlier measurements, which is reflected in the calculated PFG characteristics presented in Table I. Figure 2 shows that this depletion arises from low-energy γ rays that fall outside

TABLE I. PFG characteristics determined from previous ^{252}Cf(sf) experiments using $LaBr_3$ detectors, compared to uncorrected and corrected values from the present work. The uncertainties on the uncorrected values are statistical, propagated through the γ-ray unfolding routine. The scaling factors used to obtain the corrected values are also given. In Ref. [35], three separate measurements were conducted using $LaBr_3$ detectors, marked Q489, Q491, and 2987, respectively.

Reference	$\overline{M}_\gamma$	$\overline{E}_{\gamma,\mathrm{tot}}$ [MeV]
This work, uncorrected	6.37 ± 0.03	6.18 ± 0.05
This work, corrected	8.28 ± 0.04 [a]	6.61 ± 0.05 [b]
Scaling factors	1.30	1.07
Billnert *et al.* [34]	8.30 ± 0.08	6.64 ± 0.08
Oberstedt *et al.* [35] (Q489)	8.29 ± 0.07	6.74 ± 0.09
Oberstedt *et al.* [35] (Q491)	8.28 ± 0.08	6.76 ± 0.09
Oberstedt *et al.* [35] (2987)	8.28 ± 0.07	6.51 ± 0.07

[a]The uncertainty listed is the propagated statistical uncertainty.
[b]See footnote a.

of the ±3 ns time gate, a narrower gate relative to the time resolution than those used in Refs. [33–35]. As described above, a wider time gate could not be used in the present experiment due to contamination of PFNs. By comparing our measured ^{252}Cf(sf) PFG characteristics to those obtained by selected previous experiments (see Table I) chosen because they also use $LaBr_3$ γ-ray detectors, we estimate that about 10% of the γ-ray energy and 20% of the multiplicity are excluded due to the narrow prompt time gate. The effect of the time gate on the observed value of M_γ has recently been thoroughly discussed in Ref. [36].

In this paper, we study the E_x dependence of PFG emission from ^{241}Pu*. Because Fig. 4(a) shows that the PFG spectrum for ^{252}Cf is reproduced for $E_\gamma \gtrsim 0.5$ MeV, we will be sensitive to potential changes E_x in the spectrum of ^{241}Pu* above this γ-ray energy. Furthermore, it is reasonable to assume that the same percentage of the PFGs are lost in the ^{240}Pu(d,pf) measurement as for ^{252}Cf(sf). Therefore, significant changes in the ^{241}Pu* PFG spectrum below ≈0.5 MeV are expected to be observed as well.

In order to facilitate comparison to previous experiments despite the difference in time gates, we introduce a scaling procedure for $\overline{E}_{\gamma,\mathrm{tot}}$ and $\overline{M}_\gamma$. Here, the previous ^{252}Cf(sf) measurements are used to find the scaling parameters needed to correct the multiplicity and total energy. The scaling parameters are taken as the constant ratio between, e.g., the multiplicity found in this work and the uncertainty-weighted average $\overline{M}_\gamma$ reported by the previous studies. The scaling parameters and the corrected ^{252}Cf(sf) PFG characteristics are found in Table I. The same scaling parameters are later applied to the extracted ^{241}Pu PFG multiplicity and total energy, and from these the scaled $\overline{\varepsilon}_\gamma = \overline{E}_{\gamma,\mathrm{tot}}/\overline{M}_\gamma$ is determined.

B. FREYA simulation

The computational fission model FREYA version 2.0.3 was used to simulate the prompt fission γ rays resulting from the fission of ^{241}Pu*. In FREYA only a selected number of fissioning nuclei are included, and the fission of ^{241}Pu* is currently not among them. To implement this isotope, the fission fragment mass distribution $Y(A)$ and the total kinetic energy of the fragments TKE(A) were needed, neither of which were available from experiments. They were therefore obtained from the fission model GEF (GEneral description of Fission observables) [14]. TKE(A) and $Y(A)$ are known to change with the excitation energy of the compound nucleus, thus their energy dependencies had to be determined in order to simulate energy-dependent fission in FREYA. A five-parameter-Gaussian fit was used to parametrize $Y(A, E_x)$. TKE(A, E_x) was determined by shifting TKE(A_H) to match the evaluated PFN multiplicity for each E_x, where A_H is the mass of the heavy fragment. Further details of this procedure are found in Ref. [37]. As FREYA only simulates neutron-induced and spontaneous fission, the ^{240}Pu(d,pf) reaction was mimicked by the (n,f) surrogate reaction, see Sec. IV for further discussion regarding potential differences between the two reactions. By using the reaction ^{240}Pu(n,f) one obtain fissions of ^{241}Pu* with excitation energy $E_x = E_n + S_n$. Here S_n is the neutron separation energy of ^{241}Pu. As ^{240}Pu is not fissile, the E_x equivalent of thermal neutron-induced fission, $E_n \approx 0$ MeV, lies below the double-humped fission barrier, whose values are 6.14 ± 0.5 MeV and 5.4 ± 0.5 MeV for the inner and outer barrier, respectively [32].

A brief summary of how FREYA treats γ-ray emission is given below; a full account is found elsewhere [11,20]. Neutrons are evaporated until no longer energetically possible, which is when the excitation energy of the fragment falls below S_n, and thus γ-ray emission begins. First, statistical γ rays are sampled from a black-body spectrum, each carrying $1\hbar$ of the fragment's angular momentum. After reaching the yrast line, rotational $E2$ γ rays are emitted to exhaust the remaining excitation energy and angular momentum. Whenever available for the fragment in question, FREYA will use the evaluated discrete transitions from the RIPL-3 library [38] instead of the statistical and collective sampling.

The two FREYA input parameters $t_{\max}$ and $g_{\min}$ were considered in this work, as FREYA does not simulate photons emitted from states with half-lives longer than $t_{\max}$ or with energies lower than $g_{\min}$. In accordance with the experimental prompt time cut, $t_{\max}$ was chosen to be 3 ns. The value of $g_{\min}$ reflects the energy threshold of γ rays included in the analysis and was chosen to be 0.1 MeV, as used in previous experiments [10,16,35].

The ^{240}Pu(n,f) reaction was simulated for E_n in the range 0.0–5.0 MeV with steps of 0.5 MeV, which corresponds to the ^{241}Pu* excitation energy range 5.2–10.2 MeV. We ran 10^6 fission events per energy.

III. RESULTS

Figure 3 shows that the majority of the $(d,pf\gamma)$ events arrive when the excitation energy of ^{241}Pu* exceeds ≈5.5 MeV, and thus the onset of fission corresponds well to the values of the double-humped fission barrier reported in Ref. [32]. The prompt fission γ rays were extracted from the unfolded coincidence matrix for the ^{241}Pu excitation energy range from 5.5–8.5 MeV using E_x bins of 0.5 MeV. Outside this region few fissions are registered and spectrum is dominated by the background of random coincidences with γ rays from ^{9}Be. As stated above, the γ-ray threshold was set to 0.1 MeV in the analysis. The upper energy limit chosen in PFG studies is usually in the range 6–10 MeV and has little impact on the PFG characteristics [39]. We thus study the PFGs in the range from 0.1–10 MeV, as no γ rays with higher energy were observed.

The PFG spectra for different E_x bins is shown in Fig. 5. Note that these spectra have not been subject to the corrections described in Sec. II A. The uncertainties included for the experimental spectra are the statistical uncertainties, propagated through the γ-ray unfolding routine, as well as the statistical uncertainty on the number of fissions detected. For clarity, uncertainties are only shown for one spectrum.

To further understand the PFG behavior with E_x, the PFG characteristics were calculated from Fig. 5. The resulting values for $\overline{M}_\gamma$, $\overline{E}_{\gamma,\mathrm{tot}}$, and $\overline{\varepsilon}_\gamma$ as a function of E_x are shown in Fig. 6. The data are shown both before and after the correction procedure described in Sec. II A was applied. We emphasize that the sole effect of this correction is a scaling of all the

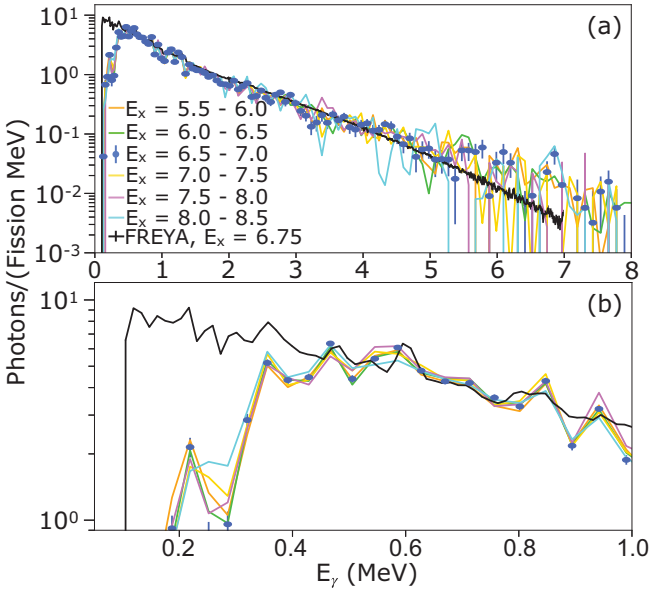

FIG. 5. Extracted, uncorrected prompt fission γ-ray spectra for ^{241}Pu for excitation energies in the range 5.5–8.5 MeV, compared to the FREYA prediction at $E_x = 6.75$ MeV. Statistical uncertainties are shown for the experimental spectrum in the excitation energy bin 6.5–7.0 MeV to increase readability. The statistical uncertainties on the FREYA spectrum are smaller than the marker size for lower energies. (b) shows the same data as in (a), magnified to highlight the low-energy region. We observe that the experimental spectra for different E_x are similar.

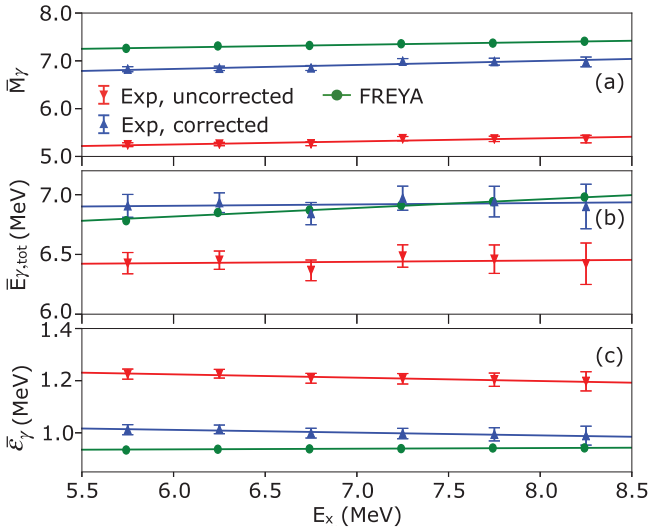

FIG. 6. Evolution of (a) $\overline{M}_\gamma$, (b) $\overline{E}_{\gamma,\mathrm{tot}}$, and (c) $\overline{\varepsilon}_\gamma$ with ^{241}Pu* excitation energy. The full red, blue, and green lines show the weighted linear interpolation of the uncorrected and corrected experimental data, and the FREYA results, respectively. The statistical uncertainties on the FREYA values are negligible. The uncertainties on the corrected values are the propagated statistical uncertainties. The uncertainty on $\overline{\varepsilon}_\gamma$ is calculated by assuming the uncertainties on $\overline{M}_\gamma$ and $\overline{E}_{\gamma,\mathrm{tot}}$ are independent.

PFG characteristics, included to facilitate comparison to the FREYA simulations and previous studies of other fissioning systems.

In order to quantify the rate of change observed in the PFG characteristics, we introduce the relative change of the PFG characteristics with excitation energy, the slopes of $\overline{M}_\gamma$, $\overline{E}_{\gamma,\mathrm{tot}}$, and $\overline{\varepsilon}_\gamma$ with increasing E_x; $\Delta\overline{M}_\gamma/\Delta E_x$, $\Delta\overline{E}_{\gamma,\mathrm{tot}}/\Delta E_x$, and $\Delta\overline{\varepsilon}_\gamma/\Delta E_x$. This introduction is justified by the observation in Fig. 6 that the PFG characteristics are to first order linear in E_x below the threshold of second-chance fission, which is supported by previous work [8]. The interpretation of, e.g., $\Delta\overline{M}_\gamma/\Delta E_x$ is how many extra γ rays are emitted per MeV increase in E_x of the fissioning nucleus.

TABLE II. PFG measurements and predictions of the PFG dependence on E_x below the threshold of second-chance fission. Where two energies were used, these are given as E_1, E_2, otherwise the energy range is given. In the case of Laborie *et al.* [15], only the two lowest incoming neutron energies are used to stay below the threshold of second-chance fission. This threshold is found by adding the S_n of the compound nucleus A from Ref. [40] and to the energy of the lower fission barrier of the (A-1) daughter nucleus [32].

Reference	Reaction	E_n [MeV]	E_x [MeV]	$\Delta\overline{M}_\gamma/\Delta E_x$ [MeV^{-1}]	$\Delta\overline{E}_{\gamma,\mathrm{tot}}/\Delta E_x$	$\Delta\overline{\varepsilon}_\gamma/\Delta E_x$
This work, experiment	^{240}Pu(d,pf)	–	5.75–8.25	0.06 ± 0.02	0.01 ± 0.05	−0.01 ± 0.01
This work, experiment, corrected	^{240}Pu(d,pf)	–	5.75–8.25	0.08 ± 0.03	0.01 ± 0.06	−0.01 ± 0.01
This work, FREYA-2.0.3	^{240}Pu(n,f)	0.00–5.00	5.24–10.24	0.06	0.07	0.00
Previous experiments:						
Fréhaut *et al.* [19] (1983)	^{235}U(n,f)	1.15–5.42	7.69–11.97	N/A	0.14 ± 0.01	N/A
Rose *et al.* [8] (2017)	^{239}Pu(d,pf)	–	4.81–8.49	0.23 ± 0.20	0.27 ± 0.07	0.00 ± 0.03
Rose *et al.* [8] (2017)	^{233}U(d,pf)	–	5.12–9.68	0.12 ± 0.23	0.13 ± 0.10	0.00 ± 0.03
Laborie *et al.* [15] (2018)	^{238}U(n,f)	1.60, 5.10	6.41, 9.91	0.05 ± 0.27	−0.06 ± 0.25	−0.02 ± 0.01
Qi *et al.* [16] $LaBr_3$ (2018)	^{238}U(n,f)	1.90, 4.80	6.71, 9.61	0.34 ± 0.18	0.39 ± 0.25	0.01 ± 0.04
Qi *et al.* [16] PARIS (2018)	^{238}U(n,f)	1.90, 4.80	6.71, 9.61	0.19 ± 0.16	0.24 ± 0.22	0.01 ± 0.04
Predictions/Evaluations:						
Oberstedt *et al.* [41] (2017)[a]	^{240}Pu(n,f)	0.00–5.00	5.24–10.24	0.42 ± 0.03	0.13 ± 0.08	−0.02 ± 0.01
ENDF-B/VIII.0, Stetcu *et al.* [42] (2020)	^{239}Pu(n,f)	0.00–5.00	6.53–11.53	0.51 ± 0.09	0.43 ± 0.07	0.00 ± 0.00

[a]The systematics for predicting PFG characteristics presented in Ref. [41] are applied to the ^{240}Pu(n,f) reaction, where the necessary input data were taken from the ENDF/B-VIII.0 evaluation.

The PFG properties show little change with increasing E_x, a feature that is evident when studying the extracted values for $\overline{M}_\gamma$, $\overline{E}_{\gamma,\mathrm{tot}}$, and $\overline{\varepsilon}_\gamma$ in Fig. 6. This is reflected in the relative changes: weighted linear interpolation gives $\Delta\overline{M}_\gamma/\Delta E_x = 0.07 \pm 0.03$ MeV^{-1}, $\Delta\overline{E}_{\gamma,\mathrm{tot}}/\Delta E_x = 0.01 \pm 0.05$, and $\Delta\overline{\varepsilon}_\gamma/\Delta E_x = -0.01 \pm 0.01$ for the uncorrected PFG characteristics. The impact of the correction on the relative changes is minimal (see Table II), and thus the use of this scaling procedure has no impact on the conclusions of the paper.

IV. DISCUSSION

A. Experiment and FREYA

The present experiment is the first measurement of prompt fission γ rays from ^{241}Pu* and direct comparisons of the PFG characteristics to previous experiments are therefore not possible. Typical values for $\overline{M}_\gamma$ and $\overline{E}_{\gamma,\mathrm{tot}}$ across different fissioning systems are in the range of 6.5–8 and 5–7 MeV, respectively [9,10]. We see from Fig. 5 that the corrected PFG characteristics for ^{241}Pu* are within these expected intervals.

When comparing the FREYA γ-ray spectrum for $E_x = 6.75$ MeV to the experimental spectrum for the excitation energy bin $E_x = 6.5 - 7.0$ MeV in Fig. 5, we see that the calculated spectrum is very similar to the measured one for $E_\gamma \gtrsim 0.5$ MeV. As discussed in Sec. II A, the discrepancies for $E_\gamma \lesssim 0.5$ MeV were expected. Figure 5(a) shows that FREYA reproduces the shapes of the γ-ray spectrum quite well for $E_\gamma \lesssim 0.5$ as well, probably due to the inclusion of discrete nuclear transitions from the RIPL-3 library in the γ-ray decay procedure. Figure 5 indicates that FREYA might underestimate the photon yield for $E_\gamma \gtrsim 5.5$ MeV, where structures seem to be present in the experimental spectra. Such structures in the high-energy tail of the PFG spectrum have previously been observed experimentally and are believed to originate from nuclear shell effects in the fission fragments [43]. Nevertheless, deviations at higher energies do not significantly affect the calculated values for the PFG characteristics due to the exponentially falling nature of the spectrum.

The similarity between the FREYA γ-ray spectra and the experimental spectra in Fig. 5(a) is reflected in the integrated characteristics shown in Fig. 6. The simulated values of $\overline{E}_{\gamma,\mathrm{tot}}$, presented in Fig. 6(b) lie within a 2σ interval across the excitation energy range studied. Furthermore, $\overline{M}_\gamma$ and $\overline{\varepsilon}_\gamma$ in Figs. 6(a) and 6(c) calculated by FREYA are within 8% of the corrected experimental values, though the calculated γ-ray multiplicity and average γ-ray energy are, respectively, higher and lower than the corrected experimental results. This deviation in the absolute characteristics might be a result of either the simple correction procedure presented in Sec. II A not being sufficiently precise or that FREYA simulates an excess of low-energy γ rays.

A striking feature of Fig. 6 is the apparent excitation energy independence of the observed PFG characteristics, reflected in Table II where the slopes of these quantities are found to be small. Only the value of $\Delta\overline{M}_\gamma/\Delta E_x$ is statistically significant in a 2σ confidence interval. This indicates that when additional E_x is supplied to the fissioning nucleus and hence to the fragments, only a small or even negligible fraction of the extra energy is released as emission of prompt γ rays.

The trend observed in Fig. 6 of small increase in the PFG characteristics with E_x is supported by FREYA as seen by the values for the relative changes in Table II, where the FREYA simulated for $\Delta\overline{M}_\gamma/\Delta E_x$, and $\Delta\overline{E}_{\gamma,\mathrm{tot}}/\Delta E_x$ are within a 1σ deviation from the experimental values. This overall agreement between the simulated and experimental relative changes indicate that the deexcitation model employed by FREYA captures the main mechanisms of excitation energy-dependent PFG emission. We note that the FREYA calculated $\Delta\overline{M}_\gamma/\Delta E_x$ and $\Delta\overline{E}_{\gamma,\mathrm{tot}}/\Delta E_x$ are weakly energy dependent, but as they change in parallel with each other, $\Delta\overline{\varepsilon}_\gamma/\Delta E_x$ is zero over this excitation energy range.

Understanding the behavior of the γ-ray emission simulated by FREYA gives insights into the physical mechanisms behind the experimentally determined slopes. As described above, $Y(A)$ is energy dependent and becomes progressively more symmetric with increasing E_n [37] and thus equivalently E_x. As $Y(A)$ changes, the weighted average of each γ-emitting fragment also changes, indirectly affecting PFG emission. However, the change of $Y(A)$ is expected to be small over the excitation energy interval studied. Furthermore, the PFN multiplicity is known to increase with higher E_x. The fission fragments are thus less neutron-rich at the onset of γ-ray emission, yielding a larger average S_n among the fragments. Because S_n is effectively the upper limit for γ-ray emission in FREYA, this might explain an increase in $\overline{E}_{\gamma,\mathrm{tot}}$ with E_x. Changes in the average S_n of the fragments have previously been linked to differences in the PFG characteristics [10].

Both of the aforementioned mechanisms could be sources of the dependences of the PFG characteristics on E_x. A glance at the trends in both the measured and simulated characteristics in Fig. 6 shows that these effects are small or even negligible, with only $\leqslant 0.07$ extra γ rays carrying $\leqslant 80$ keV more energy being emitted per MeV increase in E_x.

As we observe only a small fraction of the added extra energy results in γ-ray emission, this raises the question where the energy is distributed. Energy sharing in fission is a intricate and poorly understood process, as each fragment emerges both with kinetic and excitation energy. More neutrons are known to be emitted with increasing E_x, which implies that the neutrons carry away a portion of the added E_x. It thus seems that the fragment prefers to emit another neutron if possible, rather than an additional γ ray.

We note that though we make direct comparison between ^{240}Pu(n,f) as simulated by FREYA and the experimental surrogate reaction ^{240}Pu$(d,p\mathrm{f})$, these reactions may not populate the same states in the compound nuclei. The charged-particle reaction is expected to induce more angular momentum in the fissioning nucleus, and the PFGs are known to exhaust most of the angular momentum of the fragments. It is not clear how the angular momentum of the initial compound nucleus which fissions is related to those of the resulting fission fragments. An experiment comparing the impact of using the $(d,p\mathrm{f})$ versus (n,f) found a significant difference in the PFG characteristics [8], though this might be because of PFN

contamination. On the other hand, recent theoretical work suggests that the angular momentum of the compound system does not significantly influence the fragment spins [44]. This question of angular momentum propagation in fission will be further investigated in upcoming experiments at the OCL.

B. Previous experiments

As mentioned above, there are few experiments in the literature where the PFGs are extracted as a function of CN excitation energy. Nevertheless, a handful of measurements comparing thermal and fast neutron-induced fission have been conducted recently to provide vital information for the construction of the Generation-IV fast reactors [8,15–18]. This enables us to extract their values of $\Delta\overline{M}_\gamma/\Delta E_\mathrm{x}$, $\Delta\overline{E}_{\gamma,\mathrm{tot}}/\Delta E_\mathrm{x}$, and $\Delta\overline{\varepsilon}_\gamma/\Delta E_\mathrm{x}$ by fitting a linear slope to their results below the threshold for second-chance fission. Though the fissioning nuclei are not the same in the different experiments, we expect the mechanism for the energy sharing in fission and thus the energy dependence of the PFGs from different fissioning isotopes to be largely the same.

The deduced values for the relative changes of recent PFG measurements are presented in Table II. We have limited this table to only include experiments where the same setup was used for measurements at different E_x and where E_x is below the threshold for second-chance fission. The latter is to simplify interpretation because the fissioning nucleus is the same across the whole energy range considered.

From the extracted values of $\Delta\overline{M}_\gamma/\Delta E_\mathrm{x}$, $\Delta\overline{E}_{\gamma,\mathrm{tot}}/\Delta E_\mathrm{x}$, and $\Delta\overline{\varepsilon}_\gamma/\Delta E_\mathrm{x}$ we see that per additional MeV of excitation energy in the compound system, the previous measurements observed 0.05–0.34 more γ rays per fission, carrying 0.13–0.39 MeV extra energy. The average photon energy $\overline{\varepsilon}_\gamma$ is observed to be approximately constant. Due to the large uncertainties, the majority of the slopes are consistent with zero to a 2σ confidence level.

We see that both $\Delta\overline{M}_\gamma/\Delta E_\mathrm{x}$ and $\Delta\overline{E}_{\gamma,\mathrm{tot}}/\Delta E_\mathrm{x}$ from previous experiments are generally larger compared to the ones obtained from the current experiment. A possible reason for this is that some of the previous experiments measured PFGs solely at two different values of E_x below the second-chance fission threshold, and all the measurements have significant uncertainties. Consequently, the slopes are correspondingly uncertain. Additionally, a deviation could originate from a difference in the population of isomeric states. If more isomeric states are populated with increasing excitation energy, fewer γ rays might be captured in the prompt time gate, thus impacting $\Delta\overline{M}_\gamma/\Delta E_\mathrm{x}$, and $\Delta\overline{E}_{\gamma,\mathrm{tot}}/\Delta E_\mathrm{x}$.

Despite these possible differences, we see from Table II that the previous experiments largely agree with the values of $\Delta\overline{M}_\gamma/\Delta E_\mathrm{x}$ and $\Delta\overline{E}_{\gamma,\mathrm{tot}}/\Delta E_\mathrm{x}$ found for ^{240}Pu(d,pf) within a 2σ interval. The measurements by Qi *et al.* and Laborie *et al.* report large uncertainties, and the former give higher values for the relative change parameters. The weighted average slopes among the previous experiments are 0.21 MeV^{-1} and 0.22 for $\Delta\overline{M}_\gamma/\Delta E_\mathrm{x}$ and $\Delta\overline{E}_{\gamma,\mathrm{tot}}/\Delta E_\mathrm{x}$ respectively, where the measurement by Fréhaut *et al.* in Ref. [19] has been omitted due to a seemingly underestimated uncertainty on the slope.

C. Previous estimations of PFG dependence on E_x

Two previous works attempted to estimate the dependence on prompt fission γ-ray emission on E_x for different fissioning systems. In Ref. [41], Oberstedt *et al.* introduced an empirical parametrization to predict the PFG characteristics based on the mass and charge of the fissioning nucleus. In order to include the unknown E_x dependence of the PFGs, they assume that there is a direct relationship between the γ-ray and neutron multiplicities. Furthermore, in Ref. [42] Stetcu *et al.* recently evaluated available experimental data to recommend how the PFG characteristics are expected to change with inceased E_x.

Again, we find the values of $\Delta\overline{M}_\gamma/\Delta E_\mathrm{x}$ and $\Delta\overline{E}_{\gamma,\mathrm{tot}}/\Delta E_\mathrm{x}$ below the threshold for second-chance fission from from the evaluations presented by Oberstedt *et al.* and Stetcu *et al.* These are presented in Table II. Here we see that there is a significant gap between the parametrization and evaluation on one hand, and the experimental data on the other. The values of $\Delta\overline{M}_\gamma/\Delta E_\mathrm{x}$ from Refs. [41,42] are five times larger than those from the present experimental data, and more than twice as large as the average among previous experiments. Furthermore the value for $\Delta\overline{E}_{\gamma,\mathrm{tot}}/\Delta E_\mathrm{x}$ reported by Stetcu *et al.* is also noticeably larger than given by the experiments. The values for $\Delta\overline{\varepsilon}_\gamma/\Delta E_\mathrm{x}$ from Oberstedt *et al.* and Stetcu *et al.* accurately reflect the available experimental data.

While there is a definitive lack of experimental data to which Refs. [41,42] can benchmark their suggested dependence on E_x, neither FREYA nor CGMF [45] (calculations from the latter are presented in Ref. [42]) support a marked increase in the PFG characteristics below the threshold for second-chance fission.

In light of these results, the assumption in Ref. [41] regarding the direct dependence of the γ-ray multiplicity on the energy-dependent neutron multiplicity should be revisited. Furthermore, the ENDF-B/VIII.0 evaluation by Stetcu *et al.* seems to put a large emphasis on PFG characteristics inferred from γ-ray production cross sections measured in the 1960s, which are ambiguous and inconsistent with other experimental results (see, for example, Fig. 9 in Ref. [42]). We also note that the results from Rose *et al.* [8] regarding the E_x dependence of the PFGs from the ^{239}Pu(d,pf) reaction seem to not be included in their evaluation of PFGs from ^{239}Pu(n,f).

As the PFG dependence on E_x is desirable information both for providing correct input for fast-reactor simulations and for reaching a deeper understanding of the mechanisms behind PFG emission, the observed deviations between the parametrization/evaluation, on one hand, and experiments/fission simulations, on the other, must be further investigated and resolved.

V. CONCLUSION AND OUTLOOK

Prompt fission γ-ray characteristics resulting from the fission of ^{241}Pu* have been measured in the excitation energy region 5.75–8.25 MeV. A verification measurement of the PFG spectrum from ^{252}Cf(sf) reproduces previous

measurements for $E_\gamma \gtrsim 0.5$ MeV, while for lower γ-ray energies there is a deviation. This is attributed to the narrow time gate necessary to reject PFNs by ToF. We will use a larger distance between the target and detector in upcoming experiments to further investigate this deviation. Employing the well-known ^{252}Cf(sf) PFG characteristics, correction factors were found and applied to the ^{241}Pu* PFG characteristics in order to facilitate comparison between different experiments. FREYA reproduces the corrected values of the average total γ-ray energy ($\overline{E}_{\gamma,\mathrm{tot}}$) found in this work within a 2σ interval, and the average γ-ray multiplicity per fission ($\overline{M}_\gamma$) and average photon energy ($\overline{\varepsilon}_\gamma$) simulated by FREYA are within 8% of the experimental values across the excitation energy range studied.

To study the dependence of the PFG characteristics on E_x, new quantities that describe the energy dependence of the PFGs were extracted and analyzed. These were found to be small, with $\overline{M}_\gamma$, $\overline{E}_{\gamma,\mathrm{tot}}$, and $\overline{\varepsilon}_\gamma$ all exhibiting little to no dependence on E_x below the threshold for second-chance fission. We observe smaller changes than seen in other previous experiments, though large experimental uncertainties reported in earlier work complicate the comparison. However, two separate evaluations of the PFG dependence on E_x yield significantly larger values for $\Delta\overline{M}_\gamma/\Delta E_\mathrm{x}$ than the average among previous experiments. Therefore, more experiments must be conducted where PFGs are measured for different compound nucleus excitation energies. Such experiments are planned at the OCL and will hopefully bring a deeper understanding of the excitation energy partition in fission.

The data presented in Fig. 6 are available in Ref. [46].

ACKNOWLEDGMENTS

The authors wish to thank P. Sobas, J. C. Wikne, and J. Müller at the OCL for providing the deuterium beam over the course of the experiment. The authors thank the Lawrence Livermore National Laboratory (LLNL) for providing the ^{240}Pu target. D.G. thanks LBNL for hosting her visits to Berkeley. This project was supported by the Research Council of Norway, Grants No. 263030 and No. 261617, and by the US Department of Energy under Contracts No. DE-AC02-05CH11231 (LBNL) and No. DE-AC52-07NA27344 (LLNL). This work was performed under the auspices of the U.S. Department of Energy by Lawrence Livermore National Laboratory under Contract DE-AC52-07NA27344. A.O. acknowledges the support from the Extreme Light Infrastructure Nuclear Physics (ELI-NP) Phase II, a project cofinanced by the Romanian Government and the European Union through the European Regional Development Fund-the Competitiveness Operational Programme (1/07.07.2016, COP, ID 1334). G.M.T. acknowledges funding by the Research Council of Norway under contract 262952. A.C.L. gratefully acknowledges funding by the European Research Council through ERC-STG-2014 under Grant Agreement No. 637686.

[1] L. Meitner and O. R. Frisch, Disintegration of Uranium by neutrons: A new type of nuclear reaction, Nature (London) **143**, 239 (1939).

[2] O. Hahn and F. Strassmann, Über den Nachweis und das Verhalten der bei der Bestrahlung des Urans mittels Neutronen entstehenden Erdalkalimetalle, Sci. Nat. **27**, 11 (1939).

[3] S. Goriely, The fundamental role of fission during r-process nucleosynthesis in neutron star mergers, Eur. Phys. J. A **51**, 22 (2015).

[4] G. Rimpault, D. Bernard, D. Blanchet, C. Vaglio-Gaudard, S. Ravaux, and A. Santamarina, Needs of accurate prompt and delayed γ-spectrum and multiplicity for Nuclear Reactor Designs, Phys. Procedia **31**, 3 (2012).

[5] H. Nifenecker, C. Signarbieux, M. Ribrag, J. Poitou, and J. Matuszek, γ-neutron competition in the de-excitation mechanism of the fission fragments of ^{252}Cf, Nucl. Phys. A **189**, 285 (1972).

[6] F. Pleasonton, Fission of ^{233}U and ^{239}Pu, Nucl. Phys. A **213**, 413 (1973).

[7] A. Hotzel *et al.*, High-energy gamma-rays of 252Cf accompanying the spontaneous fission, Z. Phys. A **356**, 299 (1996).

[8] S. J. Rose *et al.*, Energy dependence of the prompt γ -ray emission from the (d, p)-induced fission of ^{234}U* and ^{240}Pu*, Phys. Rev. C **96**, 014601 (2017).

[9] S. Oberstedt, A. Oberstedt, A. Gatera, A. Göök, F.-J. Hambsch, A. Moens, G. Sibbens, D. Vanleeuw, and M. Vidali, Prompt fission γ-ray spectrum characteristics from ^{240}Pu(sf) and ^{242}Pu(sf), Phys. Rev. C **93**, 054603 (2016).

[10] L. Qi *et al.*, Potential of prompt γ-ray emission studies in fast-neutron induced fission: A first step, Eur. Phys. J. A **56**, 98 (2020).

[11] R. Vogt and J. Randrup, Improved modeling of photon observables with FREYA, Phys. Rev. C **96**, 064620 (2017).

[12] I. Stetcu, P. Talou, T. Kawano, and M. Jandel, Properties of prompt-fission γ rays, Phys. Rev. C **90**, 024617 (2014).

[13] M. J. Marcath, R. C. Haight, R. Vogt, M. Devlin, P. Talou, I. Stetcu, J. Randrup, P. F. Schuster, S. D. Clarke, and S. A. Pozzi, Measured and simulated ^{252}Cf(sf) prompt neutron-photon competition, Phys. Rev. C **97**, 044622 (2018).

[14] K. H. Schmidt, B. Jurado, C. Amouroux, and C. Schmitt, General description of fission observables: GEF model code, Nucl. Data Sheets **131**, 107 (2016).

[15] J.-M. Laborie, R. Billnert, G. Bélier, A. Oberstedt, S. Oberstedt, and J. Taieb, First experimental prompt gamma-ray spectra in fast-neutron-induced fission of ^{238}U, Phys. Rev. C **98**, 054604 (2018).

[16] L. Qi *et al.*, Statistical study of the prompt-fission γ-ray spectrum for ^{238}U(n, f) in the fast-neutron region, Phys. Rev. C **98**, 014612 (2018).

[17] A. Oberstedt, M. Lebois, S. Oberstedt, L. Qi, and J. N. Wilson, Prompt γ-ray characteristics from ^{235}U(n, f) at $\overline{E}_n = 1.7$ MeV, Eur. Phys. J. A **56**, 236 (2020).

[18] M. Lebois *et al.*, Comparative measurement of prompt fission γ-ray emission from fast-neutron-induced fission of ^{235}U and ^{238}U, Phys. Rev. C **92**, 034618 (2015).

[19] J. Fréhaut, A. Bertin, and R. Bois, Mesure de $\bar{\nu}_p$ et $\bar{E}_\gamma$ Pour la Fission de ^{232}Th, ^{235}U et ^{237}Np Induite par des Neutrons D'Energie Comprise Entre 1 et 15 MeV, in *Nuclear Data for Science and Technology*, edited by K. H. Böckhoff (Springer, Dordrecht, 1983), pp. 78–81.

[20] J. M. Verbeke, J. Randrup, and R. Vogt, Fission reaction event yield algorithm FREYA 2.0.2, Comput. Phys. Commun. **222**, 263 (2018).

[21] L. A. Bernstein, D. A. Brown, A. J. Koning, B. T. Rearden, C. E. Romano, A. A. Sonzogni, A. S. Voyles, and W. Younes, Our future nuclear data needs, Annu. Rev. Nucl. Part. Sci. **69**, 109 (2019).

[22] T. A. Laplace *et al.*, Statistical properties of ^{243}Pu, and ^{242}Pu (n,γ) cross section calculation, Phys. Rev. C **93**, 014323 (2016).

[23] M. Guttormsen, T. E. Hansen, and N. Lietaer, The SiRi particle-telescope system, Nucl. Instrum. Meth. A **648**, 168 (2011).

[24] V. W. Ingeberg, F. Zeiser, and E. Lima, oslocyclotronlab/Qkinz: Update (Version 1.3.3). Zenodo (2018), http://doi.org/10.5281/zenodo.1206099.

[25] T. Tornyi, A. Görgen, M. Guttormsen, A. Larsen, S. Siem, A. Krasznahorkay, and L. Csige, A new fission-fragment detector to complement the CACTUS-SiRi setup at the Oslo Cyclotron Laboratory, Nucl. Instrum. Meth. A **738**, 6 (2014).

[26] F. Zeiser, G. Tveten, F. Bello Garrote, M. Guttormsen, A. Larsen, V. Ingeberg, A. Görgen, and S. Siem, The γ-ray energy response of the Oslo Scintillator Array OSCAR, Nucl. Instrum. Meth. A **985**, 164678 (2021).

[27] V. W. Ingeberg *et al.*, Characterization of the Oslo scintillator array OSCAR (unpublished).

[28] F. Zeiser, G. M. Tveten, F. L. Bello Garrote, M. Guttormsen, A. C. Larsen, V. W. Ingeberg, A. Görgen, and S. Siem, The energy response of the Oslo Scintillator Array OSCAR-Draft state Aug 2018, arXiv:2008.06240v1 [physics.ins-det] (2018) (draft version of Ref. [26]).

[29] F. Zeiser and G. M. Tveten, oslocyclotronlab/OCL_GEANT4: Geant4 model of OSCAR, OSCAR Response Function oscar2017scale1.15 (Version v1.0.3). Zenodo (2017), http://doi.org/10.5281/zenodo.1339347.

[30] M. Guttormsen, T. S. Tveter, L. Bergholt, F. Ingebretsen, and J. Rekstad, The unfolding of continuum y-ray spectra, Nucl. Instrum. Methods Phys. Res. A **374**, 371 (1996).

[31] J. E. Midtbø, F. Zeiser, E. Lima, A.-C. Larsen, G. M. Tveten, M. Guttormsen, F. L. Bello Garrote, A. Kvellestad, and T. Renstrøm, A new software implementation of the Oslo method with rigorous statistical uncertainty propagation, Comput. Phys. Commun. **262**, 107795 (2021).

[32] S. Bjørnholm and J. E. Lynn, The double-humped fission barrier, Rev. Mod. Phys. **52**, 725 (1980).

[33] V. V. Verbinski, H. Weber, and R. E. Sund, Prompt gamma rays from ^{235}U(n,f), ^{239}Pu(n,f), and spontaneous fission of ^{252}Cf, Phys. Rev. C **7**, 1173 (1973).

[34] R. Billnert, F.-J. Hambsch, A. Oberstedt, and S. Oberstedt, New prompt spectral γ-ray data from the reaction ^{252}Cf(sf) and its implication on present evaluated nuclear data files, Phys. Rev. C **87**, 024601 (2013).

[35] A. Oberstedt, R. Billnert, F.-J. Hambsch, and S. Oberstedt, Impact of low-energy photons on the characteristics of prompt fission γ-ray spectra, Phys. Rev. C **92**, 014618 (2015).

[36] A. Oberstedt, A. Gatera, A. Göök, and S. Oberstedt, Time response and its impact on prompt fission γ-ray spectra characteristics, Eur. Phys. J. A **56**, 196 (2020).

[37] R. Vogt, J. Randrup, D. A. Brown, M. A. Descalle, and W. E. Ormand, Event-by-event evaluation of the prompt fission neutron spectrum from ^{239}Pu(n,f), Phys. Rev. C **85**, 024608 (2012).

[38] R. Capote *et al.*, RIPL - reference input parameter library for calculation of nuclear reactions and nuclear data evaluations, Nucl. Data Sheets **110**, 3107 (2009).

[39] A. Oberstedt *et al.*, Improved values for the characteristics of prompt-fission γ-ray spectra from the reaction ^{235}U(n_{th},f), Phys. Rev. C **87**, 051602(R) (2013).

[40] Data extracted from the ENDSF database using NNDC's Chart of Nuclides, https://www.nndc.bnl.gov/nudat2/.

[41] A. Oberstedt, R. Billnert, and S. Oberstedt, Predictions of characteristics of prompt-fission γ-ray spectra from the n + ^{238}U reaction up to $E_n = 20$ MeV, Phys. Rev. C **96**, 034612 (2017).

[42] I. Stetcu, M. B. Chadwick, T. Kawano, P. Talou, R. Capote, and A. Trkov, Evaluation of the prompt fission gamma properties for neutron induced fission of ^{235,238}U and ^{239}Pu, Nucl. Data Sheets **163**, 261 (2020).

[43] H. Makii *et al.*, Effects of the nuclear structure of fission fragments on the high-energy prompt fission γ-ray spectrum in ^{235}U(n_{th}, f), Phys Rev. C **100**, 044610 (2019).

[44] R. Vogt and J. Randrup, Angular momentum effects in fission, Phys. Rev. C **103**, 014610 (2021).

[45] P. Talou, I. Stetcu, P. Jaffke, M. E. Rising, A. E. Lovell, and T. Kawano, Fission fragment decay simulations with the CGMF code, arXiv:2011.10444v1.

[46] D. Gjestvang *et al.*, Zenodo repository for data in Fig. 6 from the article Excitation energy dependent prompt fission γ-ray emission from ^{241}Pu*, doi: 10.5281/zenodo.4333545 (2020).

Paper II

Angular momentum generation in nuclear fission

II

Angular momentum generation in nuclear fission

J. N. N Wilson, D. Thisse, M. Lebois, N. Jovančević, D. Gjestvang, R. Canavan, M. Rudigier, D. Etasse, R-B. Gerst, L. Gaudefroy, et al.

Article

Angular momentum generation in nuclear fission

J. N. Wilson[1]✉, D. Thisse[1], M. Lebois[1], N. Jovančević[1], D. Gjestvang[2], R. Canavan[3,4], M. Rudigier[3,5], D. Étasse[6], R-B. Gerst[7], L. Gaudefroy[8], E. Adamska[9], P. Adsley[1], A. Algora[10,11], M. Babo[1], K. Belvedere[3], J. Benito[12], G. Benzoni[13], A. Blazhev[7], A. Boso[4], S. Bottoni[13,14], M. Bunce[4], R. Chakma[1], N. Cieplicka-Oryńczak[15], S. Courtin[16], M. L. Cortés[17], P. Davies[18], C. Delafosse[1], M. Fallot[19], B. Fornal[15], L. Fraile[12], A. Gottardo[20], V. Guadilla[19], G. Häfner[1,7], K. Hauschild[1], M. Heine[16], C. Henrich[5], I. Homm[5], F. Ibrahim[1], Ł. W. Iskra[13,15], P. Ivanov[4], S. Jazrawi[3,4], A. Korgul[9], P. Koseoglou[5,21], T. Kröll[5], T. Kurtukian-Nieto[22], L. Le Meur[19], S. Leoni[13,14], J. Ljungvall[1], A. Lopez-Martens[1], R. Lozeva[1], I. Matea[1], K. Miernik[9], J. Nemer[1], S. Oberstedt[23], W. Paulsen[2], M. Piersa[9], Y. Popovitch[1], C. Porzio[13,14,24], L. Qi[1], D. Ralet[25], P. H. Regan[3,4], K. Rezynkina[26], V. Sánchez-Tembleque[12], S. Siem[2], C. Schmitt[16], P.-A. Söderström[5,27], C. Sürder[5], G. Tocabens[1], V. Vedia[12], D. Verney[1], N. Warr[7], B. Wasilewska[15], J. Wiederhold[5], M. Yavahchova[28], F. Zeiser[2] & S. Ziliani[13,14]

When a heavy atomic nucleus splits (fission), the resulting fragments are observed to emerge spinning[1]; this phenomenon has been a mystery in nuclear physics for over 40 years[2,3]. The internal generation of six or seven units of angular momentum in each fragment is particularly puzzling for systems that start with zero, or almost zero, spin. There are currently no experimental observations that enable decisive discrimination between the many competing theories for the mechanism that generates the angular momentum[4–12]. Nevertheless, the consensus is that excitation of collective vibrational modes generates the intrinsic spin before the nucleus splits (pre-scission). Here we show that there is no significant correlation between the spins of the fragment partners, which leads us to conclude that angular momentum in fission is actually generated after the nucleus splits (post-scission). We present comprehensive data showing that the average spin is strongly mass-dependent, varying in saw-tooth distributions. We observe no notable dependence of fragment spin on the mass or charge of the partner nucleus, confirming the uncorrelated post-scission nature of the spin mechanism. To explain these observations, we propose that the collective motion of nucleons in the ruptured neck of the fissioning system generates two independent torques, analogous to the snapping of an elastic band. A parameterization based on occupation of angular momentum states according to statistical theory describes the full range of experimental data well. This insight into the role of spin in nuclear fission is not only important for the fundamental understanding and theoretical description of fission, but also has consequences for the γ-ray heating problem in nuclear reactors[13,14], for the study of the structure of neutron-rich isotopes[15,16], and for the synthesis and stability of super-heavy elements[17,18].

[1]Université Paris-Saclay, CNRS/IN2P3, IJC Laboratory, Orsay, France. [2]Department of Physics, University of Oslo, Blindern, Oslo, Norway. [3]Department of Physics, University of Surrey, Guildford, UK. [4]National Physical Laboratory, Teddington, UK. [5]Technische Universität Darmstadt, Fachbereich Physik, Institut für Kernphysik, Darmstadt, Germany. [6]LPC Caen, Caen, France. [7]Institut für Kernphysik, Universität zu Köln, Cologne, Germany. [8]CEA/DAM Bruyères-le-Châtel, Arpajon, France. [9]Faculty of Physics, University of Warsaw, Warsaw, Poland. [10]IFIC, CSIC-University of Valencia, Valencia, Spain. [11]Institute for Nuclear Research (Atomki), Debrecen, Hungary. [12]Grupo de Fisica Nuclear & IPARCOS, Universidad Complutense de Madrid, CEI Moncloa, Madrid, Spain. [13]INFN, Milan, Italy. [14]Dipartimento di Fisica, Universitá degli Studi di Milano, Milan, Italy. [15]Institute of Nuclear Physics, Polish Academy of Sciences, Krakow, Poland. [16]Université de Strasbourg, CNRS, IPHC UMR 7178, Strasbourg, France. [17]RIKEN Nishina Center, Hirosawa, Japan. [18]School of Physics and Astronomy, University of Manchester, Manchester, UK. [19]Subatech, IMT-Atlantique, Université de Nantes, Nantes, France. [20]INFN Laboratori Nazionali di Legnaro, Legnaro, Italy. [21]GSI Helmoltzzentrum für Schwerionenforschung GmbH, Darmstadt, Germany. [22], Université de Bordeaux, CNRS, Gradignan, France. [23]European Commission, Joint Research Centre, Geel, Belgium. [24]TRIUMF, Vancouver, British Columbia, Canada. [25]Grand Accélérateur National d'Ions Lourds, Caen, France. [26]Institute for Nuclear and Radiation Physics, Katholieke Universiteit Leuven, Leuven, Belgium. [27]Extreme Light Infrastructure-Nuclear Physics, Horia Hulubei National Institute for Physics and Nuclear Engineering, Bucharest-, Măgurele, Romania. [28]Institute for Nuclear Research and Nuclear Energy, Bulgarian Academy of Sciences, Sofia, Bulgaria. ✉e-mail: jonathan.wilson@ijclab.in2p3.fr

The stability of heavy atomic nuclei is governed by a delicate balance between the Coulomb repulsion of the protons that attempt to deform the nucleus, the nuclear surface tension driving the nucleus towards spherical configurations, and quantum shell effects, which add extra stability for certain nuclear shapes. Fission occurs when there is a perturbation of this balance in favour of the Coulomb repulsion. It is an exothermic, dynamical process that begins as an instability in the nuclear shape, which, after passing the point of no return (the saddle point), becomes more and more elongated. The nascent fragments form a neck as they move rapidly apart, which quickly snaps (scission). Shell effects in the nascent fragments give rise to certain favoured mass splits, which for low-energy fission of actinide nuclei (typically containing about 240 nucleons) produces a light fragment of mass $A \approx 100$ and a heavy fragment of mass $A \approx 140$. After scission, the decay of each excited fragment is a statistical process. It initially proceeds through efficient removal of excitation energy via emission of typically 0–2 neutrons and 1–3 high-energy γ-rays. Subsequently, the emission of several more γ-rays, which usually carry away two units of angular momentum each, removes the majority of the angular momentum and the remaining excitation energy. This prompt de-excitation process ends at the fragment ground states, usually within a few nanoseconds[19].

There are many competing theories for how a fissioning nucleus generates its intrinsic angular momentum, and where in the above sequence of events it occurs. One class of explanations proposes that it arises from the excitation of collective vibrational modes such as bending, wriggling, tilting and twisting of the system before it splits (pre-scission). These theories suggest that the vibrations are either initiated by thermal excitations[4–6], arise from quantum fluctuations[7,8], or both[9]. Post-scission theories suggest that the angular momenta are generated either from Coulomb forces[10] or from deformed fragments that have coupled orientations[11,12]. Since the angular momentum is quickly carried away by the γ-rays, the experimental study of the generation mechanism necessarily involves detailed observation of the prompt γ-ray emission.

Experimental attempts to understand the intrinsic spin generation started with low-resolution detection of prompt fission γ-rays correlated with the indirect detection (plastic scintillator[20] and surface barrier detectors[21]) of fragment mass, which revealed saw-tooth shapes in the γ-ray yields that are strongly related to spin. The major difficulty was the separation of γ-rays emitted from the two fragments, and the existence of these patterns was called into question in a later experiment where no saw-tooth pattern was observed[22]. Another experimental approach involves spectroscopy of isomeric (long-lived) excited states found in certain nuclei. Measurements of isomer population are highly sensitive to small relative changes in spin. However, only a small subset of all the isotopes produced in fission have such isomeric states and it is difficult to measure trends over a large range in mass[23]. In this work, we use a third technique[24] based on high-resolution spectroscopy, which allows both separation of γ-rays from the two fragments and the study of trends over large mass ranges.

To probe intrinsic generation of angular momentum also requires systems with initial spin of zero or almost zero, namely spontaneous fission or neutron-induced fission. Heavy-ion or charged-particle-induced fission reactions are unsuitable because they generate high initial angular momenta[25], which can obscure the origin of the intrinsic spin.

We present here unique and extensive experimental data obtained from fission experiments carried out at the ALTO facility of the IJC Laboratory in Orsay, France, with the LICORNE directional neutron source[26,27] coupled to the high-performance ν-Ball γ-ray spectrometer[28]. We carried out high-resolution spectroscopy of fast-neutron-induced fission of ^{232}Th and ^{238}U, and the spontaneous fission of ^{252}Cf with the addition of an ionization chamber[29].

Results

For each of the three systems studied we identified characteristic γ-ray decay patterns of excited states in around 30 even–even nuclei (with even numbers of both protons and neutrons). For each even–even fission fragment we extracted the average spin after neutron emission using a method developed at the University of Manchester[24], which combines all the available γ-ray transition intensity and coincidence information (see Methods).

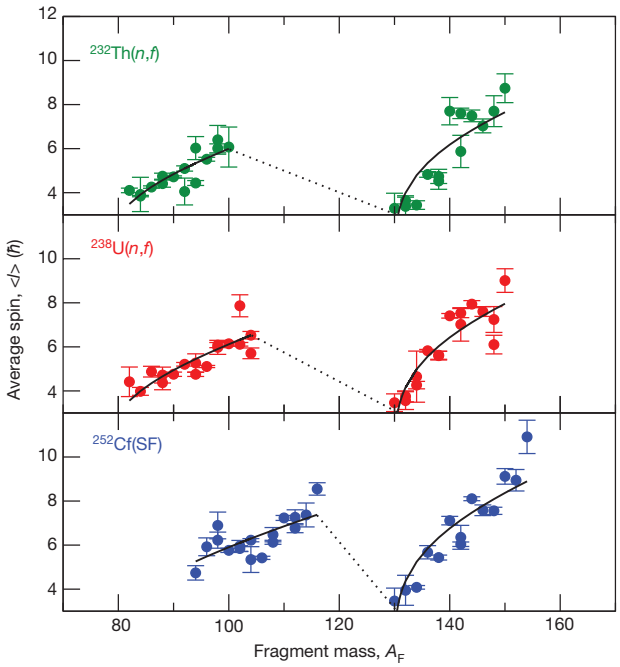

Fig. 1 | Dependence of average spin on fragment mass. Average spins extracted for even–even nuclei produced in fast-neutron-induced fission of ^{232}Th, ^{238}U and the spontaneous fission of ^{252}Cf are presented along with statistical uncertainties (error bars represent ±1 standard deviation, s.d.). Single-parameter fits to the data are shown in black lines. The fitting parameterization developed to explain the mechanism that generates angular momentum is presented in the section 'Discussion'.

Our results (Fig. 1) definitively confirm that fragment spins vary strongly as a function of fragment mass in saw-tooth distributions, similar to the patterns previously observed in γ-ray yields[20,21]. We note that a given fragment spin appears to depend only on the fragment mass, with no observable relationship to the mass of the system that emits it nor to the mass or charge of the partner nucleus with which it emerged. This observation does therefore not support theoretical explanations based on post-scission Coulomb effects[10], where a dependence of spin on the product of the fragment charges, Z_1Z_2, would be expected.

Additionally, large asymmetries in average spin are observed for certain fragment pair combinations (for example, ^{86}Se and ^{150}Ce from ^{238}U(n,f)), where the spin of the heavy fragment can be more than double that of its light partner. The existence of such asymmetries does not support the post-scission explanation based on coupled orientations of deformed fragments[11,12], which explicitly predicts spins of equal magnitudes. Indeed, the existence of such large spin asymmetries provokes the question of how spin generation could possibly occur pre-scission if the fragments are in contact and participating in a correlated collective motion. In that case, expected fragment spins at scission would be $+I$ and $-I$ units. To investigate further, we studied the correlation between spins of the most strongly populated fragments in the ^{238}U(n,f) reaction. For a given nucleus, γ-ray transitions of increasing spin were selected from its partner nucleus, constraining the partner population to higher and higher spins. We then examined how the average spin of the given nucleus evolved in response (Fig. 2). For example, the most strongly populated partner nucleus of ^{96}Sr is ^{140}Xe.

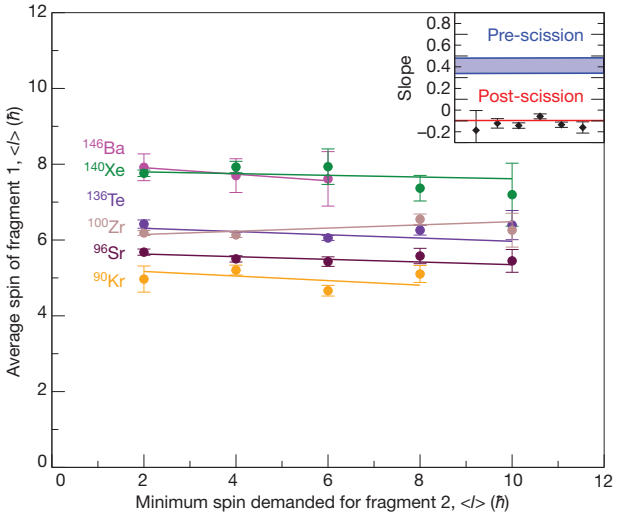

Fig. 2 | Correlation between fragment spins. Correlations between fragment and partner spins for the six most strongly populated fragments in the ^{238}U(n,f) reaction with associated statistical uncertainties (error bars represent ±1s.d.). Weighted linear fits to the data points for each nucleus are shown. The fitted slopes are compared to the expected slopes for the spin mechanisms pre-scission with correlated spins ('Pre-scission') or post-scission with uncorrelated spins ('Post-scission') in the inset. The blue band ('Pre-scission') was determined from Monte-Carlo simulations of the de-correlating effects of the neutrons and statistical γ-rays (see Methods and Extended Data Fig. 3).

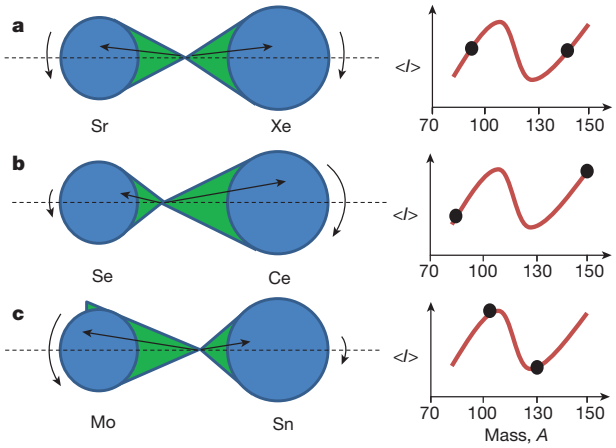

Fig. 3 | Schematic diagram of post-scission angular momentum generation. Independent torques for different scission configurations are shown, with neck nucleons displayed in green. The straight black arrows illustrate sizes and example directions of the linear momentum vectors that generate the associated angular momenta. The corresponding positions on the saw-tooth distribution of the resulting average spins are shown on the right.

By demanding observation of a γ-ray emitted from the lowest 8^+ state in ^{140}Xe we constrain this nucleus to be populated with average spins of higher than 8 units of angular momentum. The corresponding average spin in ^{96}Sr is deduced by measuring the corresponding coincident γ-ray intensities. By varying the spin conditions and the isotopes studied, we obtain the fragment spin correlations.

The observed slopes are clearly consistent with zero, suggesting an uncorrelated, post-scission spin-generation mechanism. The overall slope from the combined data is within a 2σ confidence interval of [−0.04, 0.01], compatible with no significant correlation between fragment spins and incompatible with correlated pre-scission spin generation. The data do not support pre-scission theoretical explanations[4–9], confirming what was suspected from the large spin asymmetries (Fig. 1). It appears that each fragment has no 'knowledge' of the spin generated in its partner.

This unexpected conclusion may resolve the historical controversy surrounding previous experimental results[20–22]. For fragment spins that are generated independently, the event-by-event correlations measured in ref. [22] would not be expected to generate a saw-tooth pattern in the γ-ray yield measurements. Hence, this absence of the saw-tooth pattern may support rather than contradict our current findings.

Discussion

A post-scission, uncorrelated origin of angular momentum suggests that the fragments have become two separate, independent quantal systems. This can be viewed from both macroscopic and statistical/single-particle points of view.

Post-scission generation of two independent torques

Macroscopically, we suggest that fragments acquire their spin in a process analogous to the snapping of an elastic band. A neck forms between the two emerging fragments, which undergoes first a stretching, then a rupture and finally a relaxation during which the potential energy from the deformed neck (analogous to stretched elastic) transforms into kinetic energy. For asymmetric fission of the actinide nuclei we assume a double cluster, with the cores of the nascent fragments lying near doubly closed shells and the remaining nucleons from the neck shared between them after rupture (Fig. 3).

We suggest that the nucleons from both halves of the ruptured neck drive the generation of angular momentum in each fragment. The relative sizes of torques will depend on the number of neck nucleons and thus the precise location of the neck rupture, that is, the configuration at scission. Classically, the neck would rupture in the middle at its weakest point. However, in the subatomic world a gap can appear at any point[30], with decreasing probabilities for more extreme partitions. We suggest that how the system arrives at a specific scission configuration will not have any subsequent impact on the generation of post-scission spin and that the fragments retain no 'memory' of their formation after scission.

At scission, the former neck nucleons are located far from the centres of mass of the newly born fragments in two very elongated configurations. Such extreme elongations have large surface energies, which provide the restoring forces towards more spherical shapes. Fluctuations in the aggregate direction of motion of these former neck nucleons generate the two independent torques. Small angular deviations from the fission axis of the collective nucleon motion must occur, owing to Heisenberg's uncertainty principle for spin/orientation of a system[31]. Uncertainties in the direction of the resulting linear momentum along the fission axis will result in small perpendicular components that will generate a distribution of angular momenta. Angular momenta in both fragments will point in a plane perpendicular to the fission axis, consistent with previous experiments[1], although there will be no correlation or constraint on their relative orientations. The resulting orbital angular momentum, $\mathbf{I}_o$, of the fragments with respect to each other, generated by the components of the motion perpendicular to the fission axis, ensures the conservation of the total angular momentum: $\mathbf{I}_1+\mathbf{I}_2+\mathbf{I}_o=\mathbf{0}$.

The dramatic fragment shape-change from elongated to more spherical shapes will also generate heat as the surface energy converts into internal excitation energy, setting the stage for subsequent evaporation of neutrons. Angular momentum, excitation energy and emitted neutron multiplicity will thus be strongly correlated with each other.

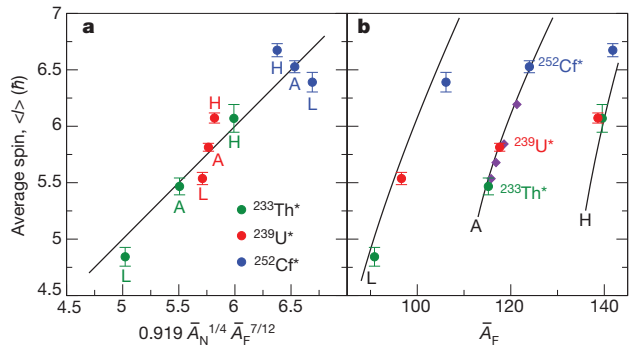

Fig. 4 | Relationship between average fragment spins and average masses. Fragment yield-averaged data with statistical uncertainties (error bars represent ±1s.d.) are shown. **a**, Data are compared to predictions from the parameterization for the three fissioning systems, with light peak (L), heavy peak (H) and average for the system (A) marked. The superscripts are the exponents in the fitting function of equation (2); see also Extended Data Fig. 4. **b**, The same data are plotted as a function of the average fragment mass $\bar{A}$ with the black lines showing predictions for other systems from the parameterization. Purple diamonds show specific predictions for the major fissile isotopes, ^{233,235}U, ^{239}Pu and in addition, ^{245}Cm. The asterisks conventionally denote that the nucleus is a compound nuclear system, thus indicating the absorption of a neutron in the cases of ^{238}U + n = ^{239}U* and ^{232}Th + n = ^{233}Th*. However, ^{252}Cf* has not absorbed a neutron since it undergoes spontaneous fission.

Indeed, similar saw-tooth distributions are known to occur in average neutron multiplicities as a function of fragment mass[32,33].

Comparison of the variation in average spins to that expected from statistical theory

In the statistical/single-particle view, if the newly formed fragments are independent, then their excited states would be expected to have an angular momentum occupation according to statistical theory. For an excited nucleus, the probability distribution, $P(I)$, of angular momenta, I, was first derived by Hans Bethe[34] and is expected to be:

$$P(I|\sigma^2) = \frac{2I+1}{2\sigma^2}\exp\left(-\frac{(I+1/2)^2}{2\sigma^2}\right) \quad (1)$$

where σ is known as a spin-cutoff parameter describing the width of this distribution and is directly related to the average spin value, $I \approx 1.15\sigma$. From statistical theory (see Methods) we derive a smooth parameterization that can be tested for compatibility with our average spin data (Fig. 1):

$$I = c\,A_N^{1/4}\,A_F^{7/12} \quad (2)$$

where c is a constant and the only free fitting parameter, A_F is the fragment mass, and A_N is the mass of neck nucleons. For light and heavy fragments we use values of $A_N = (A_F - 78)$ and $A_N = (A_F - 130)$ near the doubly magic Ni and Sn shell closures. The derivation presented here has limitations and is not intended as a full description, but as an illustration of the idea (see Methods). An extended theoretical description would involve more complex dependencies of the parameters owing to structure effects.

Six independent fits using the above parameterization for each light and heavy peak in the three different systems were performed. The fitted constants are remarkably similar, with a mean of $c = 0.196$ and standard deviation of $\sigma_c = 0.009$, a relative variation of only about 4%, suggesting that the fragment spins fall on a universal curve. This simple parameterization thus appears to capture the main ingredients of the spin–mass relationship. We conclude that the experimentally observed variation in the average spins is thus consistent with what is expected from statistical theory for a post-scission, uncorrelated, spin-generation mechanism. There may be other second-order effects (for example, Coulomb forces) that are not yet accounted for, but these are clearly small.

A concise suggestion for the mechanism that generates the intrinsic angular momentum in the light of our data is as follows, although we recognize that other interpretations may also be possible. A fissioning nucleus that starts with zero or near-zero spin undergoes: (i) unstoppable shape instability from Coulomb forces; (ii) formation of a neck between the two emerging fragment clusters; (iii) neck stretching and rupture (scission) with the birth of two deformed, newly independent quantal systems; (iv) shape relaxation of each fragment as the surface potential energy converts to excitation of the internal nucleonic degrees of freedom; (v) the resulting occupation of different angular momentum states occurring in accordance with statistical theory for two independent excited nuclei. In the equivalent macroscopic picture, the last two steps can also be seen as: (iv) a shape relaxation where aggregate collective motions of the nucleons have off-axis components generating two independent torques; (v) the statistical distributions of torques creates two independent distributions of spin.

Consequences

Understanding the angular momentum generated in fission is important for fundamental reasons, but also has consequences for other fields. In nuclear energy applications, fragment spin is related to reactor γ-ray heating effects[13,14], either through the number of prompt γ-rays that transport it during reactor operation, or the delayed γ-rays from isomeric states that contribute to the decay heat after reactor shutdown. For these reasons, many recent measurements of prompt γ-ray characteristics, such as the average multiplicity M_γ, have been carried out[35–37]. At present, only purely empirical connections between these characteristics and the mass of the fissioning system have been made[38]. However, we are now able to understand better the underlying fundamental relationships if we combine our data with known fragment yield information (Fig. 4). Here, we manage to relate two independent average quantities, the mass and the spin, for light, heavy and average fragment masses, and use our parameterization to make predictions for other systems.

We also note that fission is a production mechanism used to study the structure of exotic nuclei[15,16]. Thus, understanding spin generation will allow determination of which excited nuclear states can be accessed. Finally, outside the actinide region of the periodic table, fragment-yield distributions evolve as a result of the changing influence of shell closures. For example, a transition from asymmetric to symmetric fission occurs for nuclei beyond ^{258}Fm (ref. [39]). In the recently discovered region of β-delayed fission[40] around ^{180}Hg, the shell effects that drive the configuration at scission are not well understood. For fission regions that are less well explored, measurements of spin-sensitive γ-ray data could yield valuable information on neck formation and the relevant shell closures involved.

Conclusion

A full theoretical description of nuclear fission requires the incorporation of the mechanism that generates intrinsic angular momentum. We have presented extensive experimental data on fragment spins in different systems from which it is now finally possible to discriminate between the many competing theoretical explanations of this mechanism. We show that fragment spins are uncorrelated, revealing the post-scission nature of the mechanism. Theoretical explanations based on pre-scission collective vibrations[4–8], post-scission Coulomb excitations[10] or coupling through fragment deformations are not supported by our data[9,11]. A parameterization based on the expected occupation of

spin states according to statistical theory describes the experimentally observed mass dependence of average spins well.

Online content

Any methods, additional references, Nature Research reporting summaries, source data, extended data, supplementary information, acknowledgements, peer review information; details of author contributions and competing interests; and statements of data and code availability are available at https://doi.org/10.1038/s41586-021-03304-w.

1. Wilhelmy, J. B., Cheifetz, E., Zared, R. C., Thompson, S. G. & Bowman, H. R. Angular momentum of primary products formed in the spontaneous fission of ^{252}Cf. *Phys. Rev. C* **5**, 2041 (1972).
2. Schmidt, K.-H. & Jurado, B. Review on the progress in nuclear fission—experimental methods and theoretical descriptions. *Rep. Prog. Phys.* **81**, 10630 (2018).
3. Andreyev, A. N., Nishio, K. & Schmidt, K.-H. Nuclear fission: a review of experimental advances and phenomenology. *Rep. Prog. Phys.* **81**, 016301 (2018).
4. Rasmussen, J. O., Nörenberg, W. & Mang, H. J. A model for calculating the angular momentum distribution of fission fragments. *Nucl. Phys. A* **136**, 465 (1969).
5. Moretto, L. G. & Peaslee, G. F. & Wozniak, G. J. Angular-momentum-bearing modes in fission. *Nucl. Phys. A* **502**, 453 (1989).
6. Mişicu, S., Săndulescu, A., Ter-Akopian, G. M. & Greiner, W. Angular momenta of even-even fragments in the neutronless fission of ^{252}Cf. *Phys. Rev. C* **60**, 034613 (1999).
7. Shneidman, T. M. et al. Role of bending mode in generation of angular momentum of fission fragments. *Phys. Rev. C* **65**, 064302 (2002).
8. Gönnenwein, F., Tsekhanovich, I. & Rubchenya, V. Angular momentum of near-spherical fission fragments. *Int. J. Mod. Phys. E* **16**, 410–424 (2007).
9. Bonneau, L., Quentin, P. & Mikhailov, A. N. Scission configurations and their implication in fission-fragment angular momenta. *Phys. Rev. C* **75**, 064313 (2007).
10. Hoffman, M. M. Directional correlation of fission fragments and prompt gamma rays associated with thermal neutron fission. *Phys. Rev.* **133**, B714 (1964).
11. Mikhailov, I. N. & Quentin, P. On the spin of fission fragments, an orientation pumping mechanism. *Phys. Lett. B* **462**, 7 (1999).
12. Bertsch, G. F., Kawano, T. & Robledo, L. M. Angular momentum of fission fragments. *Phys. Rev. C* **99**, 034603 (2019).
13. Rimpault, G. et al. Needs of accurate prompt and delayed γ-spectrum and multiplicity for nuclear reactor designs. *Phys. Proc.* **31**, 3–12 (2012).
14. Lemaire, M., Vaglio-Guadard, C., Lyoussi, A. & Reynard-Carette, C. For a better estimation of gamma heating in nuclear material-testing reactors and associated devices: status and work plan from calculation methods to nuclear data. *J. Nucl. Sci. Technol.* **52**, 9 (2015).
15. Dudouet, J. et al. ^{96}Kr–low-Z boundary of the island of deformation at N=60. *Phys. Rev. Lett.* **118**, 162501 (2017).
16. Ha, J. et al. Shape evolution of neutron-rich ^{106,108,110}Mo isotopes in the triaxial degree of freedom. *Phys. Rev. C* **101**, 044311 (2020).
17. Zagrebaev, V. I., Aritomo, Y., Itkis, M. G., Oganessian, Yu. Ts. & Ohta, M. Synthesis of superheavy nuclei: how accurately can we describe it and calculate the cross sections? *Phys. Rev. C* **65**, 014607 (2001).
18. Itkis, M. G., Vardaci, E., Itkis, I. M., Knyazhev, G. N. & Kozulin, E. M. Fusion and fission of heavy and superheavy nuclei (experiment). *Nucl. Phys. A* **944**, 204–237 (2015).
19. Talou, P. et al. Late-time emission of prompt fission γ rays. *Phys. Rev. C* **94**, 064613 (2016).
20. Armbruster, P., Labus, H. & Reichelt, K. Investigation on the primary spins of the ^{235}U fission fragments. *Z. Naturforsch.* **26a**, 512–522 (1971).
21. Pleasonton, F. Prompt γ-rays emitted in the thermal-neutron induced fission of ^{233}U and ^{239}Pu. *Nucl. Phys. A* **213**, 413–425 (1973).
22. Glässel, P., Schmid-Fabian, R. & Schwalm, D. ^{252}Cf fission revisited—new insights into the fission process. *Nucl. Phys. A* **502**, 315–324 (1989).
23. Naik, H., Dange, S. P. & Singh, R. J. Angular momentum of fission fragments in low energy fission of actinides. *Phys. Rev. C* **71**, 014304 (2005).
24. Abdelrahman, Y. et al. Average spins of primary fission fragments. *Phys. Lett. B* **199**, 504–508 (1987).
25. Boutoux, G. et al. Study of the surrogate-reaction method applied to neutron-induced capture cross sections. *Phys. Lett. B* **712**, 319–325 (2012).
26. Lebois, M. et al. Development of a kinematically focused neutron source with the p(^{7}Li,n)^{7}Be inverse reaction. *Nucl. Instrum. Meth. Phys. Res. A* **735**, 145–151 (2014).
27. Wilson, J. N. et al. The LICORNE neutron source and measurements of prompt γ-rays emitted in fission. *Phys. Proc.* **64**, 107–113 (2015).
28. Lebois, M. et al. The ν-ball spectrometer. *Nucl. Instrum. Meth. Phys. Res. A* **960**, 163580 (2020).
29. Gaudefroy, L. et al. Impact of Coriolis mixing on a two-quasi-neutron isomer in ^{164}Gd and other N=100 isotones. *Phys. Rev. C* **97**, 064317 (2018).
30. Brosa, U., Grossmann, S. & Müller, A. Nuclear scission. *Phys. Rep.* **197**, 167–262 (1990).
31. Franke-Arnold, S., Barnett, S. M., Leach, J., Courtial, J. & Padgett, M. Uncertainty principle for angular position and angular momentum. *New J. Phys.* **6**, 103 (2004).
32. Terrell, J. Neutron yields from individual fission fragments. *Phys. Rev.* **128**, 2925 (1962).
33. Göök, A., Hambsch, F. & Vidali, M. Prompt neutron multiplicity in correlation with fragments from spontaneous fission of ^{252}Cf. *Phys. Rev. C* **90**, 064611 (2014).
34. Bethe, H. A. An attempt to calculate the number of energy levels of a heavy nucleus. *Phys. Rev.* **50**, 332 (1936).
35. Oberstedt, A. et al. Improved values for the characteristics of prompt-fission γ-ray spectra from the reaction ^{235}U(n_{th},f). *Phys. Rev. C* **87**, 051602(R) (2013).
36. Chyzh, A. et al. Systematics of prompt γ-ray emission in fission. *Phys. Rev. C* **87**, 034620 (2013).
37. Qi, L. et al. Statistical study of the prompt-fission γ-ray spectrum for ^{238}U(n, f) in the fast-neutron region. *Phys. Rev. C* **98**, 014612 (2018).
38. Valentine, T. E. *Evaluation Of Prompt Fission Gamma Rays For Use In Simulating Nuclear Safeguard Measurements*. Oak Ridge National Laboratory Report TM-1999/300, https://www.osti.gov/servlets/purl/753485-4TSmOw/webviewable/ (US Department of Energy Office of Scientific and Technical Information, 2001).
39. Flynn, K. F. et al. Distribution of mass in the spontaneous fission of ^{256}Fm. *Phys. Rev. C* **5**, 1725 (1972).
40. Andreyev, A. et al. New type of asymmetric fission in proton-rich nuclei. *Phys. Rev. Lett.* **105**, 252502 (2010).

Methods

Experimental setup

Samples of ^{238}U (81 g) and ^{232}Th (129 g) were irradiated with a pulsed neutron beam from the LICORNE neutron source (400-ns period) in the centre of the v-Ball spectrometer for total acquisition times of 216 h and 450 h, respectively. The average neutron energy that provoked fission was 1.9 MeV. Triggerless data from the 184 detectors in the v-Ball array were written to disk at high data rates of typically 1–3 million γ-ray hits per second, and processed later offline. Each detected γ-ray energy was associated with a unique 64-bit time stamp accurate to sub-nanosecond precision, thanks to the state-of-the-art FASTER digitization system[41]. γ-ray coincidence events were identified offline with a minimum trigger condition defined as at least two unsuppressed high-resolution germanium (Ge) detectors and at least one other detector module (bismuth germinate (BGO) or $LaBr_3$) firing within a short 80-ns time window. These events were subsequently sorted into two- and three-dimensional histograms for further offline analysis. An additional dataset was gathered from the ^{252}Cf spontaneous fission source inside an ionization chamber[29] placed in the centre of the v-Ball array for 52 h. With this latter setup, one fragment was detected in-flight, while the other fragment was stopped in the backing of the sample.

Data analysis

Examples of γ-ray coincidence spectra are shown in Extended Data Fig. 1 and Extended Data Fig. 2, which support the main findings of the Article. The lack of dependence of the ^{140}Xe intensity pattern on the fissioning system is shown in Extended Data Fig. 1, and the lack of correlation between ^{140}Xe and ^{96}Sr fragment intensity patterns is shown in Extended Data Fig. 2.

The main experimental data on average spins after neutron emission presented in this Article rely on a method initially developed at Manchester University in the late 1980s and described fully in ref. [24]. It will henceforth be referred to as the Manchester Spin Method (MSM).

The MSM relies on measuring the relative intensity of every resolvable γ-ray transition for a given nucleus populated in the reaction of interest. At each level with spin I, the intensity difference between the observed ingoing and outgoing transitions is computed. This difference is defined as the direct side-feeding, S, of the state. The average spin populated is therefore the side-feeding-weighted average of the level spins over all n levels, $\langle I \rangle = \sum_{i=1..n} I_i S_i / \sum_{i=1..n} S_i$. A further small correction in the result is necessary to account for the angular momentum carried away by the statistical transitions, which depends on the reaction and is deduced from γ-ray decay models at around one extra unit in the case of fission.

The MSM condenses all the available γ-ray intensity and coincidence data for a given nucleus into a single number: the average spin after neutron emission. It is thus a powerful experimental tool with which to study angular momentum effects in nuclear reactions. The method measures a cumulative intensity flow through many different excited states, all of which will eventually reach the ground state. There is a redundancy in the measured information and the method has a low sensitivity to individual γ-ray intensities (that is, a large perturbation in the intensity value of any particular γ ray from the decay pattern has a small impact on the result). For example, the inclusion or exclusion of the intensities of transitions from states other than those with the lowest energy for a given spin (so-called yrast states) levels in the calculation is seen to have very little impact on the result (see Methods section 'Non-inclusion of weaker transitions'). If the yrast sequence of transitions is observed, then an average spin can be extracted from the data.

We note that the first experiment where the MSM was applied used only 12 Compton suppressed small-volume Ge detectors to study heavy-ion induced fission. In this work, we measure neutron-induced fission with a high-performance third-generation γ-ray spectrometer with 106 large-volume, Compton-suppressed Ge crystals (that is, γ-rays that scatter out of the Ge crystal and into the surrounding BGO scintillator are vetoed) and state-of-the-art, triggerless signal digitization technology.

Application of the MSM to v-Ball data

We measured the average spin in around 30 even–even nuclei in each system (see Extended Data Tables 1, 2 and 3). Even–even nuclei have relatively simple, well known decay schemes and are generally much easier to study. Even–odd and odd–odd isotopes often have highly fragmented decay patterns with many low-energy transitions, which are difficult to detect. The presence of a neutron beam pulsation, or—as for the case of the spontaneously fissioning ^{252}Cf(SF)—direct detection of one of the fission fragments in the ionization chamber, is crucial for distinguishing between γ rays from prompt fission and those from subsequent fragment β-decays. This latter source of γ rays is usually associated with low multiplicity events ($M_\gamma \approx 2$–3), but for certain isotopes can be comparable to that of fission. Emission of γ-rays after β-decays is uncorrelated in time, whereas 95% of prompt fission γ-rays are emitted within a few nanoseconds of the beam pulse or fission event. Without the beam pulsation, γ-rays from β-decay and prompt fission events are difficult to discriminate. This can lead to difficulties in extracting fragment average spin from intensity measurements, since population of nuclei via both processes occurs. The closer to stability the nucleus, the more of a problem this represents. ^{252}Cf(SF) has been extensively studied with spectroscopy over the last twenty years[42,43] but mostly from datasets without direct fission fragment detection, where the primary focus has been on extending knowledge on the nuclear structure of exotic neutron-rich nuclei. Spin effects in ^{252}Cf(SF) may have been difficult to study without an ability to discriminate γ-rays from fission and β-decay.

γ-ray coincidence data and efficiency calibrations

Application of the MSM requires determination of the γ-ray full energy peak detection efficiency over a wide range of energy: 100 keV to 5 MeV. Each of the three systems studied (^{232}Th, ^{238}U, ^{252}Cf) has its own unique efficiency curve owing to different target/chamber geometries producing slightly different self-shielding effects at lower energies. These were determined by combining GEANT IV[44] simulations of the setup for the highest-energy part (2–5 MeV), source measurements, and measurements from the fission coincidence data for the lowest-energy part (100–500 keV). For the lowest part of the energy range, self-shielding effects in the massive ^{232}Th and ^{238}U targets are particularly important, and are difficult to simulate owing to the complex, non-uniform distribution of fissions within these targets. The drop in efficiency below 200 keV is substantial and is measured from the experimental data by gating on γ-ray yrast cascades in rotational nuclei (for example, Ce and Mo) from above and measuring efficiency ratios for the transitions below. Uncertainties on these efficiencies are included in the data analysis for the measurement of γ-ray intensities and in the subsequent deduction of average spins after neutron emission.

Fitting procedures

Global fits of many thousands of γ-ray coincidences were performed in two dimensional (2D) γ–γ coincidence matrices using the Radware software package[45]. Two dimensional analysis is essential to measure 4+ state side-feedings. Since many nuclei share similar transition energies, a global 2D fitting procedure is needed for accurate measurements of transition intensities. Odd–even and odd–odd nuclei also need to be included so that all the possible coincidences can be identified in a particular matrix slice or region. Level scheme information from the evaluated ENSDF libraries[46] containing level spins, excitation energies, transition energies and coincidence relationships are used as the starting point for each nucleus. Peak width parameters are fixed from a pre-determined width calibration as a function of energy.

The intensities, G_k, and energies of the observable transitions are then fitted simultaneously for all nuclei in a global fit with thousands of free parameters. Subsequent local fits for each nucleus are then performed to check convergence at the local level, with global parameters fixed and only local parameters free to vary. Global and local fits are then repeated iteratively until convergence is achieved. At each stage, Radware calculates a χ^2/degrees of freedom, which is used to verify and assure convergence for each nucleus. Additionally, Radware also allows for powerful visual comparisons between the fitted γ-ray coincidences and the experimental spectral data. This facilitates a large number of visual checks to ensure the level scheme of each fragment is correctly fitted and the local fit has fully converged. Global fits serve only as second-order corrections to fit properly the rare occasions when one fragment contains a pair of transitions of similar energies to those in another fragment.

To process the results of the fitting procedure and to extract side-feedings and average spins for each nucleus, new software has been developed that operates on the fitted intensity and peak position output from Radware. The side-feeding S_i of each level is computed from the sum of all observable transition intensities, G_k, feeding in and out of each level.

The software checks the level scheme transition intensities for self-consistency. Negative side-feedings are unphysical and if detected may signal a potential problem with the fitting of transitions feeding in or out of a particular level. Finally, the code computes the average spin for each nucleus studied by combining the level spins I_i and the side-feeding S_i information $\langle I \rangle = \sum_{i=1..n} I_i S_i / \sum_{i=1..n} S_i$.

Propagation of uncertainties and variance-covariance

The computed statistical uncertainty on the intensity of a particular transition is dependent on statistical variations in the number of counts at coincident peak positions in two dimensions. A relative uncertainty in the level of background of 5% is assumed along with a typical relative uncertainty in the detection efficiency of 3%. For transitions below 200 keV the relative uncertainty on the detection efficiency rises to 20% owing to the substantial drop in detection efficiency over this energy range.

To determine the uncertainties on the extracted average spins <*I*>, the uncertainties on the fitted experimental intensity data are propagated through the MSM. However, the intensities, G_k, and side-feedings, S_i, are not necessarily independent and correlations may exist between these parameters. Therefore, correct mathematical treatment of error propagation requires the incorporation of potential correlated sources of uncertainty. Analysis of variances and covariances are needed first for the intensities, G_k, to determine the uncertainties on the S_i and then for the side-feedings to determine the error on average spin $\sigma_{\langle I \rangle}$ in the following way:

$$\sigma^2_{\langle I \rangle} = \sum_{i=1..n} I_i^2 \sigma^2(S_i) + \sum_{i=1..n} \sum_{j=1..n\ (i \neq j)} I_i I_j \operatorname{cov}(S_i, S_j)$$

where $\operatorname{cov}(S_i, S_j)$ is the matrix of covariances.

Given that the ν-Ball detector array uses Ge detectors with excellent resolution, a high detector granularity, and a 'low' overall efficiency (~5%), the vast majority of covariances between intensity parameters are zero. Within the same level scheme, the off-diagonal elements of the variance-covariance matrix are typically (<0.05), so the independence of the G_k values can be considered a realistic assumption. However, the same cannot be said of the S_i values, which are computed from intensity differences between neighbouring transitions in the scheme. The adjacent side-feedings S_i are thus strongly correlated with each other, giving rise to both large negative and positive off-diagonal elements in the corresponding covariance matrix (about |0.4–0.8|). To perform the propagation requires the computation of a covariance matrix $\operatorname{cov}(S_i, S_j)$ for each data point of <*I*>. This is complex and laborious, and given the number of data points, each one derived from a separate level scheme and having its own unique set of coincidence relationships, this procedure for uncertainty calculation is challenging.

A more practical method for obtaining good estimates of the statistical errors associated with each average <*I*> is to fit the side-feeding distribution as in Extended Data Fig. 4 and use the resulting uncertainty on the fitted average of this distribution. Here, there may be some small dependence of the uncertainty on the exact form of the fitting function chosen. This procedure for uncertainty estimation yields uncertainties comparable in size to the application of variance–covariance analysis.

Using the example of the ^{238}U(n,f) coincidence data, the observable intensities vary from the strong, for example, ^{140}Xe $4^+ \rightarrow 2^+$ at 3.42(11)% of the total yield, to the very weak $14^+ \rightarrow 12^+$ in ^{150}Ce at 0.024(16)% of the total yield. The median relative statistical uncertainties on transition intensities from the global fit is 13%, and for level side-feedings is 24%. This gives rise to a typical relative average spin uncertainty of around 5%.

Sensitivity of the MSM

The level of accuracy, or sensitivity, of the MSM is an important question. To what extent are side-feeding distributions measured at or near the yrast line distorted by local quirks of the nuclear structure, leading to non-statistical inaccuracies in the average spin measurement for a particular nucleus? There are two empirical answers to this question, as follows. The first is addressed by the sensitivity analysis of the method to the inclusion or exclusion of non-yrast states (root-mean-square average difference 5.9%). This implies a potential variation in the sensitivity of the method in the range of 0.3$\hbar$–0.6$\hbar$ owing to the degree of incompleteness of the spectroscopic information.

A second estimation of the sensitivity, or accuracy, of the MSM can be obtained from analysis of the non-statistical variations of the data points around the fitted trends. The correlation coefficients obtained from the fits (see Extended Data Table 4) have values of typically $R^2 = 0.85$, implying that ~15% of the variation is not accounted for by the fit. The statistical uncertainties account for an additional ~5% of the variation (for example, a root-mean-square average of 5.5% for the ^{238}U(n,f) reaction). Hence ~10% of the variation of the variation remains unaccounted for. This can originate from three sources: second-order physics effects not included in the smooth parameterization, local spin mis-assignments/errors in the literature level scheme information, and local biases due to peculiarities of the local nuclear structure. The trend is measured over a range of approximately 4$\hbar$–10$\hbar$ and hence we deduce that in the worst case, the sensitivity of the method is in the range 0.4$\hbar$–1.0$\hbar$.

Corrections applied in the MSM

The MSM involves some further small corrections due to possible residual coincidences from β-decay, for the side feeding of the first 2^+ state, for the presence of isomeric states, and finally for statistical transitions from the continuum of unresolved non-yrast states. The correction methods are outlined below, followed by a description of how a transition intensity can be deduced indirectly, if it cannot be obtained directly or accurately fitted.

***β*-decay.** The experimental conditions were arranged to strongly suppress β-decay, achieved by tagging one fission fragment in the ionisation chamber for ^{252}Cf(SF) and by pulsation of the neutron beam with 400-ns period in the cases of ^{232}Th(n,f) and ^{238}U(n,f). Additional corrections were employed to remove any residual γ-ray coincidences from β-decay in the neutron-induced reaction data by subtracting an uncorrelated background. Background coincidence matrices were created using a pre-prompt trigger window 200 ns before a beam pulse of exactly the same size as the prompt window (80 ns). Typically, the correction applied is very small, since these matrices contained only 1–2% of the total counts of the prompt matrices, yet these subtractions are potentially important for the fragments closest to stability towards

the end of the β-decay chains in fission (for example, ^{98}Zr, ^{142}Ba, and so on). γ-ray coincidences from these nuclei will have larger components produced by this unwanted population process. If the correction is not applied this could lead to underestimates of the average spin in these particular nuclei owing to the presence of unwanted β-decay population pathways at lower spins.

Determination of the side-feeding of the first 2^+ state. The side feeding of the first excited state (2^+ in almost all even–even nuclei) cannot be measured directly from the γ–γ coincidences of a particular nucleus. However, as noted in the original MSM paper[29], it is possible to determine this side-feeding by selecting a strong transition in a partner fragment. The intensity ratio of the transition from the first excited state to the ground state, and the transition(s) feeding the first excited state can then be measured from the resulting spectrum and uncertainty determined. This ratio, labelled $G_{(2/4)}$ and shown in Extended Data Tables 1 and 2, is always greater than or equal to unity, since negative side-feedings are unphysical.

These ratios cannot be determined directly for all of the fragments studied, either because they and their partners are weakly populated, or because in some cases the transition energy is a doublet common to both fragment and partner, or to two neighbouring partners. We therefore fit the trends of $G_{(2/4)}$ ratios as a function of fragment mass in the light and heavy peaks for both the ^{232}Th and ^{238}U, and use the fitted values with appropriate uncertainties. The $G_{(2/4)}$ ratios for the light peak show a gradual trend towards unity at the highest masses. However, the $G_{(2/4)}$ ratio in the heavy peak is initially high (around 2.5) near the doubly magic Sn shell closure and decreases rapidly towards unity with increasing mass. In the most extreme case, the side-feeding of the 2^+ state in ^{132}Sn populated in the ^{238}U(n,f) reaction accounts for some 60% of the total side-feeding intensity. This phenomenon may thus account for some of the observed anomaly at $Z = 50$ when using the γ-ray coincidence method to determine fission yields[47].

For the ^{252}Cf(SF) system it is not possible to deduce the 2^+ side-feedings from gating on the partner fragments since the partner fragment decays in-flight, so its transitions are Doppler broadened. In the case of ^{252}Cf(SF) we use $G_{(2/4)}$ ratio values deduced from the fits to the ^{238}U(n,f) data. The ^{232}Th(n,f) $G_{(2/4)}$ ratios show similar variations with mass, but we assume that the ^{238}U(n,f) trends provide better estimates. This is preferable to assuming 2^+ state side-feeding values of zero for ^{252}Cf(SF), since it allows a better comparison of average spins in all three systems, but may necessarily introduce some small systematic bias.

Statistical transitions. The statistical side feeding transitions will also carry away a small quantity of angular momentum. In the original MSM paper calculations were used to estimate the average number of statistical transitions (2.5) and average angular momentum per transition (0.4 units)[48]. Here, we use these same values to facilitate comparison of results. These do not affect the shape of the observed saw-tooth distributions but will instead just shift them globally up or down in spin.

Isomeric states and delayed transitions. Calculating the average spin for a nucleus with a strongly populated isomer requires an additional step in the analysis. For isomeric transitions with lifetimes in the nanosecond to microsecond range, the γ-ray decay below the isomer can occur outside the trigger window and thus the γ-rays and their coincidences with states above the isomer are not observed, leading to an underestimate of the average spin if no correction is applied. The correction for ^{252}Cf(SF) data are very simple, since we can just increase the size of the prompt window from 100 ns to 4 μs. This results in an increase in the average spin of the most affected nuclei, ^{132}Sn and ^{134}Te, of 12% and 14% respectively. No other nuclei show statistically significant (>2s.d.) increases in the deduced average spin for an extended coincidence window. Applying corrections for isomers in the ^{232}Th(n,f) and ^{238}U(n,f) datasets is more difficult. The prompt window is increased from 80 ns to 400 ns, and the corresponding increase in spin for these key isomeric nuclei is measured. A further correction is then applied using an extrapolation to account for the missing isomeric coincidences beyond the 400-ns window.

For all three fissioning systems the nucleus ^{130}Sn presents a unique problem. A 10^+, 1.6-μs isomer decays to the 7^- state through an unobservable 96-keV transition and this 7^- state has a half-life of 1.7 min. Hence, there is missing intensity for this nucleus. We include ^{130}Sn in our data, but acknowledge the existence of a potential systematic error in the calculation of the average spin for this particular case. However, since the neighbouring ^{132}Sn also has a similar high-spin isomer, and the inclusion or exclusion of these decays changes the average spin by only 12%, we assume that the systematic underestimate of average spin for ^{130}Sn will be smaller than the statistical uncertainties.

Redundancy and the indirect deduction of intensity information. As mentioned previously, there is some redundancy in the γ-ray transition intensity, given that we measure a cumulative intensity flow. This redundancy can be exploited to recover missing intensity information in the rare case that it is necessary. A problem that can occur during a two-dimensional coincidence analysis is that occasionally, certain coincidences or transitions can be obscured by the presence of others if they are too close in energy. This generally presents more of a difficulty for a small number of weak transitions in nuclei with the lowest production yields. For example, there is a strong background of random 511-keV γ-rays from electron–positron annihilation. For a nucleus that has a weak transition very close to this energy it is often impossible to measure its intensity directly owing to the large statistical fluctuations present after subtraction of this dominating background.

If such doublets or multiplets are too close in energy to resolve by two-dimensional peak fitting, information on the intensity of the obscured transition can still be recovered from the intensity flows into and out of its initial and final states. For the general case, the intensity, G, of a γ-ray transition between initial state A and final state B can never be smaller than the intensity balance into state A and never be larger than the intensity balance out of state B, since this would result in negative side-feedings for A or B, which is unphysical.

If G_{Ai} and G_{Ao} are the measured ingoing and outgoing intensities from state A, and G_{Bi} and G_{Bo} those for state B, then the intensity of the missing transition intensity, G_x, must obey the following relation $(G_{Ai} - G_{Ao}) \geq G_x \geq (G_{Bo} - G_{Bi})$. The best estimate of the intensity G_x is thus the average $((G_{Ai} - G_{Ao})+(G_{Bo} - G_{Bi}))/2$ of the upper and lower bound and implies that the side-feedings of state A and state B are equal. The impact of deducing a γ-ray intensity on the average spin measured for a particular nucleus is negligible because the measurement integrates the intensity information from many transitions and the deduced intensity is usually a very good estimate of the real intensity.

Potential sources of bias

The MSM has several sources of potential bias outlined below.

Level schemes. Since we are observing neutron-rich nuclei far from stability in these experiments, the level schemes in the literature (see the ENSDF databases[46]) may have spin assignments of certain levels which are only tentative, and in some cases incorrect by 1 or 2 spin units. This may have a small impact on the average spin extracted for a particular nucleus. However, the main side-feeding branches usually occur at lower spins with the 2^+, 4^+ and 6^+ yrast levels accounting for a large fraction of the total side-feeding intensity in most cases. These states are usually well measured with unequivocal spin assignments. Mis-assignment of the spins of certain states may either slightly lower or slightly raise the average spin deduced for a particular nucleus. However, the effect will be local, can occur in either direction, and will be confined to a particular nucleus. No global systematic effect is expected.

Ground state feeding. The direct side-feeding of the ground state is impossible to measure using γ-ray spectroscopy. However, we can estimate it from an extrapolation of the spin distribution toward zero. Extended Data Fig. 4 shows how this extrapolation is performed from fits to the spin distribution associated with each data point. The extracted 0^+ feeding is given an appropriately large relative uncertainty. The 0^+ feeding is typically 3–5% of the total side-feeding intensity in most cases, but increases in the vicinity of closed-shell nuclei (up to 18% in the case of ^{132}Sn). The impact of this correction on the average spin values results in a slight lowering, which is smaller than the statistical errors. However, for ^{132}Sn and its near neighbours with substantial 0^+ feeding the average spin values drop considerably more by typically $0.3\hbar$. Performing this correction has no impact on the conclusions.

Non-inclusion of weaker transitions. A potential bias in extraction of average spin could occur as a function of the fragment yield. Nuclei that are more weakly populated in general may have fewer observable transitions and levels available for inclusion in the weighted sum. However, we conclude that the MSM method is very insensitive to the inclusion or exclusion of non-yrast levels. Provided transitions from levels in the yrast sequence are visible, a reliable extraction of average spin can be made. The non-observation of weak transitions at the top of the yrast sequence has little impact on the final result, since if the transitions are weak at this point, the side-feedings are also weak and contribute little to the result. To quantify this potential bias, average spins in the 15 most strongly populated nuclei were recalculated after fitting only the yrast sequences and ignoring the presence of all other non-yrast states and transitions. The root-mean-square difference between the two sets of values was found to be 5.9%. The transition rates of statistical side-feeding transitions are orders of magnitude faster than the intra-yrast cascade transitions and this probably accounts for why the difference is small. Finally, if the measured average spins for all nuclei studied are plotted against fragment yields, the two quantities are seen to be almost entirely uncorrelated.

The trigger condition. For the case of the ^{252}Cf(SF), the trigger condition was an anode signal of the ionization chamber corresponding to detection of one fragments in flight, with the other stopped rapidly in the backing of the sample. This gives a clean, unambiguous signal that a fission has occurred. For the ^{232}Th(n,f) and ^{238}U(n,f) reactions the fission discrimination is less perfect. Although the beam pulsation allows discarding of events which are uncorrelated in time, a minimum multiplicity condition is also used in the prompt trigger window. This is essential to distinguish fission from the complex background of other low-multiplicity processes that also occur during the beam pulse, such as inelastic scattering ^{238}U(n,n'), ^{27}Al(n,n'),^{72,73,74,76}Ge(n,n'), p(^{7}Li,^{7}Li′) Coulomb excitation of the primary beam, and the intrinsic activity of the targets. The intrinsic activity is a particular problem for the ^{232}Th target, as a fraction of its decay also occurs during the prompt beam pulse. Since the majority of γ-rays detected during the experiment come from these low-multiplicity processes, a minimum trigger condition of $M_\gamma \geq 3$ is essential in order to preferentially select fission events. For the best discrimination the trigger condition should be placed at even higher multiplicities but we have deliberately kept it at 3 to minimize any potential trigger biases, even though this results in larger backgrounds. From the ^{252}Cf(SF) data it is possible to study the impact of the multiplicity trigger condition on the results. Raising the minimum trigger condition from the ionization chamber fission tag from a minimum multiplicity of two to three has no noticeable impact on the measured average spins. Effects are, however, observed at higher-multiplicity conditions. A global increase in the average spin for all nuclei of around one spin unit is observed for an increase of around 4 units in detected multiplicity. This correlation is completely expected and gives us further confidence in the key observation of this paper, namely the absence of spin correlations between fragment partners. The reason the slope of the correlation of average spin with detected multiplicity is not larger is mostly due to the imperfections in the ν-Ball calorimeter (68% efficiency for detecting a single γ-ray at 1 MeV). An event of detected multiplicity (or fold) of 4 will thus have sizeable contributions from emitted multiplicities of 4, 5, 6, 7 and 8.

Derivation of the spin parameterization from statistical theory. The expected probability distribution, $P(I)$, of angular momenta, I, for an excited nucleus, following the work of Hans Bethe[35], is:

$$P(I|\sigma^2) = \frac{2I+1}{2\sigma^2}\exp\left(-\frac{(I+1/2)^2}{2\sigma^2}\right)$$

where σ is known as a spin-cutoff parameter describing the breadth of this distribution. In the Fermi gas model, the spin cut-off parameter depends directly on the nuclear temperature, T, and is related to the excitation energy E_x and the level density parameter, a.

$$T = \sqrt{\frac{E_x}{a}}$$

In this model, the spin cut-off parameter is then usually defined as the product of the rigid body moment of inertia, $\mathcal{I}_{rigid}$, and the temperature:

$$\sigma^2 = \mathcal{I}_{rigid}T$$

where for a spheroidal nucleus

$$\mathcal{I}_{rigid} = \frac{2}{5}A_F R^2$$

so $\mathcal{I}_{rigid} \propto A_F^{5/3}$. Using a level density parameter a that is proportional to A_F, the variation in the spin cut-off parameter with fragment mass can then be defined in the following way:

$$\sigma^2 \propto \sqrt{E_x}A_F^{7/6}$$

If we assume that the excitation energy of the fragment is proportional to the mass of the nucleons from the ruptured neck (that is, $E_x \propto A_N$), we obtain this final parameterization based on statistical theory, which can be used to fit our average spin data in Fig. 1:

$$I = c\,A_N^{1/4}A_F^{7/12}$$

where $I \approx 1.15\sigma$. This smooth parameterization of the mass dependence with only one free parameter can be used as a fitting function, analogous to the smooth fitting of nuclear mass variations with the Weissacker formula[49]. An extended theoretical description would also have additional local variations in $E_x(A_F)$, level density $a(A_F)$ and $\mathcal{I}_{rigid}(A_F)$ owing to structure effects. However, the smooth functional dependence of $I(A_F)$ captures the major ingredients of the variation.

Monte Carlo code for correlated fragment spins. For the data presented in Fig. 2, a dispersion propagation Monte Carlo code was developed to understand what experimental slopes we would expect to see if the intrinsic angular momentum were generated by pre-scission mechanisms that produce correlated spins at scission (that is, the precise width and location of case 'Pre-scission' in the inset of Fig. 2). The emission of neutrons and statistical γ-rays in each fragment will have a de-correlating effect on any spin measurements carried out at or near the yrast lines. The precise and only purpose of this code is to propagate realistic spin dispersions from scission to yrast simultaneously in both fragments owing to emission of neutrons and statistical γ rays. It allows for (i) complete user control over the spin distribution parameters at

scission, (ii) total control over the widths of the spin dispersions due to emission of both neutrons and γ-rays, and (iii) the ability to output the resulting spin distribution observed at yrast when setting conditions on the spin distribution in the partner fragment.

Dispersions in spin due to neutron emission were taken as random $\pm 0.5\hbar$ per emitted neutron. To obtain statistical γ-ray spin dispersions, the RAINIER code[50] was used to fully model the γ-decay of several representative spherical and deformed fission fragments. Typical statistical γ-ray spin dispersion distributions with a width of around $\pm 1.5\hbar$ were then imported into our Monte Carlo code.

The placement of different gating conditions at yrast on one fragment could then be simulated and the effect on the resulting spin distribution at yrast in the partner fragment could be determined (see Extended Data Fig. 3). A simulated experimental relationship between the gating condition at yrast in one fragment and the 'measured' average spin in the other could then be probed and an 'experimental' slope deduced. With these tools, a sensitivity analysis of the results to the parameters of the initial spin distribution and neutron/γ-dispersions could be performed. The blue band in the inset of Fig. 2 for case 'Pre-scission') gives a range of expected slopes (0.4–0.6) for fully correlated spins at scission for reasonable variations of these parameters. The conclusion is that statistical emission will slightly weaken any spin correlations present at scission but will not destroy them.

We also note that similar experimental data exists for 1n partners. These are not shown in Fig. 2, which would have become much too cluttered. However, the results obtained are similar, with comparable slopes observed.

An extension of this Monte-Carlo code to include the γ-ray spectrometer granularity and detection efficiency was also developed. Here, the concern was that demanding observation of a 'high spin' state in one fragment might reduce the overall efficiency of detection owing to potential biases towards higher-multiplicity events involving many detectors. Since ν-Ball is a highly granular array (106 separate Ge elements at large distances) this effect on the expected slopes proved to be completely negligible. However, for the case of very close-packed detector arrays (for example, 6 clover detectors placed in cubic geometry) small negative slopes could arise from such biases, suggesting an artificial anti-correlation between fragment spins.

Data availability

All data from which the conclusions of this paper are drawn are contained within this manuscript. All other data can be made available on reasonable request. The large quantities of raw data (approximately 120 Tb) are shared within the ν-Ball Collaboration on servers at the CNRS-IN2P3 Centre de Calcul in Lyon (https://cc.in2p3.fr). The ALTO facility of the IJC Laboratory has a transparent data management policy that complies with the relevant European directives on open data (https://ec.europa.eu/digital-single-market/en/european-legislation-reuse-public-sector-information). Raw data from the ν-Ball Collaboration will be made publicly available after a period of 5 years. Source data are provided with this paper.

Code availability

All codes used in the data analysis can be made available on reasonable request.

41. Etasse, D. et al. *Fast Acquisition System for nuclEar Research (FASTER)*; http://faster.in2p3.fr (2013).
42. Hamilton, J. et al. New insights from studies of spontaneous fission with large detector arrays. *Prog. Part. Nucl. Phys.* **35**, 635 (1995).
43. Smith, A. G. et al. Spectroscopy of neutron-rich nuclei populated in the spontaneous fission of ^{252}Cf and ^{248}Cm. *AIP Conf. Proc.* **481**, 283 (1999).
44. Agostinelli, S. et al. GEANT IV—a simulation toolkit. *Nucl. Instrum. Meth. Phys. Res. A* **506**, 250–303 (2003).
45. Radford, D. C. ESCL8R and LEVIT8R: software for interactive graphical analysis of HPGe coincidence data sets. *Nucl. Instrum. Meth. Phys. Res. A* **361**, 297-305 (1995).
46. Tuli, J. K. Evaluated nuclear structure data file. *Nucl. Instrum. Meth. Phys. Res. A* **369**, 506-510 (1996).
47. Wilson, J. N. et al. Anomalies in the charge yields of fission fragments from the ^{238}U(*n*,*f*) reaction. *Phys. Rev. Lett.* **118**, 222501 (2017).
48. Pühlhofer, F. On the interpretation of evaporation residue mass distributions in heavy-ion induced fusion reactions. *Nucl. Phys. A* **280**, 267–284 (1977).
49. Weizsäcker, C. F. Zur Theorie der Kernmassen. *Z. Phys.* **96**, 431–458 (1935).
50. Kirsch, L. E. & Bernstein, L. A. RAINIER: a simulation tool for distributions of excited nuclear states and cascade fluctuations. *Nucl. Instrum. Meth. Phys. Res. A* **892**, 30–40 (2018).
51. England, T. R. & Rider, B. F. *Evaluation And Compilation Of Fission Product Yields*. Los Alamos Report LA-UR-94-3106, ENDF-349, https://www-nds.iaea.org/endf349/ (International Atomic Energy Agency (IAEA) Nuclear Data Services, 1993).

Acknowledgements We thank the staff of the ALTO facility of the IJC Laboratory, Orsay, for providing the intense, precisely focused ^{7}Li primary beams for very long periods, thus permitting the collection of large datasets with the ν-Ball spectrometer. We thank W. Nazerewicz, S. Åberg and O. Serot for discussions of fission theory; we also thank S. Åberg and O. Serot for assistance with the theoretical interpretation of our experimental results. We thank G. Kessedijan for assistance with variance–covariance calculations. Finally, we thank the Gammapool international consortium for the loan of the germanium clover detectors used to construct the spectrometer. This work was supported by the IN2P3/CNRS, France, the STFC UK Nuclear Data Network, the STFC (grants ST/L005743/1 and ST/P005314) (PHR), the Marion Redfearn Trust (RCL). P.H.R., M.B., A. Boso and P.I. acknowledge support from the UK Department of Business, Energy and Industrial Strategy (BEIS) via the National Measurement System. P.K., P.-A.S. and J.W. acknowledge the support from BMBF under grant NuSTAR.DA 05P15RDFN1. Funding from the HORIZON2020 programme of the European Commission is acknowledged for Transnational Access to the ALTO facility under the Integrated Infrastructure Initiative, European Nuclear Science and Applications Research 2 (ENSAR2), grant agreement number 654002. A. Blazhev, R.-B.G. and N.W. acknowledge support by the German Research Foundation (DFG grant BL 1513/1-1). L.F., V.V., J.B. and V.S.-T. acknowledge funding from the Spanish MINECO via FPA2015-65035-P and RTI2018-098868-B-I00. A.A. acknowledges funding Spanish MINECO via FPA2017-83946-C2-1-P and Ministerio de Ciencia e Innovacion grant PID2019-104714GB-C21. B.F. acknowledges funding from the Polish National Science Centre under contracts 2014/14/M/ST2/00738 and 2013/08/M/ST2/00257. M.P. acknowledges funding from the Polish National Science Centre under contracts UMO-2019/33/N/ST2/03023, UMO-2020/36/T/ST2/00547 and A.K., K.M. and E.A. under contract UMO-2015/18/E/ST2/00217. D.G. acknowledges funding from the Norges Forskningsråd (Research Council of Norway) 263030. S.L., G.B., C.P., S.Z., L.W.I, A.G. and S.B. acknowledge funding from the Italian Istituto Nazionale di Fisica Nucleare (INFN).

Author contributions J.N.W. participated in the construction of the ν-Ball spectrometer, contributed to the experimental data taking, organised the ν-Ball international collaboration, performed the analysis work presented here and wrote the main body of the paper. D.G. helped with experimental and theoretical discussions, interpretation of results, manuscript preparation and resubmissions, calculations, plots and bibliography. D.T. constructed the spectrometer, calibrated and optimized the spectrometer, kept the spectrometer running, contributed to the experimental data taking, performed data processing of the large quantities of triggerless data and helped distribute it to the collaboration. M.L. organized the ν-Ball project, led the construction of the spectrometer, organised the experimental campaign, kept the spectrometer running, contributed to the experimental data taking and measured ν-Ball performances. M.R., N.J., R.C., G.H., R.L. and R.-B.G. helped with the cabling of the ν-Ball spectrometer, supported the running of the spectrometer (filling with liquid nitrogen, monitoring detectors, and so on), calibrated and optimized the spectrometer, contributed to the experimental data taking and performed offline data analysis. D.E. developed and helped deploy the digital electronics used for the ν-Ball Data Acquisition System). L.G. developed and deployed the ^{252}Cf ionization chamber. S.O., C.S., T.K., P.H.R., A. Blazhev, N.W., S.L., B.F., A.A., M.F., L.F. and others contributed to the theoretical discussions and interpretation of results. S.S. helped with organization, discussions and interpretation, bibliography and manuscript preparation. F.Z. carried out fragment decay simulations using the RAINIER code. All listed collaborators helped keep the experiment, the spectrometer and the data acquisition systems running over the period of 7 weeks during which the data were collected.

Competing interests The authors declare no competing interests.

Additional information

Supplementary information The online version contains supplementary material available at https://doi.org/10.1038/s41586-021-03304-w.

Correspondence and requests for materials should be addressed to J.N.W.

Peer review information *Nature* thanks Cedric Simenel, Patrick Talou and the other, anonymous, reviewer(s) for their contribution to the peer review of this work. Peer reviewer reports are available.

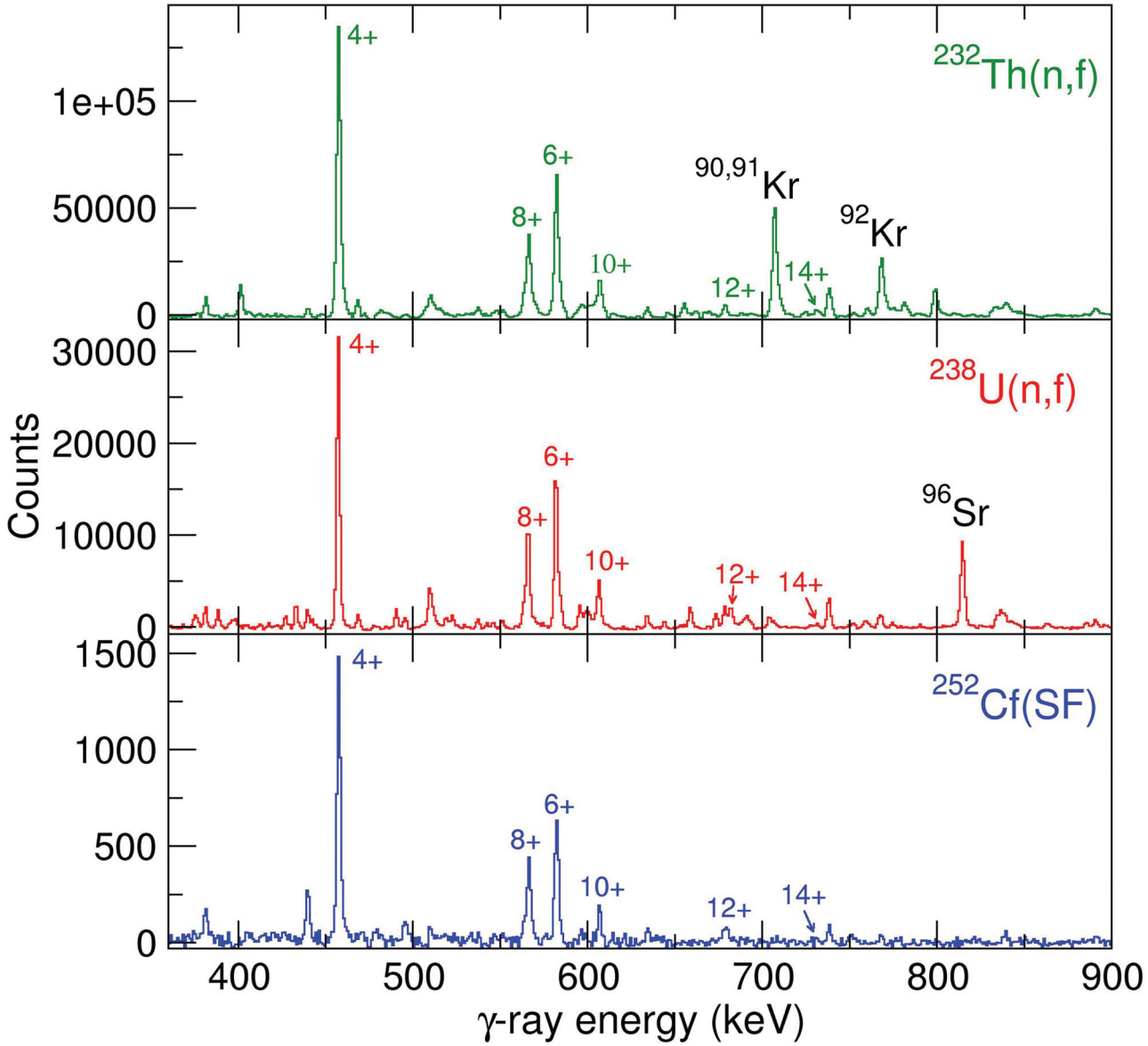

Extended Data Fig. 1 | γ-ray coincidence spectra for ^{140}Xe. Spectra are gated by the $2^+ \rightarrow 0^+$ transition for the three different fissioning systems studied in this work. The spins of states emitting the yrast sequence of transitions are marked. Strong γ-rays from the binary partner fragments are indicated. γ-rays from fragment partners in ^{252}Cf(SF), such as ^{112}Ru, were detected in flight and are thus not visible owing to Doppler broadening. The ^{252}Cf(SF) spectrum has many fewer counts, but similar experimental sensitivity is achieved owing to the elimination of backgrounds from other processes by direct detection of the fission fragment in the ionization chamber with the γ–γ coincidences.

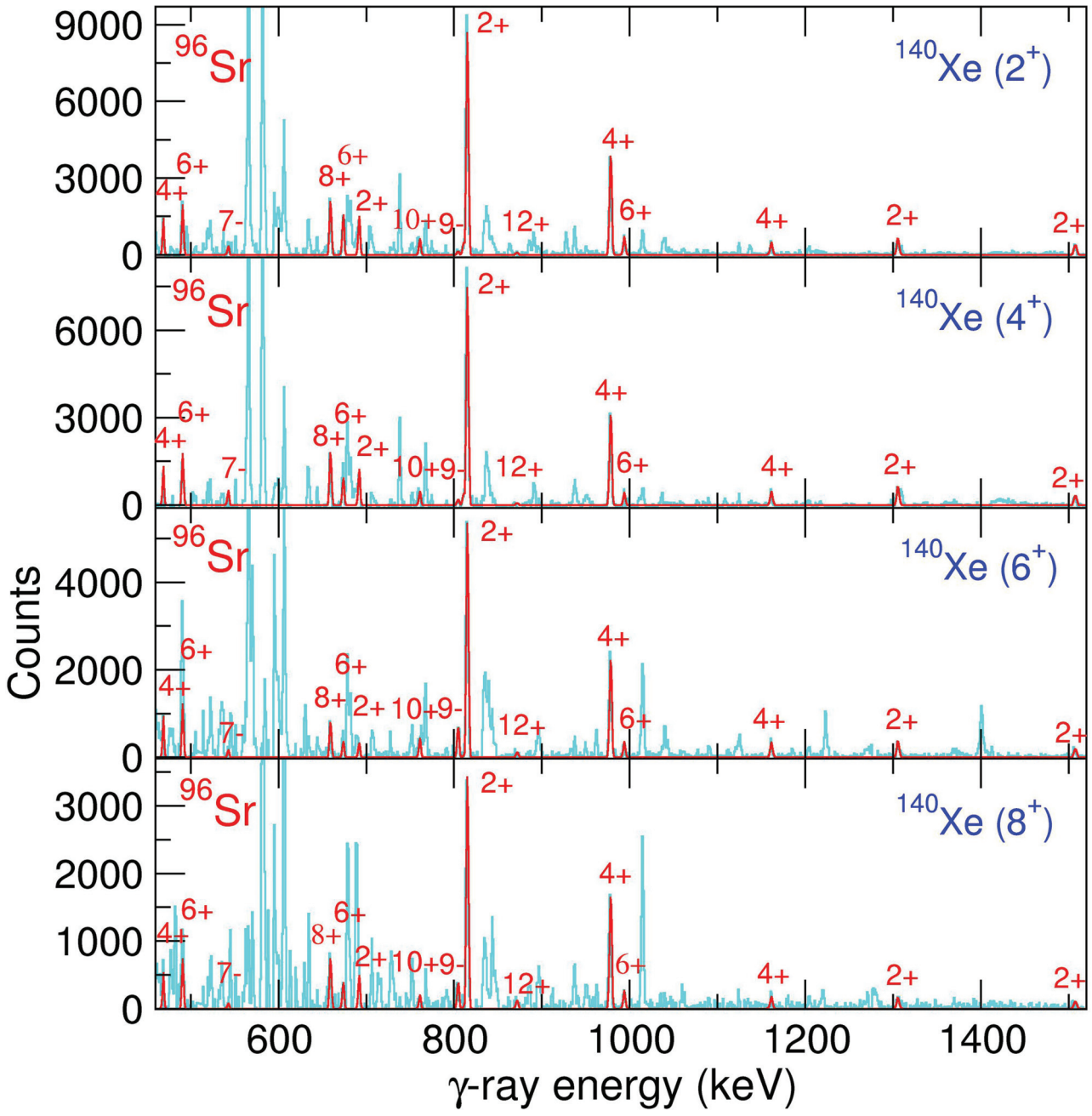

Extended Data Fig. 2 | Coincident γ-ray spectra from the ^{238}U(*n*,*f*) reaction gated on transitions from ^{140}Xe emitted from states of increasing spin. The fits to transitions decaying out of specific states of the partner nucleus ^{96}Sr are shown in red. The 492-keV transition from the 6+ state in ^{96}Sr in the third panel is deduced from its neighbours rather than fitted, owing to contamination. The intensity pattern is not observed to vary and the average spins in ^{96}Sr show no notable changes. The relationships between partner spins for several more nuclei are shown in Fig. 2.

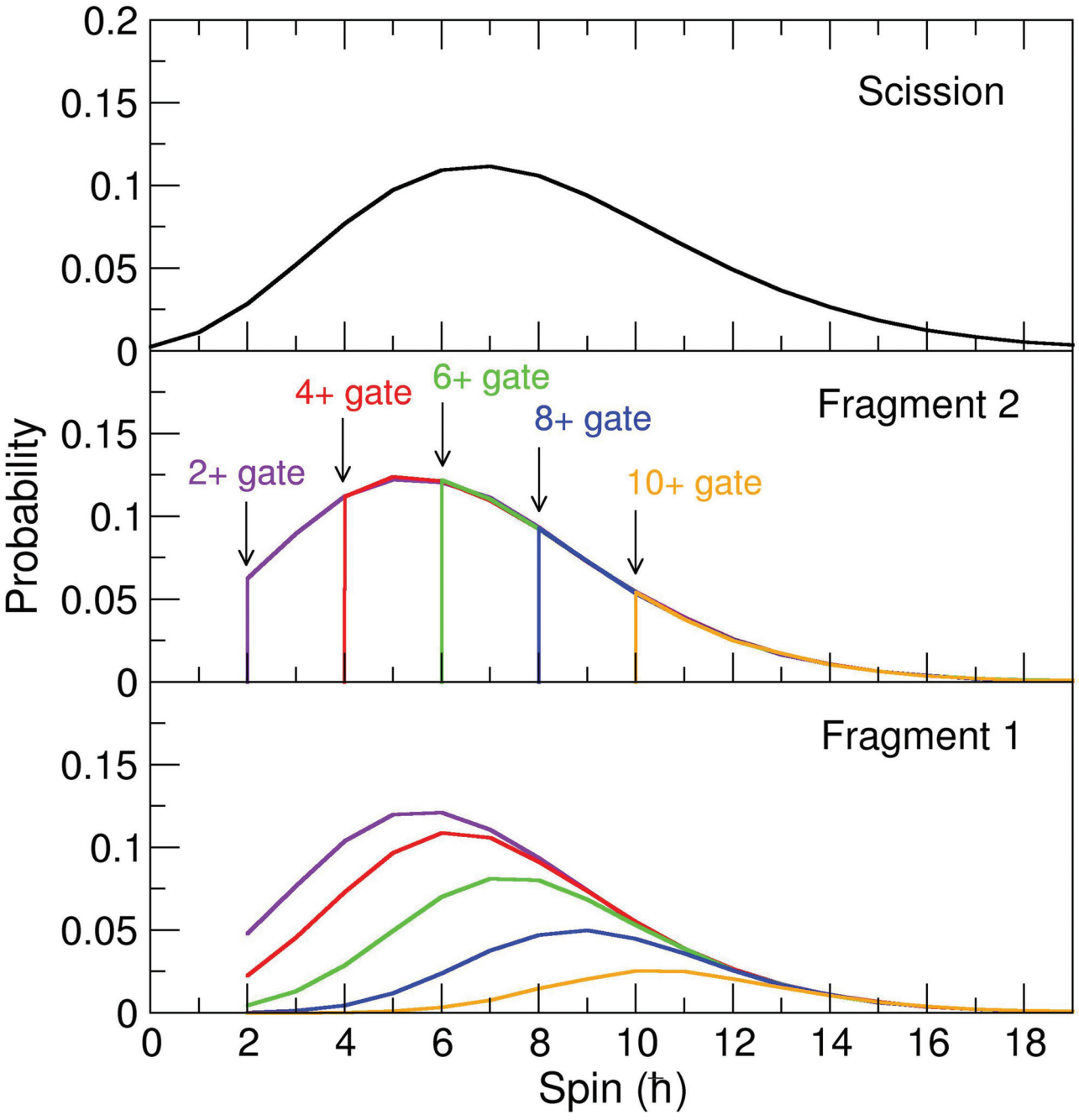

Extended Data Fig. 3 | Monte Carlo simulations of events with correlated spins at scission. Placing conditions on the minimum spin at yrast of events in fragment 1 affects the yrast distributions of event spins in fragment 2.

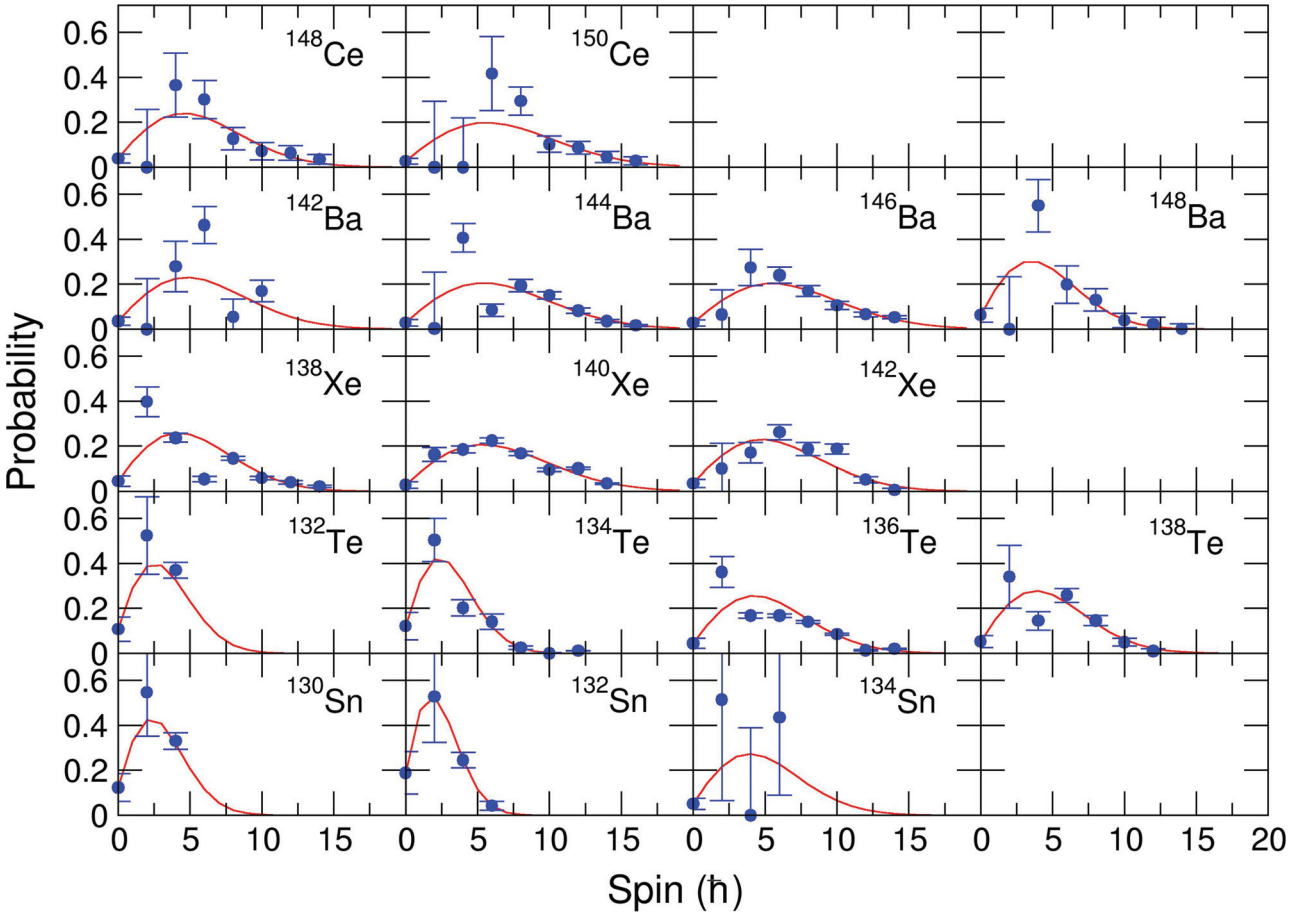

Extended Data Fig. 4 | Examples of experimental spin distributions for a range of nuclei observed in the ^{238}U(*n*,*f*) reaction. Statistical uncertainties are shown. To eliminate the odd–even staggering effect and facilitate easy visualization, side-feedings of odd spins are redistributed equally between the two neighbouring even spins. The red curves are fits to the experimental data with one free parameter and are used to extract 0+ side-feedings via an iterative procedure.

Extended Data Table 1 | ^{232}Th(*n*,*f*) average spin data

Nucleus	<I>	$\sigma_{<I>}$	$G_{(2/4)}$	$\sigma_{G(2/4)}$	0^+ feed	Yield(%)
^{82}Ge	4.10	0.10	-	-	0.11	0.64
^{84}Ge	3.92	0.78	-	-	0.09	0.32
^{84}Se	3.85	0.03	-	-	0.17	1.09
^{86}Se	4.26	0.05	1.13	0.16	0.11	4.68
^{88}Se	4.41	0.16	-	-	0.10	2.21
^{88}Kr	4.75	0.14	1.99	0.35	0.12	0.85
^{90}Kr	4.72	0.04	-	-	0.08	5.34
^{92}Kr	5.10	0.12	1.94	0.19	0.07	3.92
^{94}Kr	6.02	0.52	-	-	0.05	0.60
^{92}Sr	4.05	0.61	1.57	0.41	0.09	0.20
^{94}Sr	4.44	0.11	1.44	0.04	0.10	2.04
^{96}Sr	5.52	0.09	1.07	0.10	0.06	3.54
^{98}Sr	6.01	0.20	-	-	0.06	1.32
^{98}Zr	6.40	0.65	-	-	0.04	0.37
^{100}Zr	6.07	0.91	-	-	0.03	0.88
^{130}Sn	3.29	0.68	-	-	0.15	0.84
^{132}Sn	3.64	0.15	2.64	1.40	0.19	1.54
^{132}Te	3.38	0.48	-	-	0.13	0.35
^{134}Te	3.44	0.20	3.51	0.48	0.18	3.11
^{136}Te	4.83	0.13	2.18	0.15	0.07	3.44
^{138}Te	4.74	0.32	-	-	0.07	0.76
^{138}Xe	4.53	0.38	-	-	0.13	2.08
^{140}Xe	7.70	0.62	1.25	0.10	0.02	5.73
^{142}Xe	7.60	0.24	1.12	0.15	0.04	2.25
^{142}Ba	5.87	0.73	1.27	0.14	0.05	0.64
^{144}Ba	7.49	0.27	1.00	0.04	0.03	4.49
^{146}Ba	7.03	0.31	1.12	0.11	0.04	2.76
^{148}Ce	7.70	0.70	1.00	0.25	0.03	0.56
^{150}Ce	8.74	0.65	-	-	0.03	0.41

Measured values are given for average spin, <I>, its associated uncertainty $\sigma_{<I>}$, the measured intensity ratio $G_{(2/4)}$ and its associated uncertainty, $\sigma_{G(2/4)}$, the 0^+ feeding value and the fragment yield. Fragment yields are taken from the evaluated nuclear data files ENDF.BVII[51].

Extended Data Table 2 | ^{238}U(*n*,*f*) average spin data

Nucleus	<I>	$\sigma_{<I>}$	$G_{(2/4)}$	$\sigma_{G(2/4)}$	0^+ feed	Yield(%)
^{82}Ge	4.41	0.67	-	-	0.09	0.12
^{84}Se	3.98	0.18	-	-	0.16	0.17
^{86}Se	4.88	0.24	1.48	0.30	0.07	0.84
^{88}Se	4.72	0.36	1.20	0.23	0.10	0.54
^{88}Kr	4.37	0.32	-	-	0.10	0.37
^{90}Kr	4.76	0.10	-	-	0.08	1.85
^{92}Kr	5.21	0.08	1.66	0.37	0.06	2.50
^{94}Kr	5.27	0.42	1.60	0.31	0.05	0.73
^{94}Sr	4.76	0.10	1.22	0.09	0.09	1.51
^{96}Sr	5.11	0.05	1.31	0.06	0.06	4.13
^{98}Sr	6.08	0.12	0.95	0.14	0.04	2.27
^{98}Zr	5.98	0.32	0.94	0.10	0.06	0.49
^{100}Zr	6.14	0.11	-	-	0.05	3.30
^{102}Zr	6.12	0.08	1.11	0.12	0.05	4.09
^{104}Zr	5.71	0.24	-	-	0.06	1.01
^{102}Mo	7.87	0.50	-	-	0.02	0.08
^{104}Mo	6.53	0.17	1.45	0.30	0.04	1.08
^{130}Sn	3.46	0.40	-	-	0.12	1.65
^{132}Sn	3.75	0.25	2.84	0.64	0.19	1.88
^{134}Sn	4.65	1.16	-	-	0.05	0.18
^{132}Te	3.56	0.40	-	-	0.10	0.47
^{134}Te	4.26	0.17	2.33	0.24	0.12	3.95
^{136}Te	5.82	0.06	1.61	0.11	0.04	3.53
^{138}Te	5.60	0.20	1.56	0.21	0.05	0.55
^{138}Xe	5.62	0.18	-	-	0.05	2.04
^{140}Xe	7.41	0.10	1.16	0.03	0.03	4.04
^{142}Xe	7.53	0.21	1.12	0.11	0.04	1.53
^{142}Ba	7.02	0.76	-	-	0.04	0.69
^{144}Ba	7.94	0.16	1.43	0.35	0.03	2.46
^{146}Ba	7.60	0.22	1.07	0.06	0.03	1.98
^{148}Ba	6.10	0.42	-	-	0.06	0.25
^{148}Ce	7.24	0.59	-	-	0.04	0.75
^{150}Ce	9.01	0.54	-	-	0.03	0.86

Measured values are given for average spin, <I>, its associated uncertainty $\sigma_{<I>}$, the measured intensity ratio $G_{(2/4)}$ and its associated uncertainty, $\sigma_{G(2/4)}$, the 0^+ feeding value and the fragment yield. Fragment yields are taken from the evaluated nuclear data files ENDF.BVII[51].

Extended Data Table 3 | ^{252}Cf(SF) average spin data

Nucleus	<I>	$\sigma_{<I>}$	0^+ feed	Yield(%)
^{94}Sr	4.74	0.33	0.11	0.55
^{96}Sr	5.92	0.40	0.05	0.89
^{98}Sr	6.89	0.61	0.03	0.37
^{98}Zr	6.22	0.37	0.05	0.59
^{100}Zr	5.76	0.10	0.06	2.06
^{102}Zr	5.84	0.13	0.06	1.45
^{104}Zr	5.34	0.59	0.07	0.22
^{102}Mo	5.96	0.25	0.05	0.46
^{104}Mo	6.22	0.07	0.05	2.83
^{106}Mo	5.42	0.07	0.07	3.47
^{108}Mo	6.13	0.09	0.05	0.67
^{108}Ru	6.47	0.32	0.06	1.98
^{110}Ru	7.23	0.11	0.04	3.62
^{112}Ru	6.77	0.20	0.04	0.94
^{112}Pd	7.26	0.34	0.04	0.75
^{114}Pd	7.37	0.54	0.03	1.82
^{116}Pd	8.55	0.28	0.03	0.82
^{130}Sn	3.46	0.59	0.12	0.36
^{132}Sn	3.95	0.68	0.11	0.14
^{134}Te	4.08	0.08	0.13	2.35
^{136}Te	5.67	0.30	0.03	0.91
^{138}Xe	5.43	0.11	0.04	3.63
^{140}Xe	7.11	0.19	0.03	2.55
^{142}Xe	6.35	0.54	0.04	0.37
^{142}Ba	6.04	0.10	0.05	2.70
^{144}Ba	8.11	0.09	0.03	3.37
^{146}Ba	7.58	0.24	0.04	0.98
^{148}Ce	7.56	0.16	0.03	2.35
^{150}Ce	9.12	0.35	0.02	0.94
^{152}Nd	8.94	0.49	0.02	0.83
^{154}Nd	10.91	0.76	0.01	0.42

Measured values are given for average spin, <I>, its associated uncertainty $\sigma_{<I>}$, the measured intensity ratio $G_{(2/4)}$ and its associated uncertainty, $\sigma_{G(2/4)}$, the 0^+ feeding value and the fragment yield. Fragment yields are taken from the evaluated nuclear data files ENDF.BVII[51].

Extended Data Table 4 | Fitting parameters for the light and heavy peak data for the three fissioning systems

System	Mass peak	Fitted constant c	Correlation coefficient R^2
^{232}Th(n,f)	light	0.189	0.837
^{238}U(n,f)	light	0.192	0.806
^{252}Cf(SF)	light	0.186	0.803
^{232}Th(n,f)	heavy	0.195	0.848
^{238}U(n,f)	heavy	0.202	0.854
^{252}Cf(SF)	heavy	0.213	0.884

The fitting function is defined as $\langle l \rangle = c A_N^{1/4} A_F^{7/12}$ with a single free parameter, c.

Paper III

What impacts the isomeric yield ratios of fission fragments?